

## **INFORMATION TO USERS**

**This manuscript has been reproduced from the microfilm master. UMI films the text directly from the original or copy submitted. Thus, some thesis and dissertation copies are in typewriter face, while others may be from any type of computer printer.**

**The quality of this reproduction is dependent upon the quality of the copy submitted. Broken or indistinct print, colored or poor quality illustrations and photographs, print bleedthrough, substandard margins, and improper alignment can adversely affect reproduction.**

**In the unlikely event that the author did not send UMI a complete manuscript and there are missing pages, these will be noted. Also, if unauthorized copyright material had to be removed, a note will indicate the deletion.**

**Oversize materials (e.g., maps, drawings, charts) are reproduced by sectioning the original, beginning at the upper left-hand corner and continuing from left to right in equal sections with small overlaps. Each original is also photographed in one exposure and is included in reduced form at the back of the book.**

**Photographs included in the original manuscript have been reproduced xerographically in this copy. Higher quality 6" x 9" black and white photographic prints are available for any photographs or illustrations appearing in this copy for an additional charge. Contact UMI directly to order.**

# **UMI**

**A Bell & Howell Information Company  
300 North Zeeb Road, Ann Arbor MI 48106-1346 USA  
313/761-4700 800/521-0600**



**Influence of Breaking Waves on Sediment  
Concentration Profiles and Longshore Sediment  
Flux in the Nearshore Zone**

by

**Andrea S. Ogston**

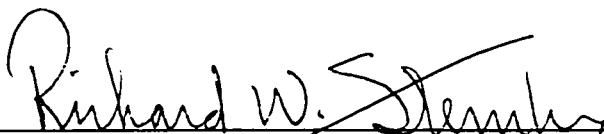
**A dissertation submitted in partial fulfillment of the  
requirements for the degree of**

**Doctor of Philosophy**

**University of Washington**

**1997**

Approved by

  
Chairperson of Supervisory Committee

**Program Authorized  
to Offer Degree**

**Oceanography**

**Date**

**December 18, 1997**

**UMI Number: 9819282**

---

**UMI Microform 9819282**  
**Copyright 1998, by UMI Company. All rights reserved.**

**This microform edition is protected against unauthorized  
copying under Title 17, United States Code.**

---

**UMI**  
**300 North Zeeb Road**  
**Ann Arbor, MI 48103**

### **Doctoral Dissertation**

In presenting this dissertation in partial fulfillment of the requirements for the Doctoral degree at the University of Washington, I agree that the Library shall make its copies freely available for inspection. I further agree that extensive copying of this dissertation is allowable only for scholarly purposes, consistent with "fair use" as prescribed in the U.S. Copyright Law. Requests for copying or reproduction of this dissertation may be referred to University Microfilms, 1490 Eisenhower Place, P.O. Box 975, Ann Arbor, MI 48106, to whom the author has granted "the right to reproduce and sell (a) copies of the manuscript in microform and/or (b) printed copies of the manuscript made from microform."

Signature



Date

12/18/97

University of Washington

**Abstract**

**Influence of Breaking Waves on Sediment  
Concentration Profiles and Longshore Sediment  
Flux in the Nearshore Zone**

by Andrea S. Ogston

Chairperson of the Supervisory Committee: Professor Richard W. Sternberg  
School of Oceanography

Two experiments provided data for the investigation of the influence of wave breaking on suspended sediment concentration profiles and sediment flux in the nearshore zone. A prototype wave basin experiment provided velocity fluctuation profiles in the upper water column and the DUCK94 field experiment provided detailed suspended sediment concentration profiles in the nearbed region.

The wave basin turbulence intensity results show wave breaking in the surf zone not only causes increased levels of turbulence near the water surface, but also causes increased levels of turbulence throughout the water column. Eddy viscosity estimates suggest wave breaking can affect mixing and diffusion throughout the entire water column. The DUCK94 sediment concentration data provided nearbed sediment eddy diffusivity estimates, and the nearbed profile was found to increase linearly with height above the bed. Also, the relationship in the nearbed between eddy diffusivity for sediment and eddy viscosity for momentum was examined, and under unbroken waves a ratio of 0.48 was found between them. Under broken waves, no relationship could be determined, suggesting methodology used to describe turbulent diffusion outside the surf zone is not necessarily applicable inside the surf zone, and bottom boundary shear may not be the primary mechanism responsible for the vertical distribution of suspended sediment.

The wave basin and DUCK94 information were combined to formulate unbroken and broken wave eddy diffusivity profiles. A simple one-dimensional model was created to examine the impacts of the eddy diffusivity profile on suspended sediment and longshore sediment flux. Under unbroken waves, the eddy diffusivity form in the upper water column is not critical because such a small amount of sediment is suspended above the wave boundary layer. Under broken waves, sediment is suspended higher in the water column and thus, the eddy diffusivity form significantly impacts the predicted suspended sediment profile. For example, the integrated suspended sediment load and longshore sediment flux (for the lower 50 cm of the water column) are under predicted by at least 25 and 33 percent, respectively, when using an eddy diffusivity profile that does not reflect wave breaking.

## TABLE OF CONTENTS

	<i>Page</i>
List of Figures .....	iv
List of Tables .....	vii
<b>CHAPTER 1. INTRODUCTION .....</b>	<b>1</b>
1.1 Suspended Sediments and Turbulence .....	1
1.2 A Diffusion Model for Suspended Sediment Transport .....	1
1.2.1 Settling Flux .....	2
1.2.2 Turbulent Flux and Eddy Diffusion Coefficients .....	3
1.2.3 Vertical Wave Advective Flux .....	6
1.3 Implications for the Surf Zone .....	7
1.3.1 Surf Zone Models .....	7
1.3.2 Objectives .....	10
<b>CHAPTER 2. ESTIMATION OF TURBULENCE INTENSITY AND EDDY VISCOSITY UNDER UNBROKEN AND BROKEN WAVES IN A WAVE BASIN .....</b>	<b>12</b>
2.1 Introduction .....	12
2.2 Wave Basin Experiment Data Set .....	12
2.2.1 Instrumentation .....	12
2.2.2 Experiment .....	14
2.2.3 Data Set Summary .....	14
2.3 Data Analysis .....	16
2.3.1 Data Processing .....	17
2.3.2 Estimates of Dissipation Rates and Turbulence Intensity .....	18
2.3.3 Estimates of Eddy Viscosity .....	18
2.4 Results .....	23
2.4.1 Turbulence Dissipation and Intensity Results .....	24
2.4.2 Comparison to Others' Work .....	24
2.4.3 Water Column Eddy Viscosity Results .....	26
2.5 Discussion .....	30
2.5.1 Wave Height Scaling .....	30



<b>CHAPTER 3. NEARBED SEDIMENT EDDY DIFFUSIVITY PROFILES FROM DUCK94 FIELD DATA.....</b>	<b>33</b>
3.1 Introduction.....	33
3.2 DUCK94 Data Set.....	33
3.2.1 Instrumentation.....	34
3.2.2 Field Experiment.....	36
3.2.3 Data Analysis.....	39
3.3 Results.....	46
3.3.1 Mean Flow and Wave Orbital Velocities.....	48
3.3.2 Friction Velocity.....	49
3.3.3 Suspended Sediment Concentration Profiles.....	51
3.3.4 Time Averaged Eddy Diffusivity Profiles.....	53
3.4 Discussion.....	53
3.4.1 Stratification Correction to Eddy Diffusivity Profile.....	53
3.4.2 Scaling.....	54
3.4.3 Relationship Between $K_s$ and $K_m$ .....	58
<b>CHAPTER 4. EVALUATION OF THE <math>K_s</math> VS <math>K_m</math> RELATIONSHIP: IMPLICATIONS FOR SURF ZONE DIFFUSION MECHANISMS.....</b>	<b>62</b>
4.1 Motivation.....	62
4.2 Relationship of $K_s$ to $K_m$ in the Nearbed for Unbroken and Broken Waves.....	62
4.2.1 Assumptions Leading to Nearbed $K_s$ Estimates.....	63
4.2.2 Assumptions Leading to $K_m$ Estimates.....	63
4.3 Discussion of $K_s$ And $K_m$ Relationship.....	64
4.3.1 Data Variability.....	69
4.3.2 Limitations in Jonsson Friction Factor Under Broken Waves.....	69
4.3.3 Limit on $K_s$ .....	70
4.4 Proposed $K_s$ and $K_m$ Relationship.....	71
4.5 Summary.....	73
<b>CHAPTER 5. COMBINED EDDY DIFFUSIVITY PROFILE AND RESULTING SUSPENDED SEDIMENT PREDICTION.....</b>	<b>76</b>
5.1 Motivation.....	76
5.2 Combined Eddy Diffusivities.....	77
5.2.1 Comparison to Other Studies.....	80
5.2.2 Formulation of Combined Eddy Diffusivity Parameterization.....	82
5.3 Prediction of Suspended Sediment Concentration Profiles.....	86
5.3.1 Physical Processes Input.....	86
5.3.2 Suspended Sediment Input.....	87

5.3.3 Eddy Diffusivity Profiles.....	87
5.3.4 Settling Velocity.....	90
5.4 Model Results.....	94
5.4.1 Suspended Sediment Profile .....	94
5.4.2 Sediment Flux Profile.....	97
5.5 Discussion .....	98
5.5.1 Implication of Model Results.....	100
 CHAPTER 6. SUMMARY AND CONCLUSIONS .....	 103
 APPENDIX A. MODEL RESULTS.....	 107
 List of References.....	 116

## LIST OF FIGURES

	<i>Page</i>
FIGURE 1.1. Eddy viscosity profiles used in modeling studies.....	5
FIGURE 1.2. Numerical model results of Johns (1983) for the simulation of turbulent processes beneath broken waves in the surf zone .....	8
FIGURE 1.3. Numerical model results of Deigaard, et al. (1986) showing the comparison between measurements of Nielsen et al. (1982) and predicted suspended sediment concentration.....	9
FIGURE 2.1. Schematic of the wave basin at Wild Rivers Waterpark in Irvine, California .....	13
FIGURE 2.2. SonTek acoustic-doppler velocimeter (ADV). .....	15
FIGURE 2.3. Ensemble-average velocities and pressure under broken wave of nominal height 0.9 m at location A.....	19
FIGURE 2.4. Representative wavenumber spectrum of vertical velocity .....	22
FIGURE 2.5. Vertical profiles of turbulence intensity, $w'$ beneath unbroken and broken waves .....	25
FIGURE 2.6. Vertical profiles of turbulence intensity, $w'$ , where $w'$ is normalized by $(gh)^{1/2}$ .....	27
FIGURE 2.7. Vertical profiles of eddy viscosity beneath unbroken and broken waves...	29
FIGURE 2.8. Eddy viscosity values from both locations A and B under unbroken and broken waves where depth below surface is normalized by wave height ..	31
FIGURE 3.1. Instrument array deployed in DUCK94 (Duck, NC) .....	35
FIGURE 3.2. Example FOBS calibration curves for four individual sensors .....	37
FIGURE 3.3. Plan view of instrument deployment scheme for total DUCK94 experiment.....	38

FIGURE 3.4. Time series of water level, waves, wind, currents and atmospheric pressure during the October phase of the DUCK94 experiment.....	40
FIGURE 3.5. Cross shore beach profile showing instrument and sediment sampling locations.....	41
FIGURE 3.6. Time series of pressure and suspended sediment concentration.....	42
FIGURE 3.7. Example data run profile of suspended sediment concentration and sediment eddy diffusivity .....	45
FIGURE 3.8. Profiles of time averaged suspended sediment concentration for unbroken and broken wave data runs .....	50
FIGURE 3.9. Profiles of time averaged sediment eddy diffusivity for unbroken and broken wave data runs.....	52
FIGURE 3.10. Profile of sediment eddy diffusivity show the impact of sediment induced stratification .....	55
FIGURE 3.11. Profiles of time averaged sediment eddy diffusivity scaled by the eddy viscosity for momentum.....	57
FIGURE 3.12. Upper water column eddy diffusivity values for the broken wave data runs with the depth below the sea surface scaled by the wave height .....	59
FIGURE 3.13. The relationship between the eddy viscosity for momentum, $K_m$ , and the sediment eddy diffusivity, $K_s$ .....	60
FIGURE 4.1. Relationship of $K_s$ to $K_m$ at 4 cmab where $K_s$ is assumed linear.....	65
FIGURE 4.2. Relationship of $K_s$ to $K_m$ at 4 cmab under unbroken wave conditions .....	66
FIGURE 4.3. Relationship of $K_s$ to $K_m$ at 4 cmab under broken wave conditions .....	68
FIGURE 4.4. Proposed relationship of $K_s$ to $K_m$ at 4 cmab.....	72
FIGURE 4.5. Conceptual sketch describing the mechanisms of sediment diffusion in the surf zone.....	74
FIGURE 5.1. Eddy diffusivity values from both the wave basin experiment and DUCK94 experiment.....	78
FIGURE 5.2. Region of overlap between the wave basin experiment and DUCK94 .....	79

FIGURE 5.3. Eddy diffusivity values above the nearbed region from both the wave basin experiment and DUCK94.....	81
FIGURE 5.4. Conceptual diagram of the eddy diffusivity profile formulated from the wave basin and DUCK94 data .....	83
FIGURE 5.5. Fit to the highest energy waves in the wave basin study at locations A and B .....	85
FIGURE 5.6. Profiles of eddy diffusivity as used in model studies and, measured and predicted suspended sediment concentration profile .....	88
FIGURE 5.7. Comparison of predicted suspended sediment concentration profiles to measurements showing the effect of settling velocity.....	91
FIGURE 5.8. Comparison of predicted suspended sediment concentration profiles to measurements showing the effect of using an elevation dependent settling velocity .....	93
FIGURE 5.9. Example unbroken wave data run profiles of eddy diffusivity, and measured and predicted suspended sediment concentration and longshore sediment flux .....	95
FIGURE 5.10. Example broken wave data run profiles of eddy diffusivity, and measured and predicted suspended sediment concentration and longshore sediment flux .....	96
FIGURE A.1. Measurements and predictions of unbroken wave data runs .....	108
FIGURE A.2. Measurements and predictions of broken wave data runs.....	112

## LIST OF TABLES

	<i>Page</i>
TABLE 2.1. Summary of wave basin velocity and pressure measurements .....	16
TABLE 3.1. Summary of 17 minute DUCK94 data runs used in this study .....	44
TABLE 3.2. Ratio of eddy diffusivity for sediment to eddy viscosity for momentum .....	61
TABLE 5.1. Sediment size and settling velocity .....	90
TABLE 5.2. Integrated concentration and flux.....	94
TABLE 5.3. Integrated sediment concentration in the lower 50 cm.....	98
TABLE 5.4. Integrated longshore sediment flux in the lower 50 cm.....	99

## ACKNOWLEDGMENTS

I would like to thank all of the members of my committee who have provided guidance in the completion of this dissertation, Dick Sternberg, Joan Oltman-Shay, Arthur Nowell, Chris Sherwood, and Catherine Petroff. I had the fortune of starting my graduate career under the best advisor, Dick Sternberg, and three of the best mentors one could ask for, Gail Kineke, Chris Sherwood, and Ed Kempema. The four of them have provided, each in their own way, the inspiration, support, and motivation to finish this dissertation. Also, they all have shown me the excitement and fun that comes with oceanography. Many friends here at the University of Washington have kept me going with their support in these last couple of years, and particularly I would like to thank my office mates Isaac Berhane, Erika McPhee, Josefa Guerra, and Judy Boughner.

Many thanks go to Chris Sherwood and Bill Asher who provided the wave basin data set and encouraged me in the analysis. The DUCK94 data collection would have been impossible without the leadership of Reggie Beach, and I appreciate all he has taught me about surf zone data collection, and the drive needed to get that data. The engineering talents and instrument making abilities of Rex Johnson and Randy Fabbro are greatly appreciated. Diane Foster and Rob Holman from OSU deserve many thanks for helping me formulate ideas and keep a sense of perspective out in field.

A special thanks go to Liz Scanland for reading, in excruciating detail, this manuscript and adding the correct punctuation, verbs, and forcing me to get to the point, and to Kevin O'Brien for the hours of cut-and-paste, and to both of them for all their help. Thanks also to Lin Sylwester who has always been incredibly responsive to my last minute graphics problems.

And finally, I thank my parents, Bill Ogston and Susanna Ogston, for all the patience and support supplied over the years.

## **CHAPTER 1. INTRODUCTION**

### **1.1 Suspended Sediments and Turbulence**

The vertical distribution of suspended sediment in the surf zone is controlled by the downward settling of sediment particles and by resuspension, and upward mixing of particles due to turbulent diffusion and wave advection. Outside the surf zone, the dominant mechanism for generation of turbulence is strong boundary shear resulting from friction at the sea bed. Sediment appears to be suspended in events within the wave current boundary layer and the suspended particles typically remain close to the bed. Inside the surf zone, however, turbulence is generated both at the sea bed and near the water surface due to wave breaking, and high concentrations of sediment can be suspended throughout the water column (Yu et al., 1993). Extensive modeling of suspended sediment transport on the continental shelf has been undertaken (e.g., Wiberg and Smith, 1983; Sherwood, 1995), and in extending these concepts to the surf zone, wave breaking must be considered. This dissertation focuses on the influence of wave breaking on the turbulent diffusion of sediment particles in the surf zone, and the resulting impact on the suspended sediment concentration profile and longshore sediment flux.

### **1.2 An Advection-Diffusion Model for Suspended Sediment Transport**

Models of suspended sediment concentration generally assume a balance exists between the downward settling of sediment particles and the upward transport by turbulent diffusion and organized vertical fluid motions. The vertical flux of sediment consists of the following balance between settling, turbulence, and vertical wave advection for the steady state condition,

$$Ws\bar{C} = \overline{w' C'} + \overline{w_w C_w} \quad (1.1)$$

where  $Ws$  is the settling velocity of the sediment particles and  $C$  is the suspended sediment concentration,  $w'$  and  $C'$  are the turbulent components of vertical fluid velocity and suspended sediment concentration, and  $w_w$  and  $C_w$  are the wave-induced components.



Assuming that upward migration of sediment results from gradient diffusion, the turbulent flux can be described by the concentration gradient times an eddy diffusion coefficient,

$$\overline{w'C} = -K_s \frac{d\overline{C}}{dz} \quad (1.2)$$

where  $K_s$  is the eddy diffusion coefficient for sediment particles. Eq. 1.1 then becomes,

$$W_s \overline{C} = -K_s \frac{d\overline{C}}{dz} + \overline{w_w C_w}. \quad (1.3)$$

This equation states that downward sediment flux due to the settling of particles is balanced by the upward gradient diffusion and the advected sediment flux due to organized wave motions. The terms of Equation 1.3 are examined in more detail below.

### 1.2.1 Settling Flux

The downward settling flux of particles is a function of the mean concentration and the settling velocity of the particles. For small particles ( $< 0.005$  cm) where the Reynolds numbers is low, the settling velocity can be described by Stokes law,

$$W_s = \frac{(s-1)gd^2}{18\nu} \quad (1.4)$$

where  $s$  is the specific gravity,  $g$  is acceleration due to gravity,  $\nu$  is the kinematic viscosity of seawater and  $d$  is the particle diameter. For the case where particles are larger and Reynolds numbers are larger, Gibbs et al. (1971) provides the following empirical adaptation of Stokes Law,

$$W_s = \frac{-3\nu + \sqrt{9\nu^2 + gd^2(s-1)(0.003869 + 0.02480d)}}{0.011607 + 0.07440d} \quad (1.5)$$

which is applied to particles with diameters between 0.0063 cm and 1 cm. This relationship is based on experiments using spheres in water and may overpredict the settling velocity of irregular shapes. For typical fine beach sand grains of diameter 200  $\mu\text{m}$ , the Stokes settling velocity is 2.6  $\text{cm s}^{-1}$  and the Gibbs settling velocity is 2.0  $\text{cm s}^{-1}$ .

### 1.2.2 Turbulent Flux and Eddy Diffusion Coefficients

The turbulent flux of sediment particles as defined by a gradient diffusion assumption is dependent upon the eddy diffusion coefficient and the vertical gradient of sediment concentration. This concept is analogous to the use of an eddy viscosity to estimate the turbulent flux of momentum introduced by Boussinesq (1877) in which the turbulent stresses are assumed to act like the viscous stresses, i.e.,

$$-\overline{u'w'} = K_m \left( \frac{d\bar{u}}{dz} \right) \quad (1.6)$$

where  $K_m$  is the eddy viscosity for momentum and  $\bar{u}$  is a mean velocity. The eddy diffusivity for sediment,  $K_s$ , has been related to eddy viscosity for momentum,  $K_m$ , by a factor  $\beta$ , ( $K_s = \beta K_m$ ), which assumes that both the eddy viscosity that is responsible for momentum flux and the eddy diffusivity that causes vertical diffusion of suspended sediments are consequences of turbulent fluctuations or eddies. The factor,  $\beta$ , has typically been taken to be a constant near 1 in the case of nonstratified flows (Glenn and Grant, 1987). There is no general agreement on the value of  $\beta$  and values both greater than and less than 1.0 have been obtained. Lees (1981) found that  $\beta$  varies inversely with suspended sediment concentration with values ranging between 1 and 10. Soulsby, et al (1986) found  $\beta$  to be on the average only about 0.2, and Dyer and Soulsby (1988) provide a discussion of  $\beta$  values found in the sea which support both  $\beta < 1$  and  $\beta > 1$ . Kawanisi and Yokosi (1997) found that  $\beta$  decreases with an increasing ratio of friction velocity to settling velocity.

#### *Eddy Viscosity Profiles*

Sediment eddy diffusivity profiles used in surf zone modeling have tended to be extensions of eddy viscosity profiles used in modeling of continental shelf processes and some of the earlier formulations of the eddy viscosity profile are discussed below. It has been difficult to test the applicability of these continental shelf eddy viscosity profiles used for surf zone processes modeling due to instrument limitations. In the nearshore, eddy

diffusivities have been previously hard to estimate from field measurements due to the detail of measurements that must be collected. New instrumentation such as the acoustic backscatter sensors (Sheng and Hay, 1995) and fiber optic backscatter sensors (Beach et al., 1992) now enable measurement of suspended sediment profiles with sufficient vertical resolution to estimate sediment eddy diffusivities.

Early work on bottom boundary layers found that a linearly increasing profile is appropriate for the constant stress layer (Kajiura, 1964 in Mei, 1989),

$$K_m = \kappa U_* z \quad (1.7)$$

where  $U_*$  is the friction velocity and is defined on the basis of the magnitude of the bed shear stress,  $[U_* = (\tau_b / \rho)^{1/2}]$  and  $\kappa$  is von Karman's constant. As depicted Figure 1.1 (line A), this linear eddy viscosity profile also has been extended beyond the bottom boundary layer and throughout the water column for surf zone conditions. For this example, the water depth  $h$  is 200 cm and  $U_*$  is 14 cm s<sup>-1</sup>. Under unidirectional flows in rivers, Smith and McLean (1977) proposed a universal curve for the eddy viscosity that reflects the decay of the linear mixing profile with height above the bed,

$$K_m = \kappa U_* h \left[ \frac{z}{h} + 1.3289 \left( \frac{z}{h} \right)^2 - 16.8632 \left( \frac{z}{h} \right)^3 + 25.2266 \left( \frac{z}{h} \right)^4 \right] \quad (1.8)$$

for  $z/h < 0.3$ . This profile is illustrated as line B in Figure 1.1 for the same conditions as line A, except the length scale,  $h$ , is set at to half the water depth.

Alternately, other investigators have found an exponential decay of  $K_m$  through the upper water column (above the  $z/h < 0.3$  criteria of Smith and McLean). For steady flow, Nowell and Long (1983) found the best fit in the reanalysis of pipe flow data to be,

$$K_m = \kappa U_* z \exp \left[ - \frac{z}{h} - \alpha \left( \frac{z}{h} \right)^2 - \frac{2}{3} \alpha \left( \frac{z}{h} \right)^3 \right] \quad (1.9)$$

where  $\alpha$  is a constant determined to be 3.34. This relationship is shown in Figure 1.1 as line C for the same conditions as line A. The resulting profile was tested in a surf zone

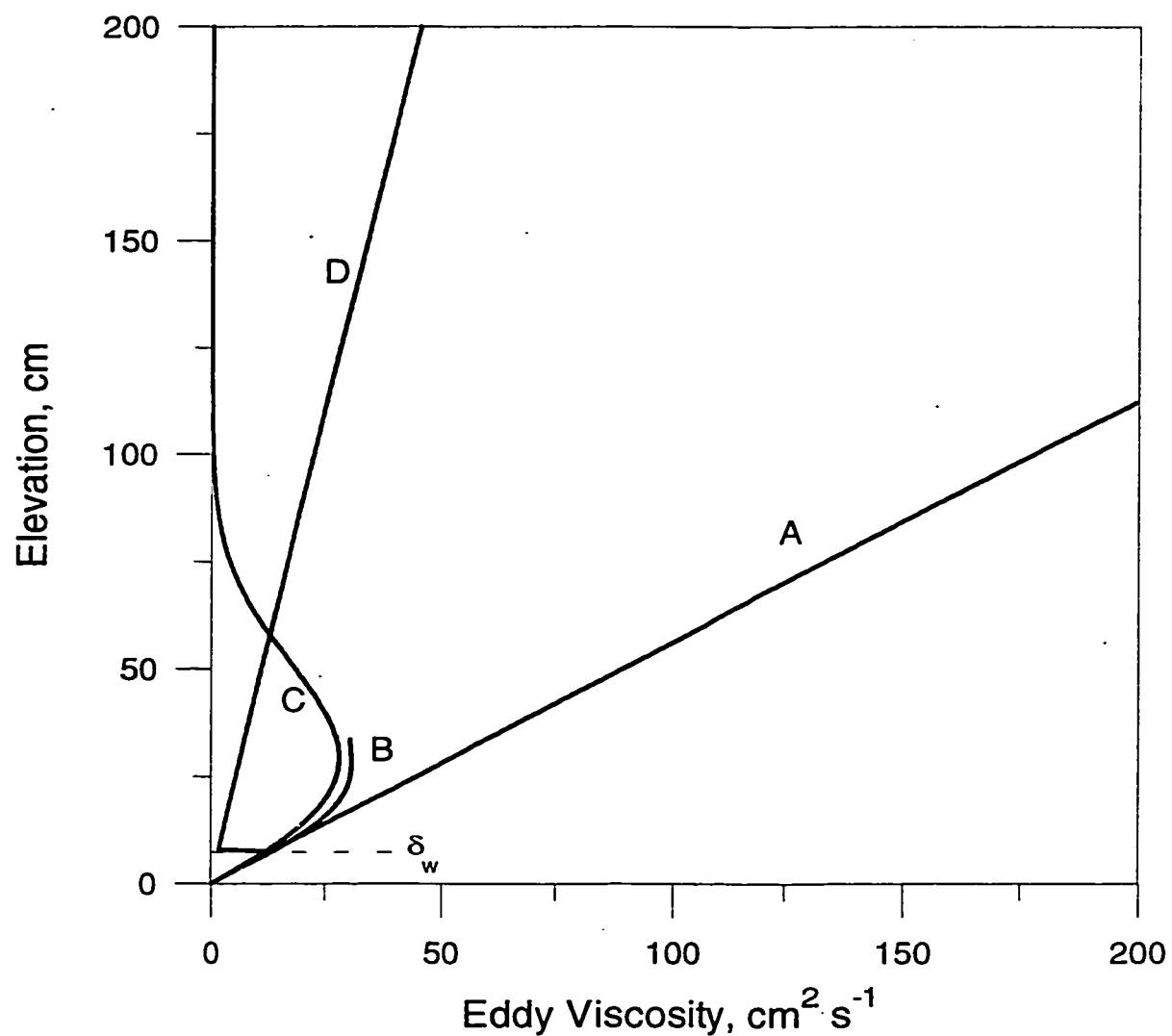


FIGURE 1.1. Eddy viscosity profiles used in modeling studies, where line A depicts a linearly increasing profile appropriate for the constant stress layer, but applied throughout the water column; line B, the profile of Smith and McLean (1977); line C, the profile of Nowell and Long (1983); and line D, the profile of Grant and Madsen (1986).

study (Beach and Sternberg, 1988) in which sediment eddy diffusivity values were computed from selected concentration profiles during relatively steady offshore flows associated with large infragravity oscillations. The Nowell and Long relationship was found to predict the data well.

Under interactions between waves and currents, Grant and Madsen (1986) used an eddy viscosity profile composed of two curves, one for the bottom wave boundary layer and one for the upper current boundary layer, i.e.,

$$K_m = \begin{cases} \kappa U_{*cw} z & z < \delta_{cw} \\ \kappa U_{*c} z & z > \delta_{cw} \end{cases} \quad (1.10)$$

where  $U_{*c}$  is the current friction velocity,  $U_{*cw}$  is the wave-current interaction friction velocity, and  $\delta_{cw}$  is the height of the wave-current boundary layer, and is shown in Figure 1.1, line D, for the same conditions as line A. A discontinuity results where the two curves meet at the top of the wave-current boundary layer.

Also, some recent studies have found a time-invariant eddy viscosity to be inadequate for prediction of third and higher harmonics of velocity and stress fields particularly in the case of steep waves (Trowbridge and Madsen, 1984; Lavelle and Mofjeld, 1983), which is the case under asymmetric surf zone waves. In this dissertation, the level of detail is such that it can be assumed that the processes suspending sediment are stationary on time scales of hours and therefore only the time-averaged case is investigated.

### 1.2.3 Vertical Wave Advective Flux

The vertical wave advective flux term is often omitted with the assumption of zero mean vertical velocity (e.g., Dyer, 1986). In a wave dominated environment, the potential exists for the vertical velocity and the suspended sediment concentration to be correlated, and therefore it is necessary to investigate the vertical wave advective flux term. Sheng and Hay (1986) found that under high energy unbroken waves, the vertical wave flux can be as large as 30 to 40 percent of the mean settling flux at 30 cmab. In the regions close

to the bed (where  $w_w$  approaches zero) the vertical wave flux was found to be small. This term will be addressed in more detail in Chapter 3.

### **1.3 Implications for the Surf Zone**

In the surf zone, breaking waves add a complicating aspect to the prediction of sediment concentration profiles. Wave breaking turbulence as well as bottom boundary layer turbulence must be considered when modeling suspended sediment profiles using an eddy diffusivity profile. Therefore, using such a profile applicable to the continental shelf (i.e., boundary shear only) may not be appropriate in surf zone conditions and may grossly affect modeled profiles of suspended sediment and sediment flux.

#### **1.3.1 Surf Zone Models**

Two models of surf zone processes provide an indication of the relative importance of wave breaking turbulence. Results from a surf zone fluids model by Johns (1983) are shown in Figure 1.2. As compared to the unbroken wave conditions where turbulent energy is restricted to the wave boundary layer (Fig. 1.2a), when wave breaking is added to the bottom boundary layer turbulence (Fig. 1.2b), high levels of turbulent energy are predicted throughout the water column. Deigaard et al. (1986) has developed a suspended sediment transport model in which surface generated turbulence is modeled in terms of the energy loss in a hydraulic jump and their results are compared to suspended sediment concentration measurements made by Nielson et al. (1982) in Figure 1.3. The solid line represents the results of their model with wave breaking included and the dashed line represents their model without wave breaking. In all cases, the inclusion of wave breaking turbulence in the model improves the comparison to Nielson's surf zone data (circles in Fig 1.3).

Although the models of Johns and Deigaard incorporated a one-equation turbulent kinetic energy closure scheme, modeling of sediment suspension in the surf zone can be accomplished by incorporating an appropriate eddy diffusivity closure scheme. In the model of Beach and Sternberg (1992), the eddy diffusivity profile did not reflect the added

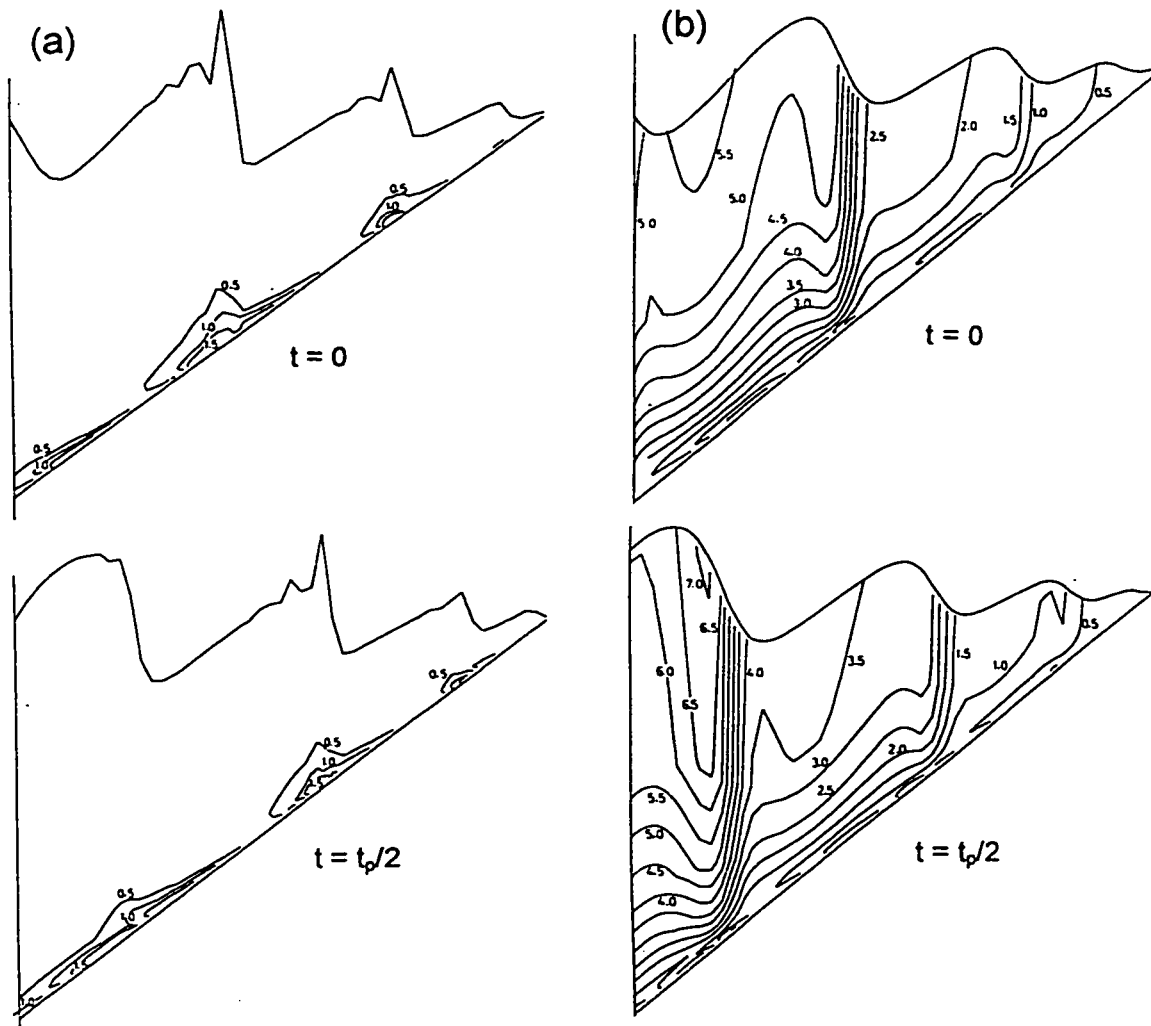


FIGURE 1.2. Numerical model results of Johns (1983) for the simulation of turbulent processes beneath broken waves in the surf zone, (a) without and (b) with the inclusion of horizontal production of turbulence from wave breaking. The contours are of scaled turbulent energy density.

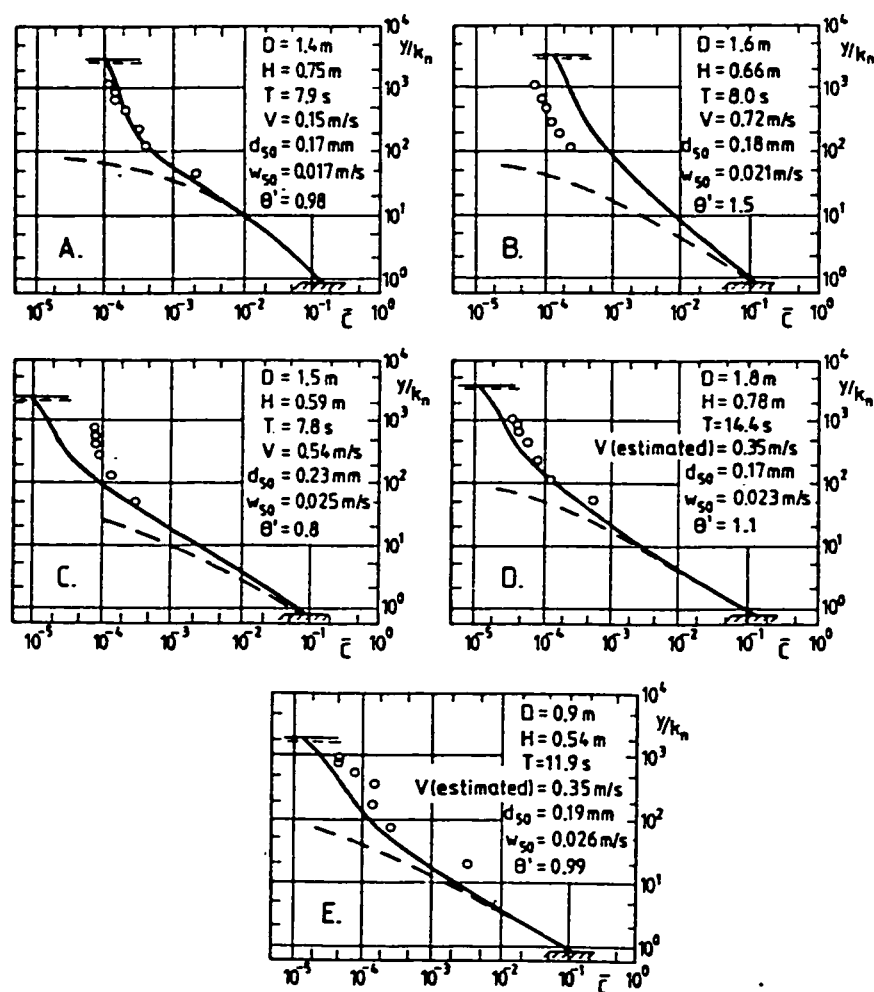


FIGURE 1.3. Numerical model results of Deigaard, et al. (1986) showing the comparison between measurements of Nielsen et al. (1982) and predicted suspended sediment concentration. The solid line is the model with wave breaking, the dashed line without wave breaking, and the circles are field measurements.



turbulence in the water column due to wave breaking. Their model of sediment suspension in the surf zone extended a wave current interaction model (Kachel and Smith, 1989) based only on bottom boundary layer processes. They found that infragravity processes could be modeled well, but that their model consistently underestimated the concentration of sediment above the bottom boundary layer.

### **1.3.2 Objectives**

The objectives of this dissertation are to use detailed suspended sediment and velocity field data to evaluate time averaged eddy diffusivity profiles used for surf zone modeling, and,

- to determine the effect of wave breaking on the form of the eddy diffusivity profile,
- to provide a rational eddy diffusivity formulation applicable for prediction of suspended sediment profiles in the surf zone,
- to examine the relationship between the eddy diffusivity for sediment and the eddy viscosity for momentum, and
- to use the formulated eddy diffusivity profile to evaluate the wave breaking impact on suspended sediment concentration profiles and sediment flux.

These goals are addressed using observations from two experiments, a prototype wave basin experiment (Asher et al., 1995) and the DUCK94 field experiment (Williams, 1995). The velocity fluctuation results from the wave basin experiment are presented in Chapter 2. These results are used to formulate an eddy diffusivity profile for the upper water column (above the wave bottom boundary layer) determined from turbulence intensity estimates under unbroken and broken waves. The wave basin experiment could not provide the bottom boundary layer information needed due to the smooth painted bottom of the basin and therefore these results are combined with field data to incorporate nearbed boundary layer characteristics. Chapter 3 presents the results from the DUCK94 field experiment from which the nearbed eddy diffusivity profile is determined from

sediment concentration profiles under real surf zone conditions. Chapter 4 looks in detail at the relationship between the eddy diffusivity for sediment and the eddy viscosity for momentum in order to formulate a method of predicting suspended sediment concentration profiles from information about the velocity field and seabed characteristics. The eddy diffusivity relationships from the two studies are combined in Chapter 5 and a mathematical formulation of the eddy diffusivity profile for both broken and unbroken waves is presented and included in a simple one-dimensional model of the vertical distribution of suspended sediments. Chapter 5 also uses the model to explore the influences of wave breaking on sediment concentration profiles and sediment flux profiles for a range of surf zone conditions found during the DUCK94 experiment. The work is summarized and conclusions are drawn in Chapter 6.

## **CHAPTER 2. ESTIMATION OF TURBULENCE INTENSITY AND EDDY VISCOSITY UNDER UNBROKEN AND BROKEN WAVES IN A WAVE BASIN**

### **2.1 Introduction**

Field studies of surf zone turbulence have been limited due to difficulties in instrumentation and in separating turbulence from mean flow and wave motions. A wave basin experiment provided the information necessary to examine the water column fluid eddy viscosity profile under prototype surf zone conditions. The 1993 Wave Basin Experiment (WABEX-93) was designed to provide a method of estimating air-sea gas transfer velocities from remote measurements of whitecap coverage. The velocity measurements made during this experiment were used to determine variance, turbulence dissipation rates, and turbulence intensity under broken and unbroken waves. Velocity results from the large scale laboratory experiment were used to parameterize an eddy viscosity profile under broken waves, and to explore the hypothesis that the turbulence created under broken waves could have a large effect of surf zone sediment transport. The wave basin study provided a means of systematic study of turbulent processes in the surf zone where the field conditions are often so complicated and chaotic that experimental methods fail.

### **2.2 Wave Basin Experiment Data Set**

Estimates of turbulence dissipation rates and intensity were made in the Hurricane Harbor surf pool at Wild Rivers Waterpark in Irvine, California. The wave basin is an unheated, freshwater recreational facility. The pool measures approximately 20 m wide by 70 m long, with a sloping bottom and depths that range from 0 to 2.4 m as drawn schematically in Figure 2.1. Overall, the experiment was designed to empirically define a method for estimating air-sea gas transfer velocities from remote measurements of fractional area whitecap coverage (Asher et al., 1995). One of the objectives of this experiment was to obtain velocity profiles and pressure measurements at multiple locations in the wave basin with resolution sufficient to estimate profiles of turbulence

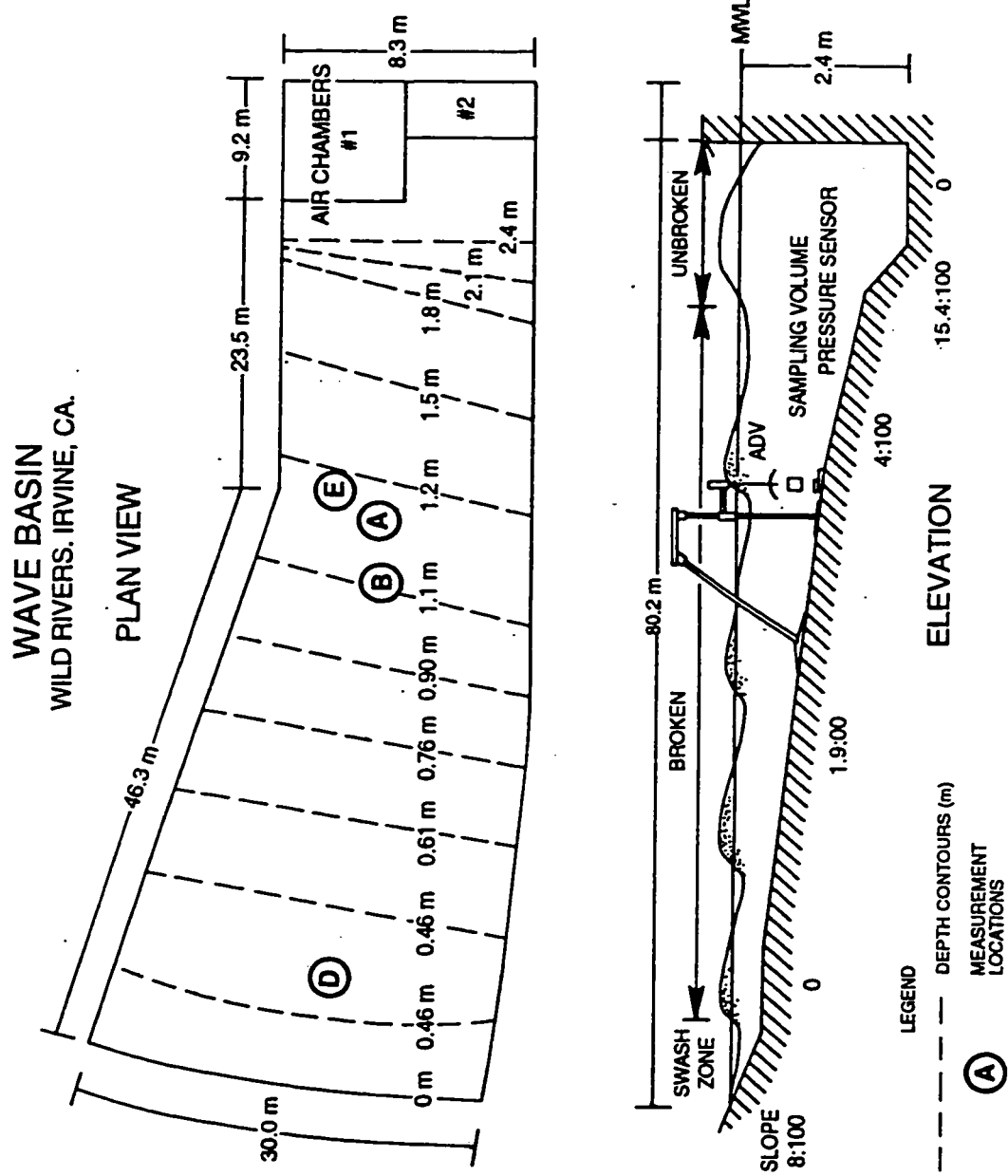


FIGURE 2.1. Schematic of the wave basin at Wild Rivers Waterpark in Irvine, California showing the five ADV measurement locations.

dissipation rate and relate those to the whitecap coverage and gas transfer due to breaking wave generated turbulence (Ogston et al., 1995). For the present study, the measurements provide a systematic approach to exploring turbulence intensity and eddy diffusion under broken and unbroken waves.

### **2.2.1 Instrumentation**

Turbulence dissipation rates were estimated from velocity measurements made with a SonTek acoustic-doppler velocimeter (ADV). The ADV measured three components of velocity in a  $0.5\text{-cm}^3$  sampling volume located 10 cm below the probe, minimizing the effect of the sensor on the flow field (Figure 2.2). Measurements were recorded at 25 Hz for runs lasting approximately 300 s (70-100 waves). Despite high concentrations of bubbles and intermittent immersion, the ADV provided high quality data for velocities approaching  $200\text{ cm s}^{-1}$ . There is no zero offset drift in the ADV velocity output; and therefore, maintenance calibration is not required unless the probe is physically damaged. A comparison of measurements between a laser doppler velocimeter and the ADV was found to have good agreement (Kraus et al., 1994) in both oscillatory and uniform flow.

In addition to the above, simultaneous measurements of pressure were made with a precision strain-gage located beneath the ADV, and video images of the water surface were recorded and later used to determine wave type and breaking location.

### **2.2.2 Experiment**

Waves were generated with four pneumatic chambers at the deep end of the wave basin. They were formed by cyclically varying air pressure in two partially filled chambers at the deep end of the pool, and then forcing water out through a grate connecting the chamber to the end of the pool. The waves which propagated and broke as they progressed across the artificial surf zone could be generated at four settings of the pneumatic chambers to heights up to 1.2 m with a fixed period of 4.2 s (see Asher et al., 1995, for details of the wave basin and wave generation). The spin-up time for the basin

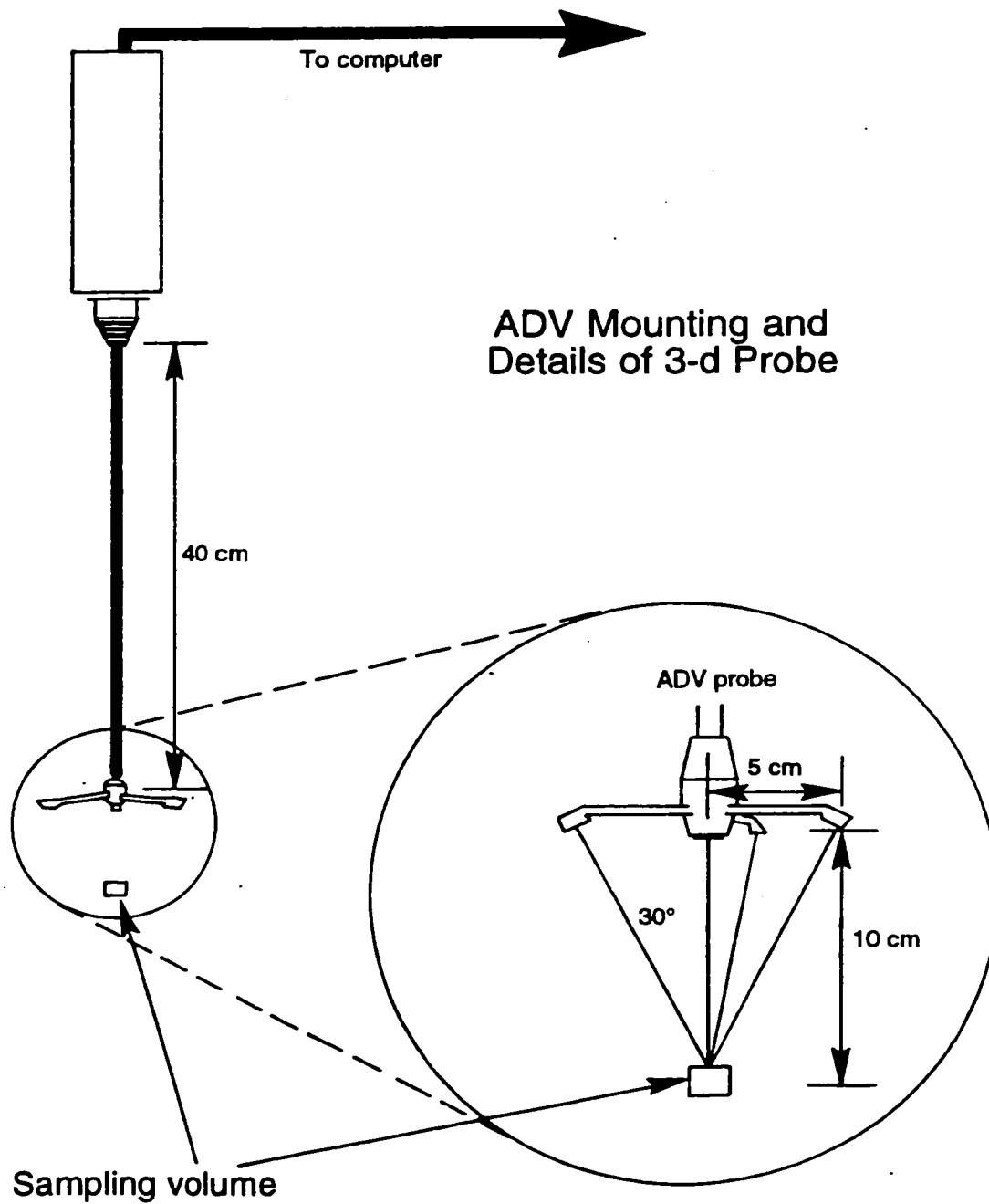


FIGURE 2.2. SonTek acoustic-doppler velocimeter (ADV). The ADV measured three components of velocity in a 0.5 cm<sup>3</sup> sampling volume located 10 cm below the probe.

Table 2.1 Summary of wave basin velocity and pressure measurements

Location	Energy Level	U (cm s <sup>-1</sup> )	Hs (cm)	h (cm)	U <sub>orb</sub> (cm s <sup>-1</sup> )
A	1	4.8	26	107	30.8
	2	3.0	45	107	47.6
	3	3.7	45	107	43.1
	4	5.3	45	107	38.4
B	1	1.6	26	87	31.8
	2	9.8	42	87	45.6
	3	34.4	27	87	45.9
	4	35.9	23	87	47.2
D	1	4.9	19	59	26.0
	2	17.7	18	59	30.5
	3	21.4	31	59	36.3
	4	8.4	23	59	30.6
E	1	4.6	26	104	34.2
	2	11.2	46	104	45.8
	3	8.7	44	104	53.5
	4	11.1	35	104	31.3

was only a few minutes, but some low-frequency fluctuations occurred. These were probably caused by seiching of the basin, periodic outbreaks of the rip currents, and timing variations in the air shunt valve.

Because the wave field was highly repeatable, profiles were made by compositing data from three to seven runs, each with the instrument mounted at the same horizontal location but at a different elevation. The profiles were obtained at two locations across the surf zone under unbroken and broken waves and at four energy levels by the wavemaker, with nominal unbroken wave heights of 0.3, 0.6, 0.9 and 1.2 m. The two ADV measurement locations are shown in Figure 2.1 (denoted A and B), as well as two locations where single point measurements were made (denoted D and E).

### 2.2.3 Data Set Summary

Data runs were typically 300 seconds in length, approximately 80 waves. A summary of the instrument locations within the tank is contained in Table 2.1. Velocity profiles for all four wave energies were measured at locations A and B. The profile at A is

composed of six vertical positions and the profile at B is composed of six or seven vertical positions, depending upon the wave magnitude. Single point measurements were made at locations D and E. At location D, which is the closest to the shoreline, measurements were made near the mid water column level. At E, the deepest location, the measurement was obtained closer to the water surface.

Mean horizontal currents at mid depth in the wave basin ranged from 1.6 to 36 cm s<sup>-1</sup>, with the variation due to the circulation patterns that would set up in the basin under specific conditions. For example, there was a strong mean current that set up at location B for the higher magnitude waves. The significant wave heights at the measurement locations ranged from 18 cm to 46 cm, with the largest wave heights not necessarily corresponding to the highest energy levels because of the change in break point location.

### **2.3 Data Analysis**

Flow beneath waves can be separated into three components: mean, periodic (wave), and fluctuating (turbulence) components. The objective of the data analysis was to quantify the turbulence component. Several approaches were considered. In laboratory studies with highly repeatable waves, all velocity deviations from the ensemble-mean wave velocity can be attributed to turbulence (Nadaoka et al., 1989). Although waves in the wave basin appeared quite regular, the detailed pressure measurements showed wave-to-wave variations in pressure. Irregularity in the wave field was most likely caused by the combined effect of variability in the wavemaker, seicheing of the basin, reflected waves, and episodic outbreaks of a rip current. Estimates of turbulence based on deviations from the ensemble-mean velocity were precluded because they would have overestimated turbulence by including nonturbulent, pressure-induced fluctuations. An alternative frequency-domain approach for extracting turbulent fluctuations from velocity records involves identifying that portion of the velocity record that is coherent with the pressure record (Kitaigorodskii et al., 1983; Agrawal and Aubrey, 1992). By assuming that pressure-coherent velocity fluctuations are caused by two-dimensional progressive



waves, noncoherent velocity fluctuations can be attributed to turbulence. However, this technique is prone to error if waves have directional spread (Herbers and Guza, 1993). Instead, the inertial dissipation method of George et al. (1994) was used, and modified to take advantage of the nearly regular wave field and the measurement capabilities of the ADV.

### **2.3.1 Data Processing**

One advantage of the ADV was its ability to rapidly re-establish good velocity measurements after the loss of acoustic signals in bubble plumes or during subaerial exposure in the trough of a wave. Initial processing identified and rejected data from times when the ADV was exposed or large amounts of bubbles were present. A preliminary criterion for rejection was based on the correlation coefficient between the transmitted acoustic signal and the received backscattered signal. Data-rejection rates increased from near zero at depth to as much as 37 percent near the surface under larger waves. Acceptable data for 70 to 100 successive waves were phase aligned using the peak in the cross covariance of the slope of the pressure signal. The ensemble mean and standard deviation for pressure and the three velocity components were then estimated (Figure 2.3). An iterative check on data was then performed: data were rejected if the velocity magnitude exceeded 3.7 standard deviations about the ensemble mean at each phase in the wave, and ensemble statistics were recalculated. Finally, mean and root-mean-square (RMS) velocities were determined for acceptable data from each data run.

### **2.3.2 Estimates of Dissipation Rates and Turbulence Intensity**

The existence of energy transfer from large eddies to small eddies is driven by vortex stretching and leads to viscous dissipation of energy near the Kolmogorov microscale. A turbulent flow field can be imagined as divided into all eddies smaller than a given size and all eddies larger than that size. The smaller eddies are exposed to the strain-rate field of the larger eddies. Because of the straining, the vorticity of the smaller eddies increases, with a consequent increase in their energies at the expense of the energy

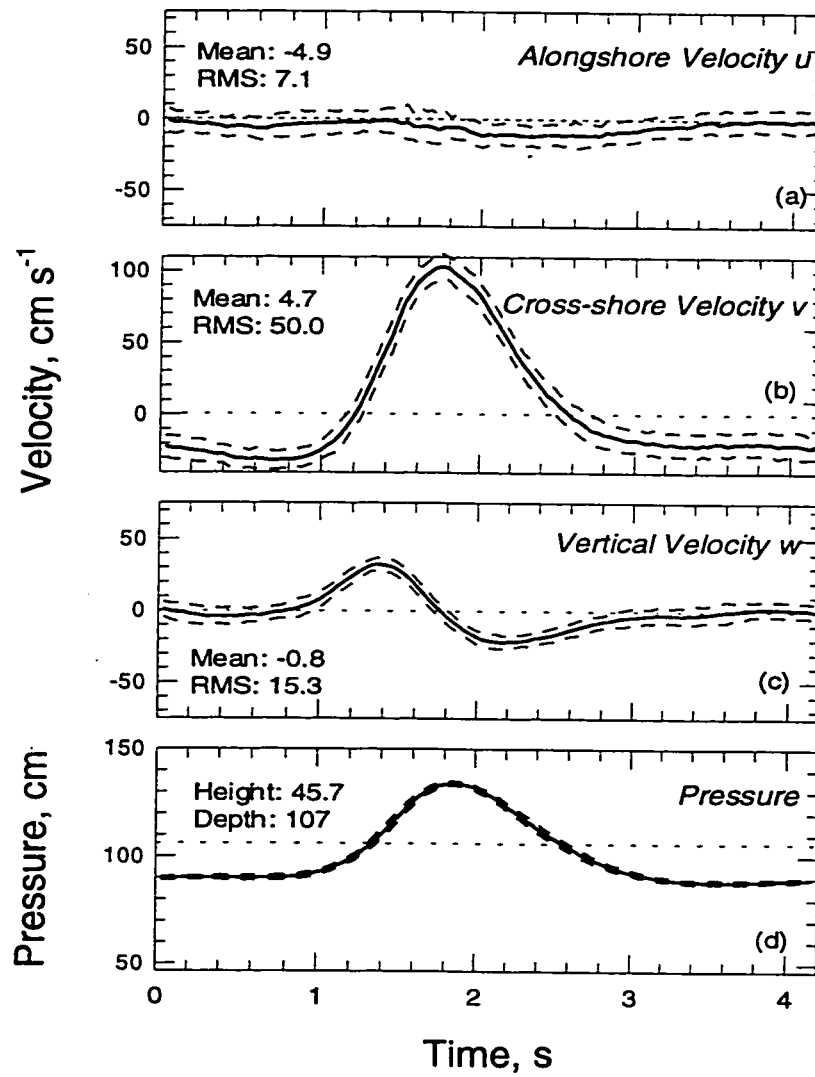


FIGURE 2.3. Ensemble-average velocities and pressure under broken wave of nominal height 0.9 m at location A, 53 cmab: a) Alongshore velocity. b) Cross-shore velocity. c) Vertical velocity. d) Pressure.

of the larger eddies. In this way there is a flux of energy from larger to smaller eddies which is finally dissipated by viscosity.

In steady flow with isotropic, fully-developed turbulence, the turbulence dissipation rate can be estimated by the magnitude of the wavenumber spectra in the inertial subrange, which takes the form:

$$E(\kappa) = \alpha \varepsilon^{2/3} \kappa^{-5/3} \quad (2.2)$$

where  $\kappa$  is wavenumber,  $E(\kappa)$  is the scalar wavenumber spectral density,  $\varepsilon$  is the turbulence dissipation rate, and  $\alpha$  is the Kolmogorov constant. The inertial subrange extends from large eddies, the scale of which is typically determined by physical dimensions of the flow (e.g., depth), to the Kolmogorov microscale, which is determined by kinematic viscosity and dissipation rate.

In the inertial subrange, the turbulence intensity can be estimated from the definition of the spectra,

$$w' = \left( \int F_{22}(\kappa) d\kappa \right)^{1/2} \quad (2.3)$$

where  $F_{22}(\kappa)$  is defined as the one dimensional spectra for variance parallel to the direction of advection of turbulence,

$$F_{22}(\kappa) = \frac{3}{4} \alpha \varepsilon^{2/3} \kappa^{-5/3} \quad (2.4)$$

(Gross et al., 1994) which upon solving for the dissipation rate and integration leads to,

$$\varepsilon = \left( \frac{4}{3\alpha} F_{22}(\kappa) \right)^{3/2} \kappa^{5/2} \quad (2.5)$$

and,

$$w' = \left( \frac{8}{3} \alpha \right)^{1/2} (\varepsilon / \kappa_o)^{1/3} \quad (2.6)$$

where  $\kappa_o$  is a wavenumber scale of turbulent eddies and  $\alpha$  has been found through laboratory and field experiments to be 0.5 (Wyngaard & Cote, 1972).

Estimates of dissipation rate were made for the wave basin data using Eq. 2.5 and the assumption that the turbulence was fully developed and isotropic. The vertical component of the ADV velocity signal was used to calculate dissipation rates because it had the highest signal-to-noise ratio of the three components. Spectral estimates were obtained using a windowing and ensemble-averaging (Welch) method. Because data were removed during initial processing, the spectra for each windowed time series was computed using a method appropriate for irregularly spaced data (Press et al., 1992). Entire data windows were omitted if more than 50 percent of the data points were missing. Spectral estimates were obtained by first detrending the data by subtracting out the ensemble-mean periodic (wave) velocity component, then computing spectra on a windowed data segment extending over three successive waves, and finally ensemble-averaging the spectra. Windowed segments were overlapped 67 percent. This yielded spectral estimates with resolved bandwidth of 0.16 Hz and 156 degrees of freedom for typical time series containing 80 waves.

The time-series data at a fixed point were used to estimate the energy density spectrum as a function of frequency, not wavenumber. The frequency spectra were converted to wavenumber spectra using Taylor's hypothesis of frozen turbulence, which assumes that the time scale of turbulent fluctuations is long compared with the time scale of the motion advecting the eddy past the sampling point. The RMS orbital velocity was used as the advective velocity for the conversion from measured frequency spectra to wavenumber spectra (Agrawal et al., 1992). An example of the wavenumber spectra generated from the vertical velocity data is shown in Figure 2.4.

Turbulence dissipation rates were estimated from the magnitude of the wavenumber spectra in the inertial subrange using Eq. 2.5. For each data run, the wavenumber spectra were individually inspected, and the magnitude of the spectra range over which the theoretical  $-5/3$  slope was found was used to estimate the dissipation rate (typically between radian wavenumbers of 0.3 and 1.5  $\text{cm}^{-1}$ ).

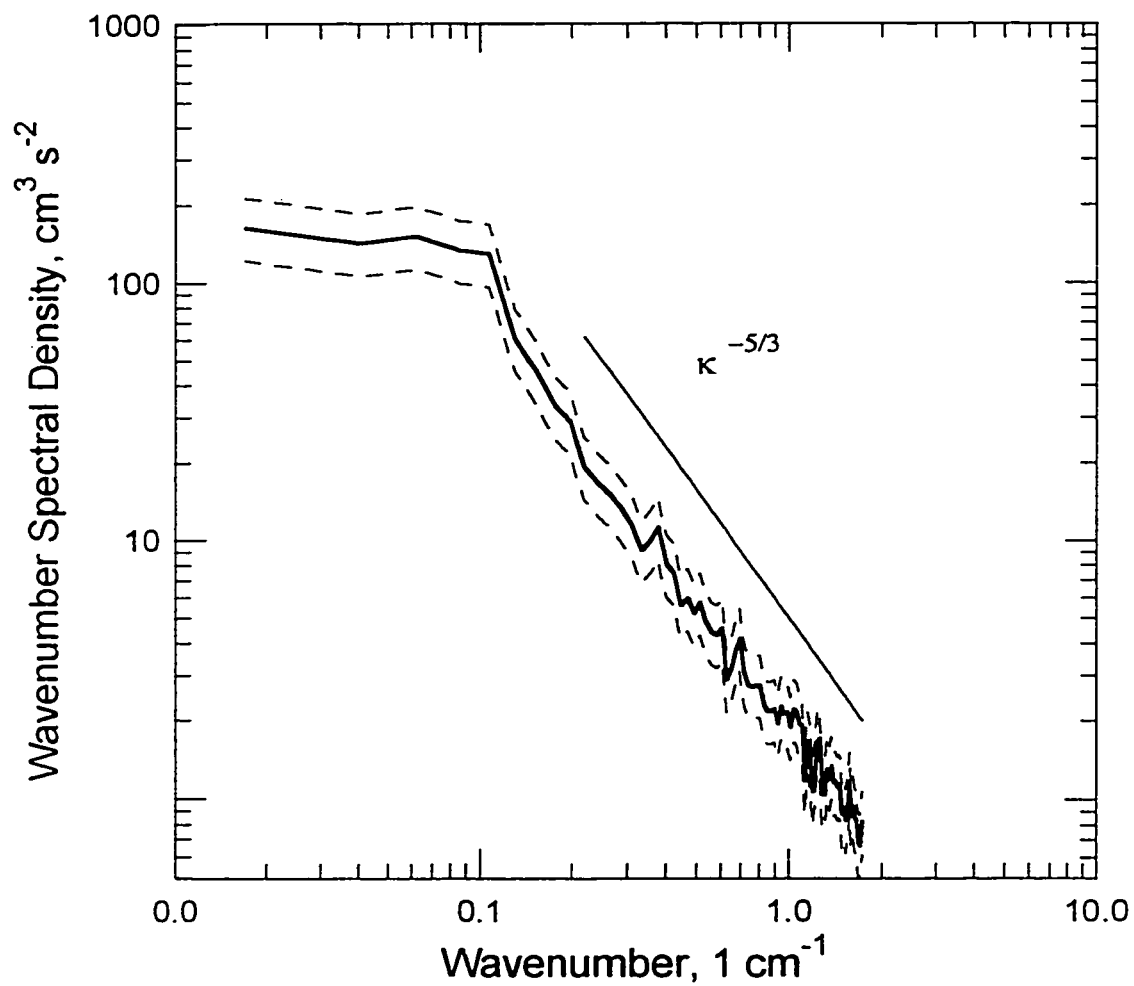


FIGURE 2.4. Representative wavenumber spectrum of vertical velocity showing inertial subrange ( $\kappa^{-5/3}$  slope) under broken wave of nominal height 0.9 m at location A, 53 cmab.

Turbulence intensities in the vertical axis were estimated using Eq. 2.6 and the estimated turbulence dissipation rates. The wavenumber scale at which most of the turbulent kinetic energy is contained for this study of breaking waves was defined at  $\kappa_0$  equal to  $0.3 \text{ cm}^{-1}$ , which corresponds to the smallest radian wavenumbers at which the inertial subrange (-5/3 slope) exists in this data.

### 2.3.3 Estimates of Eddy Viscosity

The eddy viscosity of a fluid,  $K_m$ , can be related to the turbulent kinetic energy through the Kolmogorov-Prandtl expression,

$$K_m = l\sqrt{TKE} \quad (2.7)$$

where  $l$  is the length scale of turbulent eddies, a measure of the size of those with the most kinetic energy, and  $TKE$  is the turbulent kinetic energy. The term  $\sqrt{TKE}$  is the conceptual velocity scale, which is a measure of the velocities in the eddies with the most kinetic energy. The  $TKE$  is defined by,

$$TKE = \frac{1}{2}(u'^2 + v'^2 + w'^2) \quad (2.8)$$

in which  $u'$ ,  $v'$ , and  $w'$  are the turbulence intensities in the  $x$ ,  $y$ , and  $z$  direction.

Profiles of the eddy viscosity were made for the wave basin data using Eq. 2.7, and the following assumptions. Since the turbulence intensity could only be estimated for the vertical direction ( $w'$ ) due to instrument limitations, the relationship between the three components of the  $TKE$  must be assumed. Svendsen (1987) suggests the flow generated by breaking waves might have turbulence structure similar to mixing layers of plane wakes, concluding that the contribution of  $w'^2$  to the total turbulent kinetic energy can be estimated as approximately one third. The  $TKE$  is then estimated as,

$$TKE = \frac{3}{2}(w'^2) \quad (2.9)$$

It is necessary to prescribe the variation of the length scale throughout the water column. Near the bed, the length scale of the turbulence is limited due to the proximity of

the bed. In this region, a linear variation with distance above bed has been found both in experiments (Pedersen, et al., 1993) and modeling of bottom boundary layers (Johns, 1983). In this study, the length scale is defined to be equal to the distance above the bed up to a maximum value determined in the upper water column.

In the upper part of the water column the presence of the bed has a limited impact on the turbulence. The conditions are similar to those of free turbulence and the length scale therefore is taken to be a constant. Although other studies have found the length scale proportional to the water depth ( $l = 0.2 - 0.3 h$ ; Svendsen, 1987), the length scale must be proportional to the size of the breaking waves that are generating the turbulence in the upper water column. Since the wave height to water depth is relatively constant in the surf zone, prescribing the length scale either by relationship to the water depth or to the breaking wave height yields a similar result. For this study, the length scale is defined by the wave height ( $l = 0.25 H_s$ ). This corresponds to the length scale defined through analysis of measurements in jets and shear layers ( $l = 0.1 h$ ; Svendsen, 1987), and a wave height to water depth ratio of 0.4.

## 2.4 Results

The conditions at each measurement location and wave generator setting are summarized in Table 2.1. Video of the wave basin during the experiment was used to determine whether waves were broken or unbroken at the measurement location. For the profiles at locations A, B, and the single point at location E, the waves were unbroken for the first, and broken for the second through fourth energy levels. At the single point location D, the waves were unbroken for the first and second, and broken for the third and fourth energy levels.

### 2.4.1 Turbulence Dissipation and Intensity Results

Profiles of  $w'$  beneath broken and unbroken waves are shown in Figures 2.5a and 2.5b at the two profile locations in the wave basin. Elevation is normalized by the water depth, so that a normalized elevation of 1.0 is at the mean water surface. Under unbroken

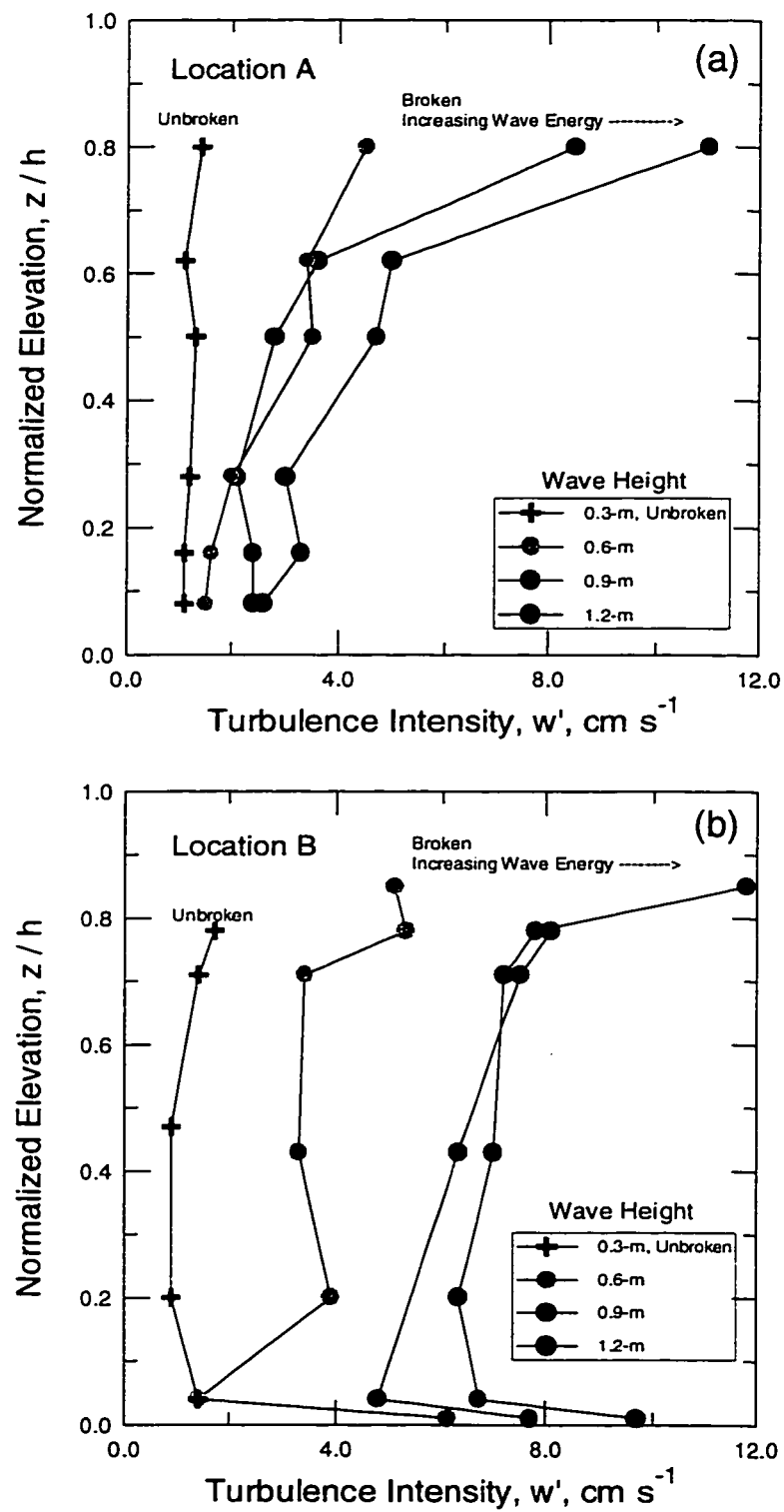


FIGURE 2.5. Vertical profiles of turbulence intensity,  $w'$ , beneath unbroken (crosses) and broken (circles) waves at a) location A and, b) location B.



waves,  $w'$  profiles were generally low in magnitude and vertically uniform. Beneath broken waves measured at location A (Figure 2.5a),  $w'$  was highest near the surface and increased with increasing wave height. Turbulence intensities throughout the water column were also seen to follow this pattern.

Profiles of  $w'$  at location B (Figure 2.5b) are similar to profiles at location A (Figure 2.5a), although the mid water column  $w'$  are higher at B, and there is at B little difference in  $w'$  between the 0.9-m and 1.2-m wave conditions. Strong rip currents at B (see Table 2.1) could be responsible for the shear in the mid water column resulting in increased  $w'$  for the mid water column compared with A. Alternatively, the increased distance from breaking (cross-shore location) at B could have allowed homogenization of turbulence through the water column. Similar values of  $w'$  for wave heights of 0.9 m and 1.2 m could indicate a saturation value for  $w'$  at some distance from the break point. At location B, velocity measurements were made very close to the pool bottom, and observed increases in  $w'$  at less than 1 cmab are likely associated with shear induced turbulence in the wall boundary layer (Figure 2.5b).

#### 2.4.2 Comparison to Others' Work

Very few studies have explored the diffusion of sediment with an emphasis on turbulence due to both wave breaking and bottom friction in the surf zone. Studies in the nearshore, but seaward of the surf zone, have typically used acoustic instrumentation (Sheng and Hay, 1995; Lee and Hanes, 1995). Acoustic measurements are not possible within the surf zone due to interference from high suspended sediment concentrations and bubbles. Turbulence intensity results from the wave basin analysis were compared to field measurements of both George et al. (1994) and Foster (1996) who used hot film anemometers inside the surf zone. A comparison to George is shown in Figure 2.6 where the fluctuating velocity component is Froude scaled (normalized by  $(gh)^{1/2}$ ). For this comparison, it is assumed that turbulence is isotropic, so that the  $u'$  in George and the  $w'$  in the present study should be of equal magnitude. In Figure 2.6a, all of the wave basin

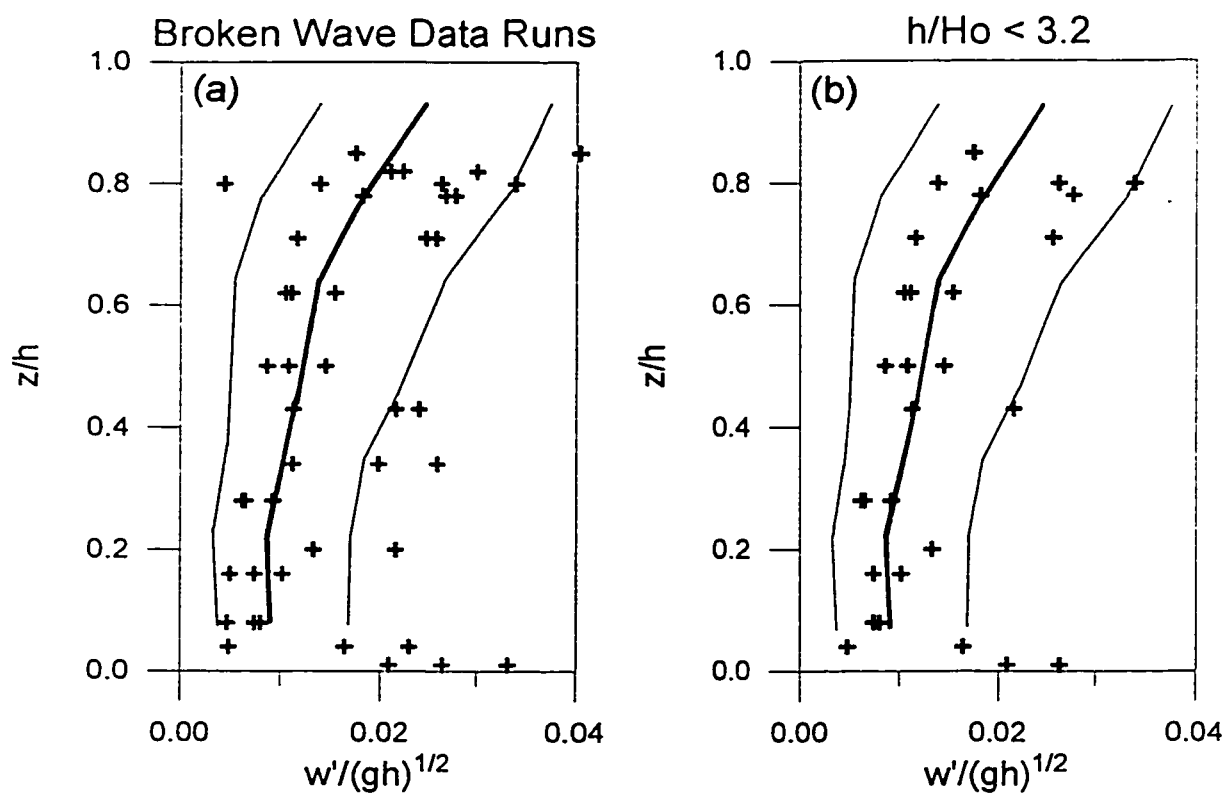


FIGURE 2.6. Vertical profiles of turbulence intensity,  $w'$ , where  $w'$  is normalized by  $(gh)^{1/2}$  for a) all broken wave data points and, b) data points where  $h/H_o < 3.2$ . The bold line connects mean  $u'$  values of George et al.(1993) in seven vertical bins and the lighter lines indicated  $\pm 1$  standard deviation.

data under broken waves is shown with symbols, and the uncertainty bounds of the George et al. (1994) measurements are shown in solid lines. The trend in the data appears similar to George's but there are many points that fall outside his uncertainty bounds. When limited to runs where  $h/H < 3.2$  (Figure 2.6b) as in George et al. (1994), the wave basin data fall well within the boundary of uncertainty in George's data.

In Foster (1996) measurements were made in the bottom boundary layer on a nearshore bar crest under a mix of broken and unbroken waves. The results were reported within wave phase divisions and can not be directly compared to time averaged values of the present study. Foster found that turbulence intensities,  $u'$ , ranging between 0 to 15 cm s<sup>-1</sup> in the bottom 15 cm of the water column, were highly intermittent and a function of wave phase. Time averaged turbulence intensities in the bottom 15 cm in the present wave basin study were found to range from 1 to 8 cm s<sup>-1</sup> and were found to be a function of wave height and cross shore location.

### 2.4.3 Water Column Eddy Viscosity Results

Profiles of eddy viscosity values beneath unbroken and broken waves at locations A and B are shown in Figures 2.7a and b, respectively, where the elevation is normalized by that water depth. At both locations it can be seen that beneath unbroken waves (cross symbols in Fig. 2.7a and b), the eddy viscosity is low and vertically uniform throughout the water column. Under broken waves, not only is eddy viscosity observed to be high very near the water surface as expected (due to the mixing induced by the breaking of waves), but is also significantly higher throughout the water column than for unbroken waves.

Differences between eddy viscosity estimates in the mid water column are apparent between the two locations. At location A (Fig. 2.7a), the magnitude of the eddy viscosity appears to be a function of the unbroken wave height, whereas at location B (Fig. 2.7b), this relationship is less clear. A possible explanation for this difference is distance from the breakpoint between the two locations. Location A is closer to the breakpoint, and

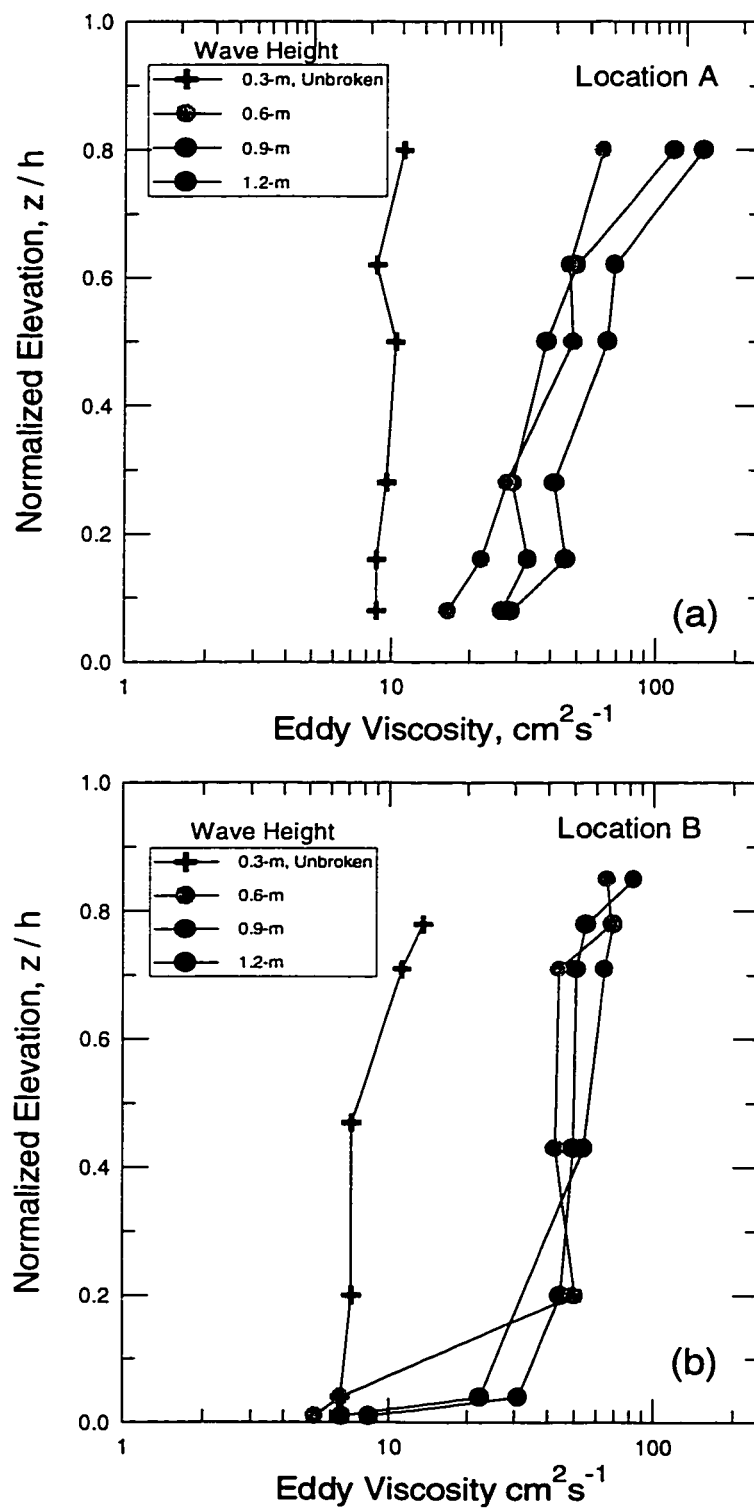


FIGURE 2.7. Vertical profiles of eddy viscosity,  $K$ , beneath unbroken (crosses) and broken (circles) waves at a) location A and, b) location B.

perhaps the high levels of mixing do not have time to diffuse as deeply into the water column as at location B which is farther from the breakpoint.

At location B an increase in the turbulence intensities very near the bed was seen (see Fig. 2.5b) due to the ADV being deployed at an elevation of less than 1.0 cm from the pool bottom. This increase is not seen in the eddy viscosity near the bottom which reflects the limitations that the length scale prescription has on the diffusion processes very close to the bed.

## **2.5 Discussion**

The turbulence intensity results show that wave breaking in the surf zone not only causes increased levels of turbulence near the water surface, but also causes increased levels of turbulence throughout the water column. The eddy viscosity profiles suggest that wave breaking can affect mixing and diffusion in the entire water column. Because the diffusion of sediment can be related to the eddy diffusion of momentum ( $K_s = \beta K_m$ ), this implies that suspended sediment profiles would look different between broken and unbroken wave conditions. The wave basin had painted surfaces and did not have sediment on the bed in order to test this concept. To apply the information gained in the wave basin to field conditions, it is important to scale the results.

### **2.5.1 Wave Height Scaling**

Turbulence intensities were found to increase with increasing wave height for the broken waves and found to decay exponentially into the water column. It is hypothesized that the level of turbulence in the water column under broken waves will be a function of the wave height and the depth below the water surface. When the vertical axis is scaled by these parameters, the eddy viscosity values separate into the unbroken and broken wave groups as seen in Figure 2.8. The broken wave data appear to fall in a slightly S-shaped pattern. There is more spread in the data close to the water surface where the larger waves appear to cause significantly larger eddy viscosity values and also deep into the

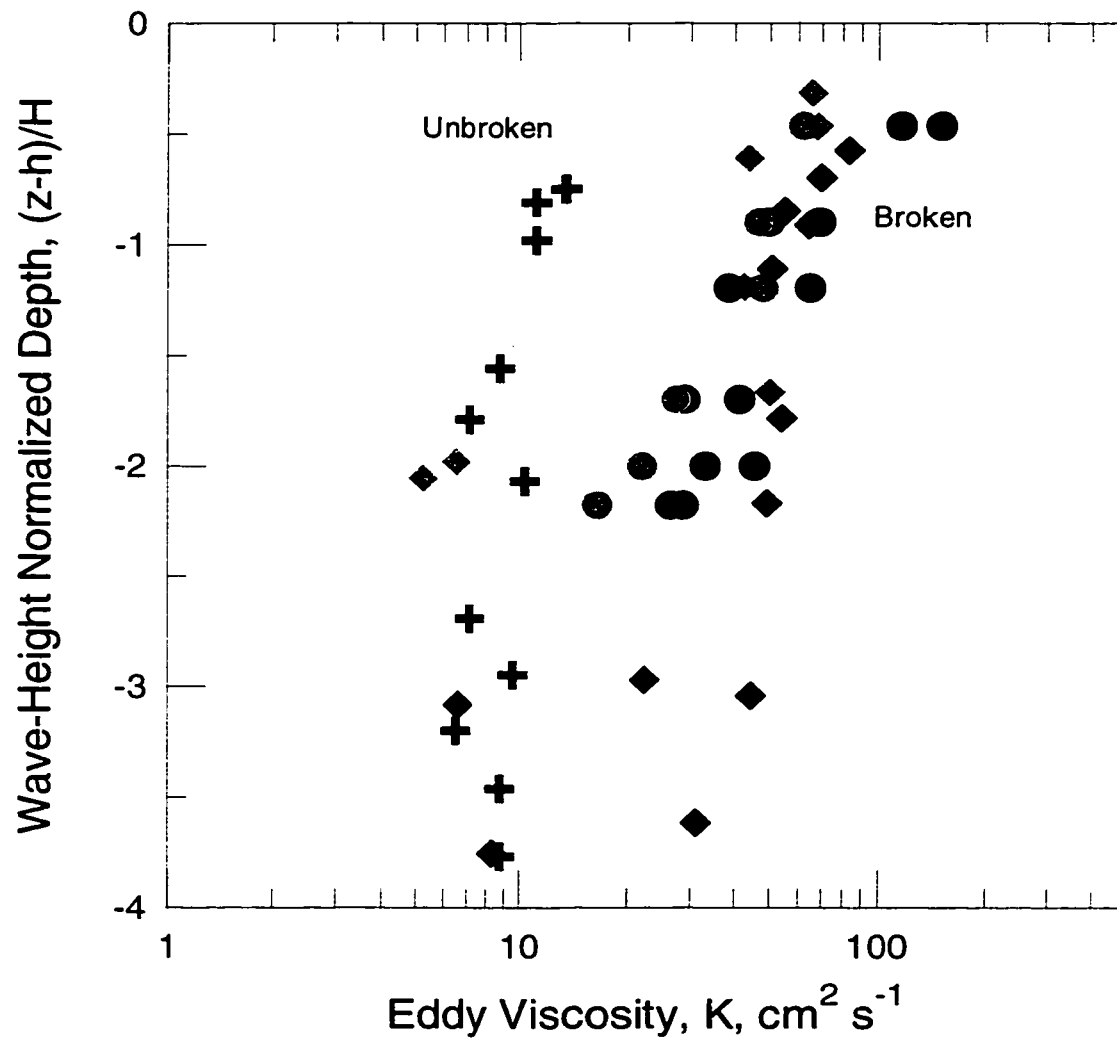


FIGURE 2.8. Eddy viscosity values from both locations A and B under unbroken (crosses) and broken (circles) waves where the depth below the water surface is normalized by the wave height.

water column where the distance from the breakpoint may influence the depth to which the breaking generated turbulence is felt.

The broken wave estimates measured very near the bed are influenced by bottom boundary layer processes and tend to fall outside the broken wave group, closer to the unbroken wave data (the four diamond symbols in alignment with the the cross symbols). This is consistent with the assumption that the turbulent length scales are limited by the proximity to the bed.

## **CHAPTER 3. NEARBED SEDIMENT EDDY DIFFUSIVITY PROFILES FROM DUCK94 FIELD DATA**

### **3.1 Introduction**

Turbulent diffusion of sediment in the surf zone can be attributed to two processes: bottom friction and wave breaking. In the previous chapter the eddy diffusivity profile in the upper water column due to wave breaking was examined. In this chapter the eddy diffusivity for sediment near the bed is explored, and estimates for nearbed friction velocity are made using the assumption that the diffusion is controlled by boundary shear generated turbulence. Detailed measurements of suspended sediment concentration are used to examine the eddy diffusivity near the bed under both unbroken and broken waves, and the results are compared to other studies done both in and outside the surf zone. The objectives of this chapter are:

- to determine the form of the nearbed eddy diffusivity profile for sediment under unbroken and broken waves, and
- to develop a nearbed eddy diffusivity formulation applicable for surf zone prediction of suspended sediment profiles.

### **3.2 DUCK94 Data Set**

Field measurements of suspended sediment concentration and fluid velocity were made during the months of August and October, 1994, at the U.S. Army Corps of Engineers Field Research Facility at Duck, North Carolina, as part of a large multi-investigator experiment (DUCK94). Instrumentation was developed prior to this experiment at the University of Washington, and was specifically designed for nearshore experiments investigating sediment dynamics in the surf zone. General design considerations required the instruments be small and relatively non-intrusive to the flow, and rugged enough to withstand harsh surf zone conditions. Both current meters and fiber optic suspended sediment sensors were developed specifically for the DUCK94 field experiment.



### 3.2.1 Instrumentation

#### *VEMA*

Electromagnetic current meters (EMCM) have been used successfully in the surf zone due to their small size and lack of moving parts (typically 4 cm diameter Marsh McBirney EMCM). Unfortunately, they can not be used close to the bed (15 cmab recommended) or close to each other (~50 cm between sensors) due to deformation of the magnetic field. In order to overcome these two problems, current meters were developed with a smaller electromagnetic field allowing multiple sensors to be arranged vertically for nearbed use. The Vertical ElectroMagnetic current meter Array (VEMA) consists of four sensors in a vertical array and is designed to be deployed as close as 6 cm from the bed for the bottom sensor and up to 50 cm from the bed for the top sensor (see sketch in Figure 3.1). The current meters were sampled at up to 16 Hz, but internal filtration required block averaging to 2 Hz for this analysis.

The VEMAs were calibrated in a tow tank to determine the linear instrument gains. Offsets were determined in the field when possible by deploying the current meters with the U.S. Army Corps of Engineers Field Research Facility pier crane immediately following the August experiment during relatively calm conditions. The current meters were deployed for 34 minutes, then rotated 180 degrees and re-deployed for another 34 minutes. Significant offset drift was observed in at least two sensors during the course of the experiment, and data from those sensors was not used in this analysis.

#### *FOBS*

Optical Backscatterance Sensors (OBS<sup>TM</sup>, D & A Instruments) have been used extensively in the surf zone with good success (e.g., Downing, 1983; Beach & Sternberg, 1988). They are small, rugged, and appear to calibrate linearly with sand concentration. The need to measure suspended sediment concentrations very near the bed and to determine the bed location relative to sensors initiated the development of the Fiber Optic Backscatterance Sensors (FOBS, Beach et al., 1992). The present instrument consists of 19 fiber optic sensors in a vertical array spanning 50 cm as shown in Figure 3.1. The

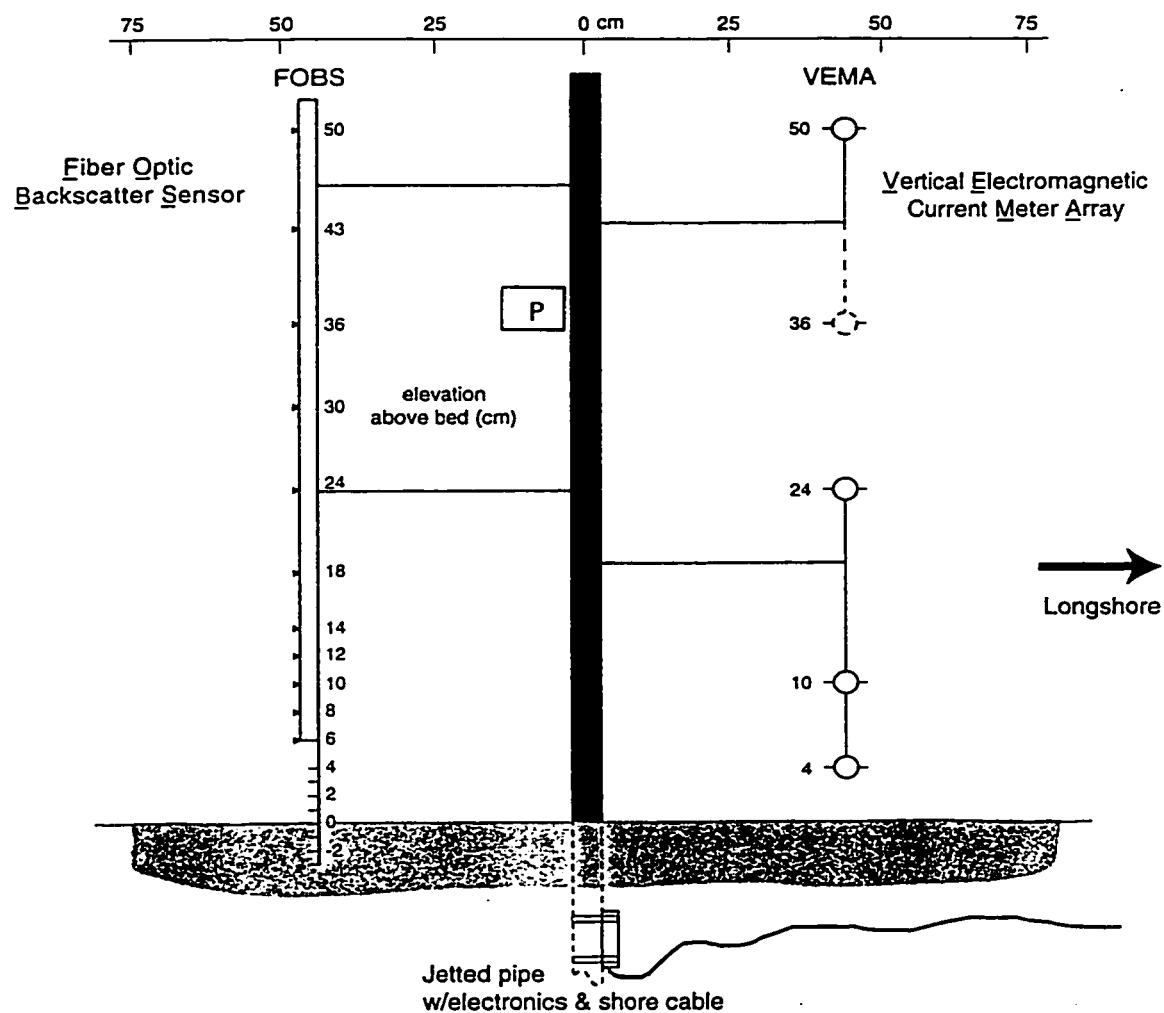


FIGURE 3.1. Instrument array deployed in DUCK94 (Duck, NC) consisting of FOBS, VEMA, and a pressure sensor.

bottom 8 sensors are positioned one cm apart in a slim probe designed to penetrate the seabed. The bed elevation can then be determined at a 1 cm accuracy by identifying sensors that are covered with sediment. The suspended sediment concentration profile can be determined between elevations of less than a cm above the bed to approximately 50 cm above the bed.

Calibrations of the FOBS were carried out prior to and immediately following the field experiments. A re-circulating tank was used with bed sediment collected in situ (Downing and Beach, 1989). The FOBS do not typically display a linear calibration as do OBS in sands, but the response seems to be adequately modeled with a third order polynomial fit (Figure 3.2). The FOBS sensors respond well in the range of concentrations between 0.1 and 100 g l<sup>-1</sup>, but above approximately 100 g l<sup>-1</sup>, the instrument response decreases with increasing concentration. This effect is also seen with the OBS in very high concentrations of fine sediments (Kineke and Sternberg, 1992). The individual sensor calibrations changed very little between the pre and post experiment calibrations for undamaged sensors.

### **3.2.2 Field Experiment**

DUCK94 was designed to be a coordinated study of nearshore processes during periods of calm and storm conditions. Multiple instrumented arrays were deployed during the months of August and October of 1994. The University of Washington and Oregon State University joint experiment consisted of two VEMA / FOBS arrays (Fig. 3.1) and a single electromagnetic current meter / FOBS array. The three arrays were deployed across the inner surf zone and trough, and at times on the nearshore bar (at locations marked A, B and C in Fig. 3.3). FOBS/VEMA arrays were deployed at Locations B and C in October (approximately 90 m and 107 m from 0 NGVD mean water level), and the single electromagnetic current meter and FOBS were deployed at Location A (70 m from shore). The average tidal range during the experiment period was 0.9 m. Data were collected for a total of 32 days during the two month-long experiments at a sampling rate of 8 or 16 Hz in August or October, respectively, for approximately 22 hours per day.

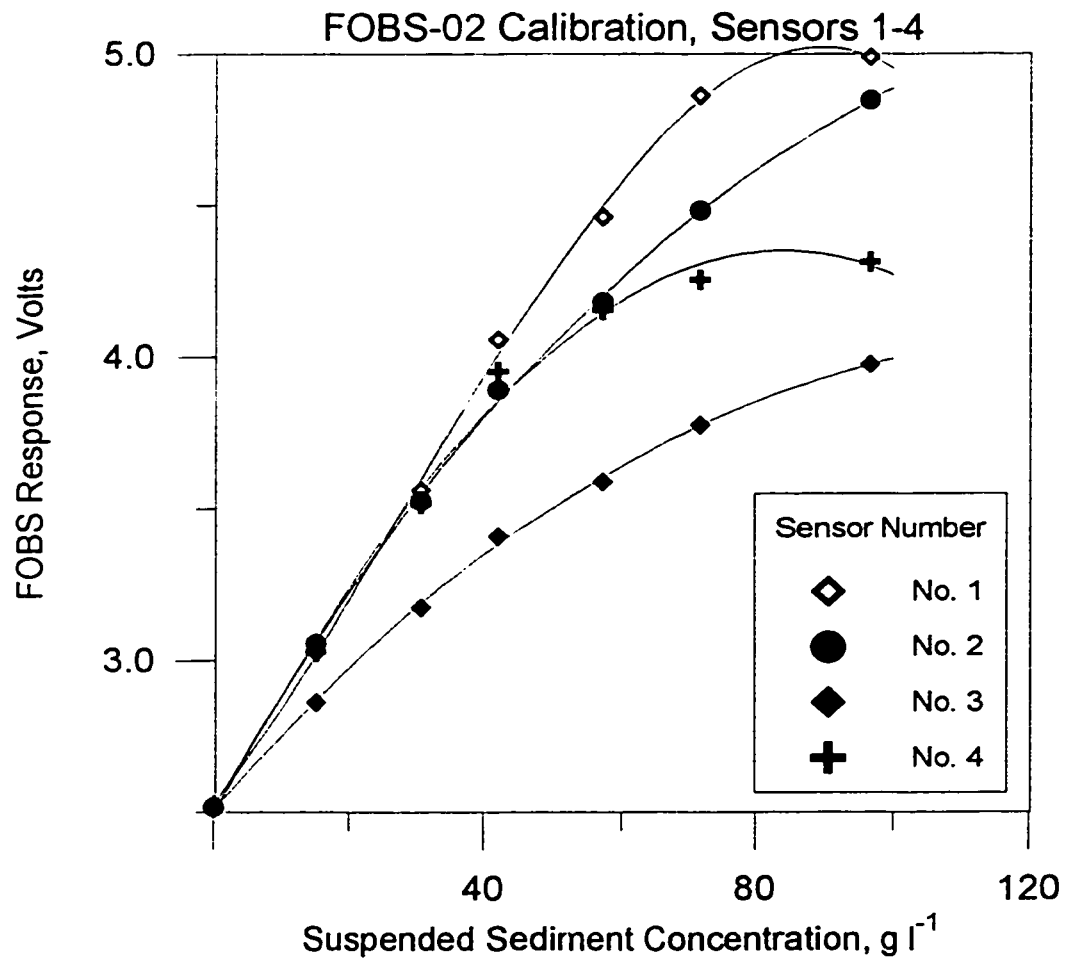


FIGURE 3.2. Example FOBS calibration curves for four individual sensors using insitu sediment samples from DUCK94.

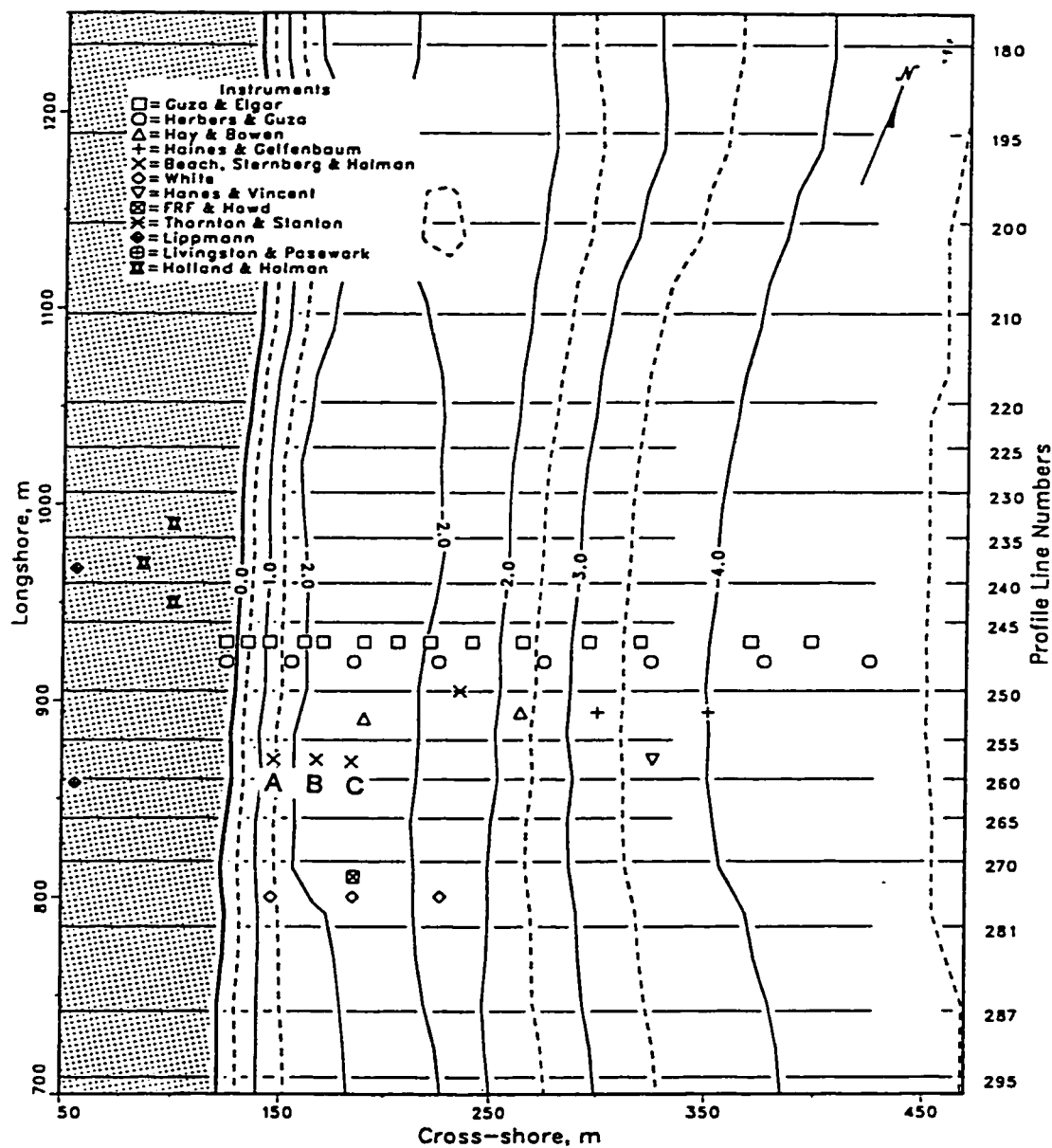


FIGURE 3.3. Plan view of instrument deployment scheme for total DUCK94 experiment. Locations A, B, and C in this study are denoted with crosses (Field Research Facility, 1994).

The August experiment was scheduled to take advantage of calm summer conditions on the East Coast. In fact, a variety of calm and storm conditions were experienced during the August study. The October experiment was scheduled to coincide with the period most likely to experience storms (northeasters). Water level, wave and wind conditions during the October experiment are shown in Figure 3.4. For this study, only data runs from the October experiment were used. Data runs were selected from a calm period during Oct. 7-9, 1994, and during a large storm with peak offshore wave heights of 4.1 m on Oct. 13-16, 1994.

Bed sediments were collected at the low tide line, trough, and bar crest on October 9th, and at the low tide line and trough on October 15, 1994 (Stauble, pers comm). The size histograms for the three sites are shown in Figure 3.5 for October 9th. At the trough location the bed sediment consisted of unimodal fine sand, and the size distribution varied only slightly between the two sampling dates. In the intertidal zone a bimodal distribution of fine sand and shell hash was seen under calmer conditions (Oct. 9), which changed to poorly sorted coarse sand under higher energy conditions (Oct. 15).

### **3.2.3 Data Analysis**

The data runs analyzed for this study were selected to demonstrate the difference between broken and unbroken wave conditions. Data runs were selected during time periods of 1) peak wave height and more narrow banded wave spectra than the average condition (long period, large swell that broke across the entire surf zone), and 2) minimal wave heights when waves were definitely not breaking. Data runs of 17 minute duration were extracted from files which covered periods of up to 3 hours. All data were collected at 16 Hz in October and were block averaged to 2 Hz for analysis. A background level of suspended sediment concentration (which can be caused by both wash load and instrument response to ambient light, water, and fiber properties) was removed from the time series by setting concentrations to zero in between wave events for each data run. An example of the time series data is shown in Figure 3.6.

The mean velocity stated throughout this paper is the velocity at the sensor closest

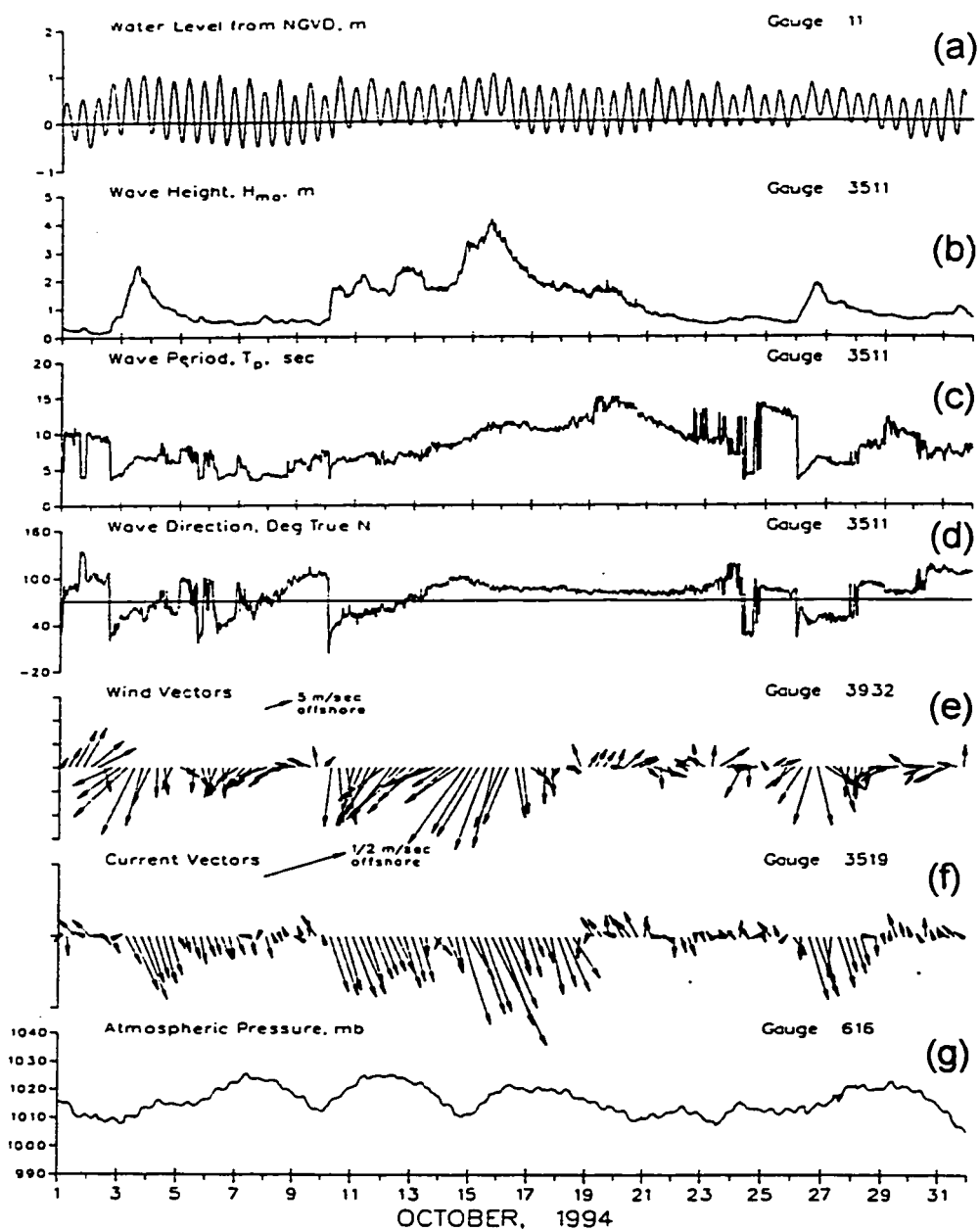


FIGURE 3.4. Time series of water level, waves, wind, currents and atmospheric pressure during the October phase of the DUCK94 experiment, a) water level from NGVD. b-d) wave height, period, and direction at the FRF 8 m array, e) wind at the end of the FRF pier, f) currents at the 8 m array, and g) atmospheric pressure, (Field Research Facility, 1994).

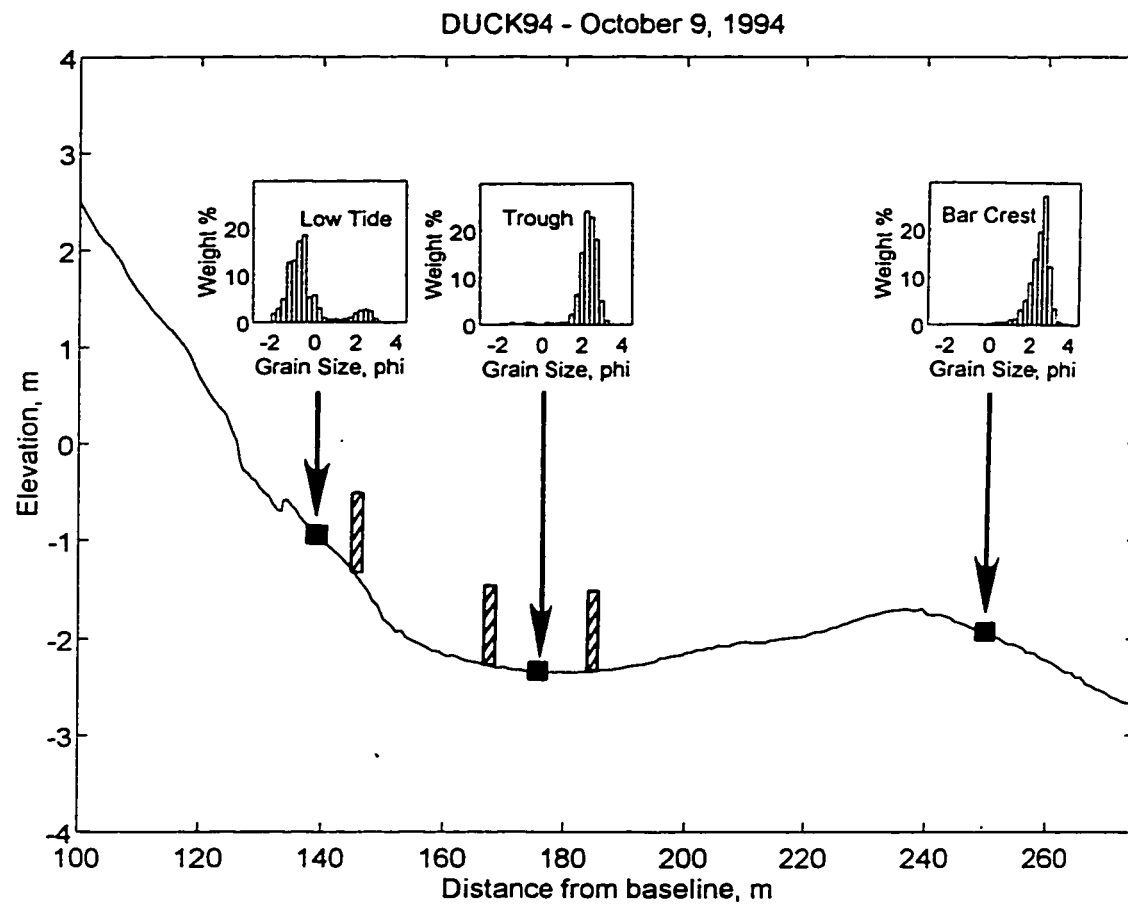


FIGURE 3.5. Cross shore beach profile showing instrument and sediment sampling locations. The sediment grain size histograms are overlain.



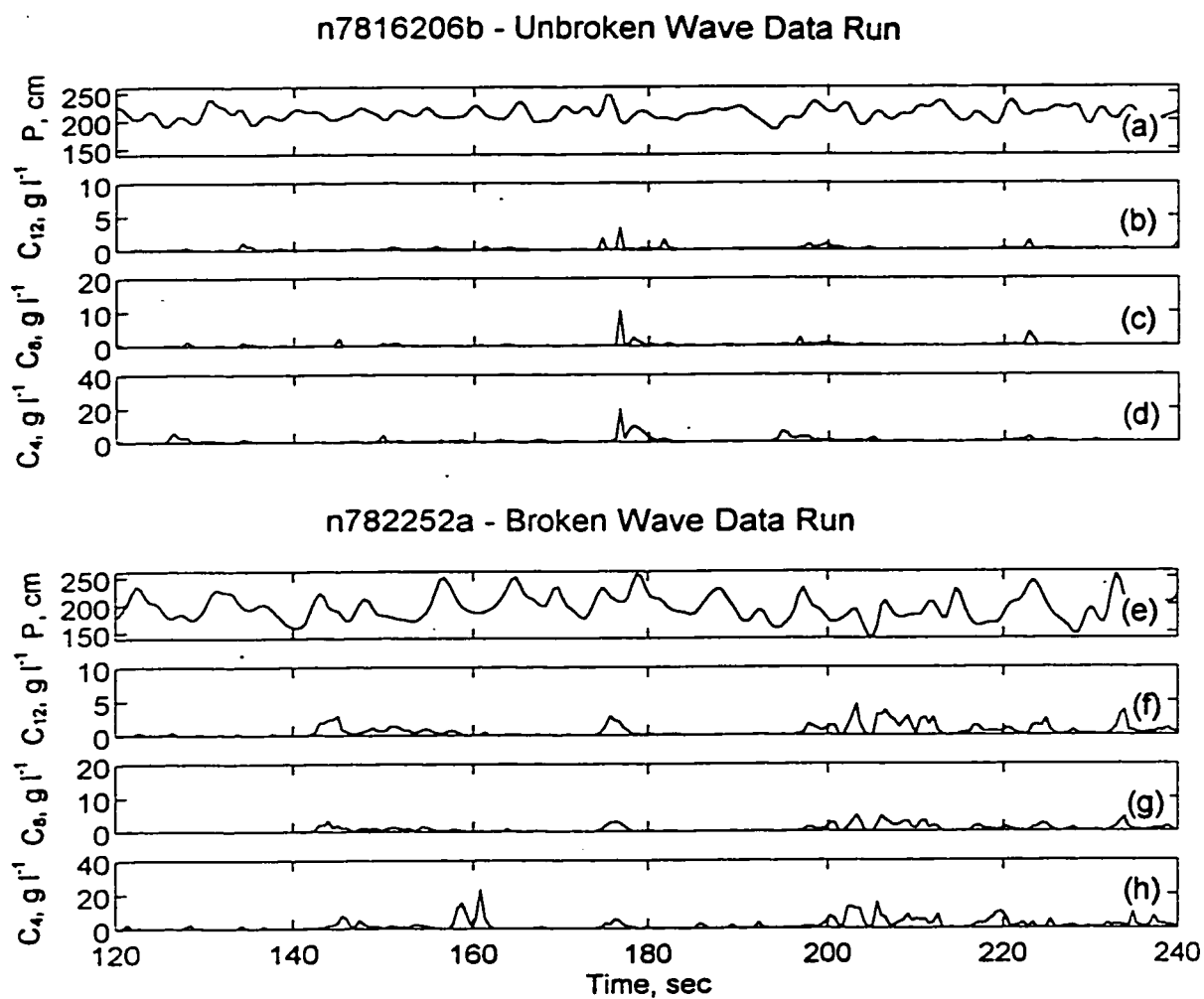


FIGURE 3.6. Time series of pressure and suspended sediment concentration at three elevations above the bed for an two example data runs; unbroken wave data run, a) pressure, b-d) suspended sediment concentration at 12, 8 and 4 cmab, and broken wave data run, e) pressure, f-h) suspended sediment concentration at 12, 8, and 4 cmab.

to 50 cm above the bed time-averaged over the 17 minutes of record. The significant wave orbital velocity,  $U_{1/3}$ , was obtained from the rms velocities in the cross and long shore directions. The significant incident wave height,  $H_{sIC}$ , was computed from the pressure energy density spectra (22 dof) between the frequency of the spectral valley between infragravity and incident motions (between 0.027 and 0.055 Hz) and 0.5 Hz. The wave period is taken at the spectral peak. The infragravity wave height,  $H_{sIG}$ , was computed from the pressure energy density spectra between frequencies of 0.004 Hz and the spectral valley.

### ***Eddy Diffusivity Calculations***

If the vertical profile of suspended sediment concentration is known, sediment eddy diffusivities can be determined from Equation 1.3,

$$K_s = \frac{Ws\bar{C} - \overline{w_w C_w}}{d\bar{C}/dz} \quad (3.1)$$

where  $Ws\bar{C}$  represents the settling flux term and  $\overline{w_w C_w}$  represents the vertical wave advection flux term, and the sum of these terms is balanced by the turbulent diffusion term,  $K_s d\bar{C}/dz$ . It is possible to estimate the vertical wave advection term using linear wave theory assumptions and horizontal velocity field measurements. The vertical velocity was estimated using linear shallow water wave theory,

$$w = \frac{z}{2\sqrt{gh}} \left( \frac{du}{dt} \right) \quad (3.2)$$

The vertical wave velocities were averaged over 1.5 second time periods throughout the data run to approximate the removal of the turbulent component. Suspended sediment concentrations were also averaged over the 1.5 second time periods, and combined with the vertical wave velocities. They were then summed to form the mean wave advective component.

Near the bed, the mean vertical advective component contributes little to the calculated eddy diffusivities because the vertical wave velocity goes to zero. Higher in the

TABLE 3.1. Summary of 17 minute DUCK94 data runs used in this study

Run No.	Time (GMT)	Date -1994	$V$ (cm/s)	$Hs_{IC}$ (cm)	$Hs_{IG}$ (cm)	$Tp$ (s)	$h$ (cm)	$Hs/h$	$U_{1/3}$ (cm/s)	$U_s$ (cm/s)
<b>***Unbroken Wave Data Runs***</b>										
n7815964C	2:07	8-Oct	12	-	-	-	320+	-	57	8.8
n7816206B	8:50	8-Oct	9	43.9	5.9	4.6	228	0.19	81	12.3
n7816206C	8:50	8-Oct	17	43.7	6.4	4.6	231	0.19	59	9.0
n7816514B	17:23	8-Oct	5	48.4	5.4	4.1	300	0.16	71	11.3
n7816514C	17:23	8-Oct	9	46.6	5.6	4.1	305	0.15	46	7.3
n7816729B	23:22	8-Oct	4	48.1	5.8	4.8	261	0.18	75	11.3
n7816729C	23:22	8-Oct	11	49.9	5.9	4.8	268	0.19	52	7.9
<b>***Broken Wave Data Runs***</b>										
n7816729A	23:22	8-Oct	1	52.1	7.3	4.8	158	0.33	74	11.2
n7817044A	8:07	9-Oct	-1	50.9	11.3	6.4	115	0.44	82	11.2
n7820881A	22:42	13-Oct	-1	95.3	29.2	7.5	211	0.45	114	14.4
n7821332A	11:14	14-Oct	-6	87.3	31.0	8.4	203	0.43	110	14.0
n7822521A	20:15	15-Oct	16	93.9	38.6	9.0	282	0.33	129	16.0
n7822655A	23:59	15-Oct	45	107.8	44.2	7.9	273	0.39	157	20.1
n7822763A	2:59	16-Oct	24	100.4	50.1	8.0	212	0.47	135	15.0

water column, however, the wave advective term can be large. As an example, eddy diffusivities were calculated both including and not including the vertical advection term, and the resulting profiles are shown in Figure 3.7. The difference between the values is greatest at the highest eddy diffusivity values (higher in the water column) and contributes less than 20 percent change in the eddy diffusivity. In this chapter, the emphasis is on the nearbed profile of eddy diffusivity, and for simplification the vertical advection term was not included in further analysis. Eq. 3.1 becomes,

$$K_s = \frac{Ws\bar{C}}{d\bar{C}/dz} \quad (3.3)$$

The detailed profiles of suspended sediment concentration obtained with the FOBS during DUCK94 enable the calculation of the sediment eddy diffusivity. The settling velocity of sediment particles was calculated based on the  $D_{75}$  of the bed sediment sample in the trough (0.18 mm), and the Gibbs settling relationship (Eq. 1.5). Selecting  $D_{75}$  to estimate the settling velocity of particles in suspension is discussed in Chapter 4.3. The

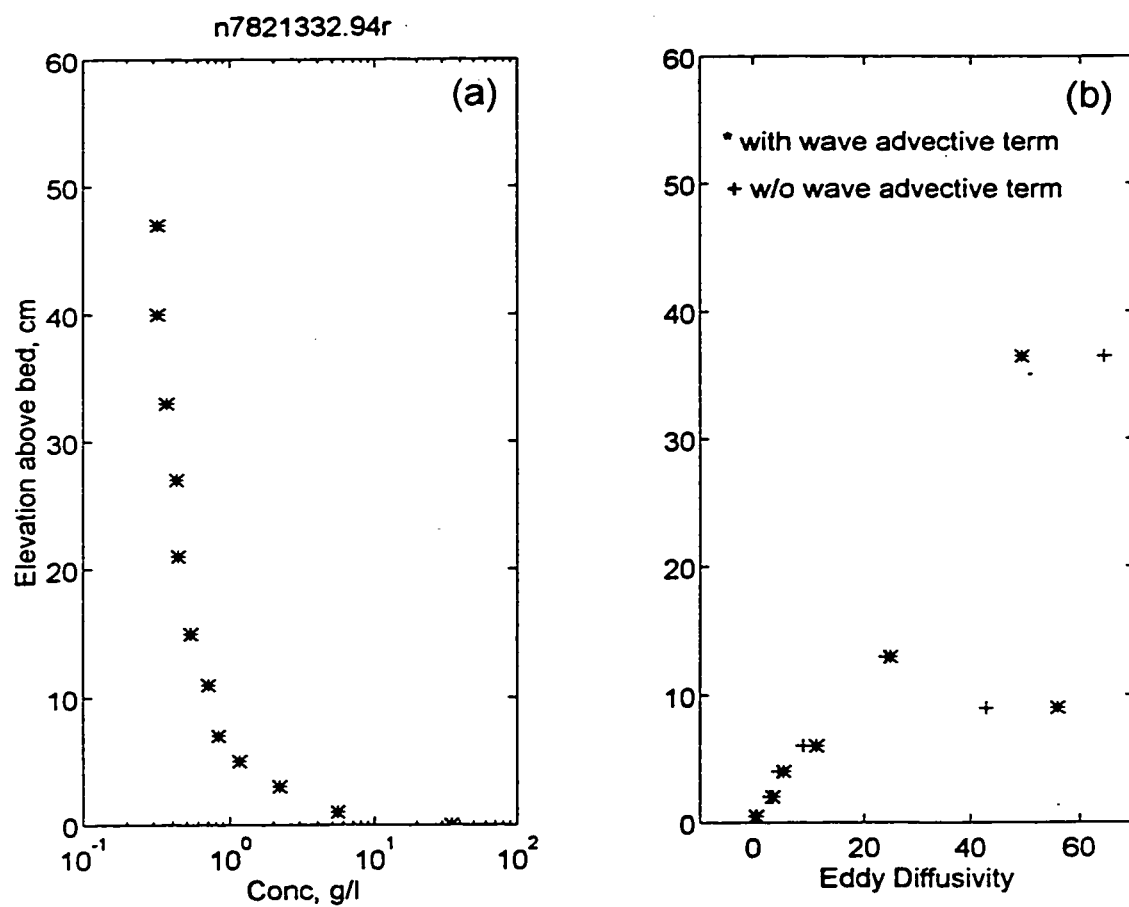


FIGURE 3.7. Example data run profile of a) suspended sediment concentration and b) sediment eddy diffusivity showing the impact of neglecting the vertical wave advection term.

sediment concentration profiles were first smoothed using a running mean to minimize error caused by the slight displacement of sensor offsets. At low values of concentration gradient ( $d\bar{C}/dz$ ), the computed eddy diffusivity values were very sensitive to small differences in offset removal; therefore, eddy diffusivity values were not computed at points where concentration gradients of less than  $0.1 \text{ g l}^{-1}$  existed between two adjacent sensors.

### 3.3 Results

Fourteen data runs were selected to represent time periods of unbroken and broken wave conditions, and wave and current environment during these runs are summarized in Table 3.1. Two criteria were used to determine the breaking state of waves during each data run, 1) the ratio of wave height to water depth, and 2) the shape of the waves. According to studies by Thornton and Guza (1982) on two separate beaches, an envelope curve relating wave height to water depth for the inner surf zone can be approximated by,

$$H_s \approx 0.55h \quad (3.4)$$

where a Rayleigh wave height distribution has been assumed, and  $H_s = 1.35 H_{rms}$ . The ratio of wave height to water depth for the data runs in the present study are lower ( $0.16 < H_s/h < 0.47$ ) than the 0.55 value found in Thornton and Guza, but the data runs can be separated using this criteria. Two groupings are evident in Table 3.1. Broken wave data runs fall in the range,  $0.33 < H_s/h < 0.47$ , and the unbroken wave data runs fall in the range,  $0.15 < H_s/h < 0.20$ . During all of the data runs with low  $H_s/h$  values, the offshore wave height was 0.6 to 0.8 m (Fig. 3.4), from which an estimate of the wave height at breaking can be obtained. Using linear wave theory and an empirically derived constant (Komar and Gaughan, 1972), the wave height at breaking was found to be 1.1 to 1.2 m. If a wave breaking criteria of  $H_b/h=0.8$  is assumed, then depth at which waves will initiate breaking can be calculated. For the low  $H_s/h$  runs, the depth at breaking was 1.4 to 1.5 m, whereas the water depth at which the data were measured ranged from 2.3 to 3.2 m, suggesting that the waves had not reached a depth at which they would break. During the

data runs with high  $H/h$  values, the offshore waveheight ranged from 0.9 to 4.0 m, and the same analysis as above was performed. The water depth for all of the high  $H/h$  data runs was below or very close to the depth of wave breaking, suggesting broken waves at the measurement locations.

To confirm the state of breaking between the two groups of data runs, the shape of the waves was examined by using the pressure signal time series. In the data runs with a high  $H/h$ , the sawtooth shape found by Yu et al. (1993) characteristic of bores or broken waves at Duck NC was seen confirming that the waves were broken. The shape of the waves in the data runs with low  $H/h$  were more symmetrical and rounded, which suggests the waves were not broken in these runs. Based on the two breaking criteria, the runs were separated into groups of broken and unbroken waves in Table 3.1.

Wave breaking type also has an important bearing on this study because breaker type (e.g., plunging vs. spilling) is found to strongly influence sediment resuspension and total sediment load (e.g., Kana, 1979; Yu et al., 1993). Compared to spilling breakers, plunging breakers are associated with stronger vortex motion and greater bed erosion and transport. Based on measurements of Kroon and Van Rijn (1992) performed in the inner surf zone, the wave height to water depth range for spilling breakings is  $0.4 < H/h < 0.6$ , which is relatively consistent with the measurements of Kana (1979). For the broken data runs used in this study, the mean  $H/h$  was 0.41, indicating spilling breakers. Another way to determine the breaker type is through the Iribaren number (Battjes, 1974),

$$\xi_b = \tan \alpha / (H_b / L_o)^{0.5} \quad (3.5)$$

where  $\alpha$  is the beach slope and  $L_o$  is the wave length (plunging breakers range:  $0.4 < \xi_b < 2.0$ ; spilling breakers range:  $\xi_b < 0.4$ ). At location A, the wave breaking Iribaren number ranged from 0.67 to 0.81 when using the beach slope,  $\tan \alpha = 0.07$ , which suggests the lower end of the plunging breaker range toward the spilling breaker range. For the broken wave data runs, wave breaking was initiated substantially farther offshore than location A, and in locations where the beach slope was less steep (Fig 3.5). The resulting Iribaren

number at the breaking location would therefore be less than at location A, suggesting that waves initiate breaking as spilling breakers. Although  $\xi_b$  does not conclusively describe the state of wave breaking for these runs, the implication of both  $H/h$  and  $\xi_b$  is that waves in the broken wave data runs were predominantly spilling breakers.

### 3.3.1 Mean Flow and Wave Orbital Velocities

Significant incident wave heights at the instrument locations for all runs range from 44 to 108 cm at wave periods of between 4.1 and 10.2 seconds. The infragravity wave height is low in all of the unbroken wave runs (5.4 to 6.4 cm), but the infragravity wave height during the broken wave runs is substantially higher (7.3 to 50.1 cm). The unbroken runs exhibit orbital velocities ( $U_{1/3}$ ) of 46 to 81 cm s<sup>-1</sup> and northward trending mean longshore currents of 4 to 17 cm s<sup>-1</sup>. The broken wave data runs have orbital velocities of 74 to 157 cm s<sup>-1</sup> and the longshore currents vary from 6 cm s<sup>-1</sup> to the south to 45 cm s<sup>-1</sup> to the north (Table 3.1).

### 3.3.2 Friction Velocity

A friction velocity can be estimated based on the currents and wave orbital velocities and the hydraulic roughness of the bed. The friction velocity is estimated using,

$$U_*^2 = f_w U_{1/3}^2 / 2 \quad (3.6)$$

where  $f_w$  is the Jonsson friction factor (Jonsson, 1966) which can be computed from the hydraulic roughness of the bed and the nearbottom wave orbital amplitude,  $A = U_{1/3} / \omega$ , based on Swart's (1974) formula. The hydraulic roughness can be estimated from the grain roughness Shield's parameter,  $\theta_{2.5}$ , based on  $2.5D_{50}$  of the bed sediment, the ripple geometry, and the wave orbital amplitude (Nielson, 1992). For this analysis, it was assumed the bed was planar during the data runs. Large bedforms were observed at times during the DUCK94 experiment (Gallagher et al., 1996), but were not typically seen inshore of the trough at the VEMA/FOBS instrument locations. Estimated friction velocities for each data run used in this study are shown in Table 3.1. The friction velocities ranged from 6.5 to 12.3 cm s<sup>-1</sup> for the unbroken runs, and from 11.2 to 20.1 cm

s<sup>-1</sup> for the broken runs.

The friction velocity estimates require the assumption of an oscillatory flow that obeys linear wave theory thus ensuring that friction at the bed is the dominant mechanism for generating turbulence. This assumption also implies that the mean velocity profile varies from a vertically uniform flow to a logarithmically decreasing boundary layer flow near the bed. In the surf zone waves are less sinusoidal, more sawtooth shaped, and the subsequent breaking creates turbulence that contributes to the turbulence levels throughout the water column. A discussion of the implications of using the Jonsson friction factor in the surf zone is included in Chapter 4.

### 3.3.3 Suspended Sediment Concentration Profiles

The time-averaged profiles of suspended sediment concentration for unbroken and broken wave conditions are shown in Figure 3.8a and b, respectively. The sediment concentration profiles for all data runs are composed of two regions. They are the nearbed region ( $z \sim 0$  to 12 cmab for the unbroken wave data runs and  $z \sim 0$  to 20 cmab for the broken wave data runs), where the mean concentration decreases rapidly with height above bed, and the upper water column region, where the concentration levels become more vertically uniform ( $z > 12$  or 20 cm, for unbroken or broken wave data runs, respectively). In the unbroken wave data runs there is low or no suspended sediment ( $< 0.1 \text{ g l}^{-1}$ ) in the upper water column. In the broken wave data runs there are substantially higher levels of suspended sediment in the upper water column (0.3 to  $1.0 \text{ g l}^{-1}$ ).

A wave boundary layer thickness can be estimated by  $\delta_w = \frac{\kappa U_*}{\omega}$  where  $\delta_w$  is the wave boundary layer thickness and  $\omega$  is the angular frequency (Wright, 1995). The computed wave boundary layer thickness ranges from 2.5 to 10.4 cm for all data runs. For unbroken wave data runs, the thickness of the observed nearbed region of the sediment concentration profiles is typically 10-15 cm, which corresponds to approximately three to four times the height of the predicted wave boundary layer thickness ( $\delta_w = 2.0$  to 4.3 cm). For the broken wave data runs, the wave boundary layer thickness is equal to or



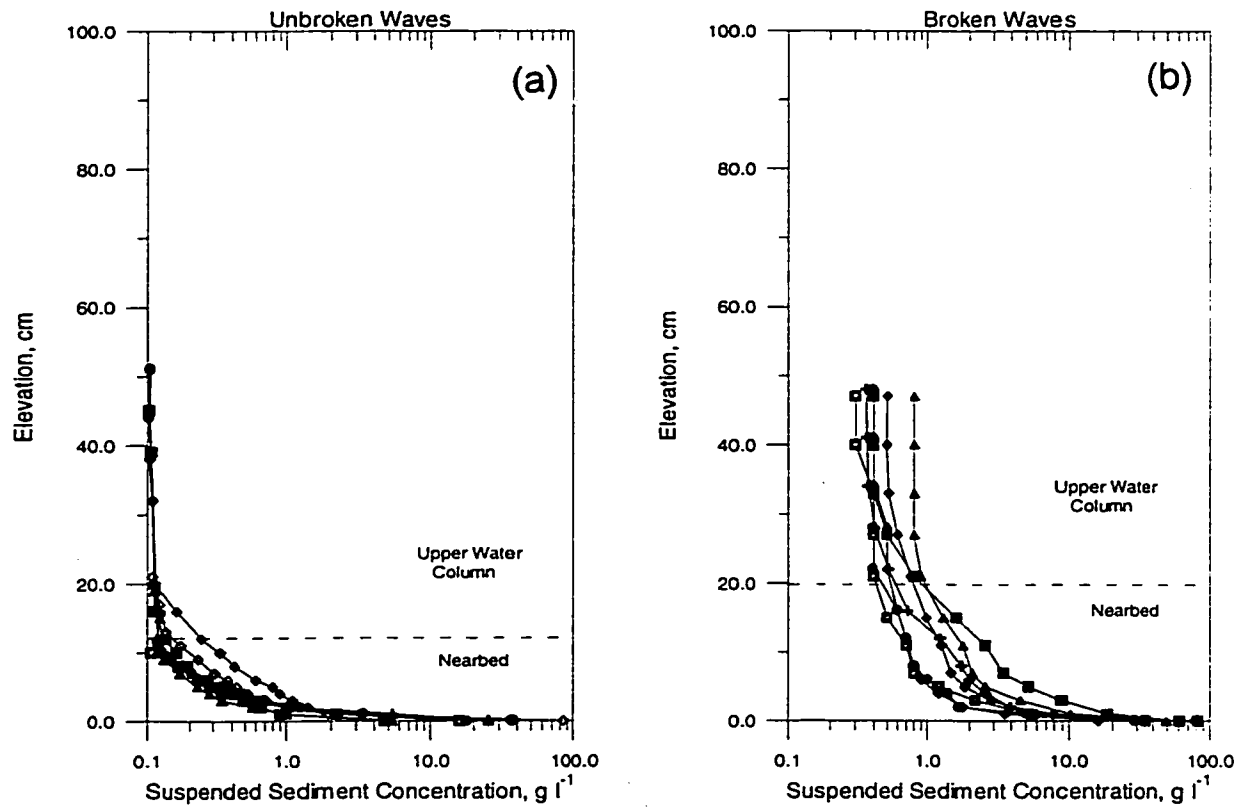


FIGURE 3.8. Profiles of time averaged suspended sediment concentration for a) unbroken wave data runs, and b) broken wave data runs. The dashed line in both panels represents the approximate location of the top of the nearbed region.

larger than that seen in unbroken conditions ( $\delta_w = 3.5$  to  $10.4$  cm), and the top of the observed nearbed layer corresponds to two to four times the calculated wave boundary layer thickness. In general, the nearbed region appears to correspond to approximately three times the wave boundary layer thickness for both unbroken and broken wave data runs.

For the unbroken wave sediment concentration profiles, maximum sediment concentrations in the nearbed region range from  $6$  to  $90 \text{ g l}^{-1}$  at an elevation of less than  $1.0$  cmab (Fig. 3.8a). The dashed line in Figure 3.8a represents the average elevation of the top of the nearbed region for the unbroken wave data runs. In the upper water column region, concentrations are close to zero or the detection limit of the FOBS instrumentation.

For the broken wave sediment concentration profiles, the maximum concentrations in the nearbed region are greater than  $80 \text{ g l}^{-1}$  at  $1.0$  cmab and decrease with height above the bed at varying rates of decay (Fig. 3.8b, dashed line as above). In the upper part of the nearbed region, ( $z \sim 10$  to  $20$  cmab) a step appears to occur in all but one broken wave concentration profile (i.e. a steep slope to the profile stepping into a relatively flat slope). The step in the concentration profile could be due to increased infragravity wave energy (see Table 3.1) during the broken runs, and perhaps the steps correspond to the top of the incident wave boundary layer and the top of the infragravity wave boundary layer. In the upper water column sediment concentration is typically uniform in the vertical and ranges from  $0.3$  to  $1.0 \text{ g l}^{-1}$ .

### 3.3.4 Time Averaged Eddy Diffusivity Profiles

Eddy diffusivity profiles were determined from the measured concentration profiles using the relationship in Eq. 3.3. The resulting  $K_z$  profiles are shown in Figure 3.9a and b for the unbroken and broken wave data runs, respectively, and the dashed line denotes the approximate boundary between the nearbed region and the upper water column. In the nearbed region, Eq. 3.3 provides a detailed estimation of the  $K_z$  profiles due to large sediment concentrations and concentration gradients. Above the nearbed region less

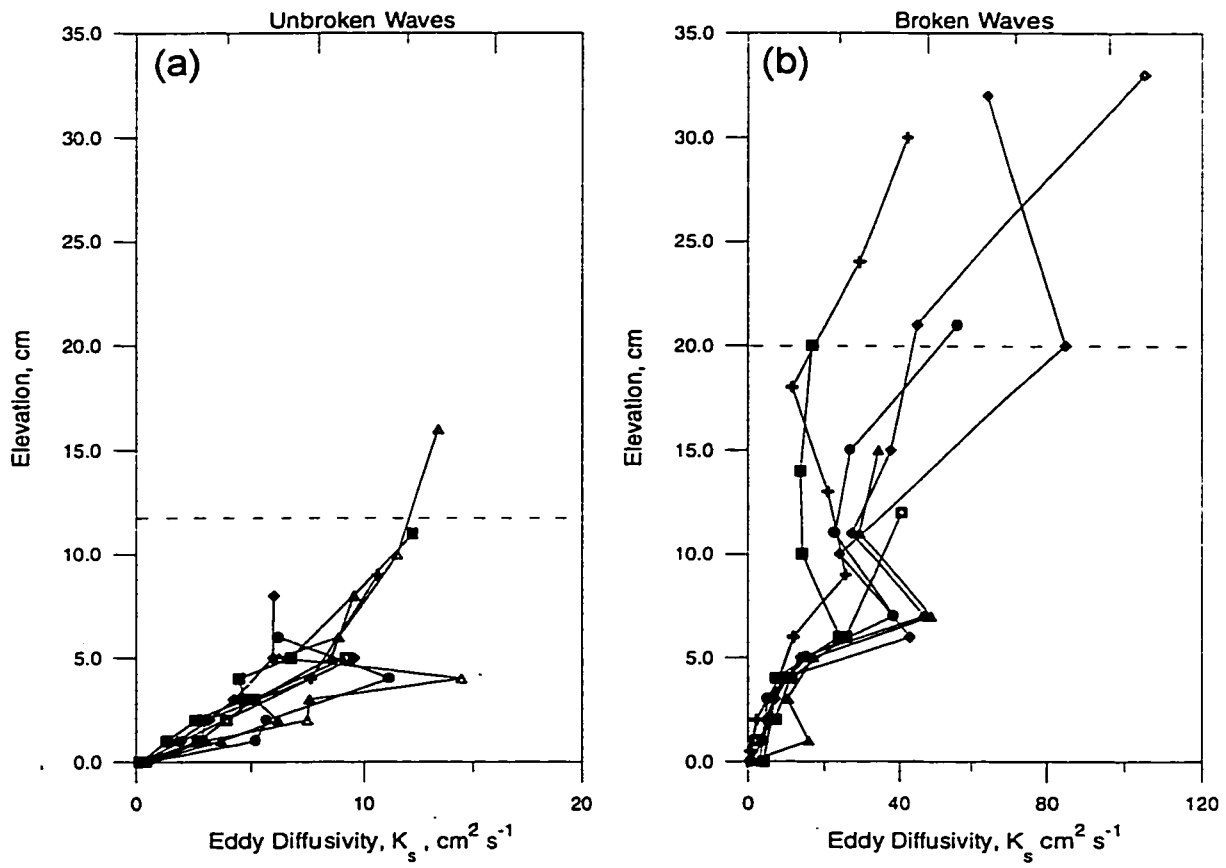


FIGURE 3.9. Profiles of time averaged sediment eddy diffusivity for a) unbroken wave data runs, and b) broken wave data runs. The dashed line in both panels represents the approximate location of the top of the nearbed region.

information can be obtained due to the small concentration gradients.

For the unbroken wave data runs,  $K_r$  values were computed at elevations of 0 to 16 cmab (Fig. 3.9a). In the nearbed region,  $K_r$  values were found to increase with height above bed up to a maximum above which they appear to become vertically uniform or to display a slight increase with height above bed. Between approximately 1 and 5 cmab the increase with height above bed appears to be linear, but with varying slope for the different runs. From 5 to 16 cmab, the increase with height above bed is minimal with maximum observable eddy diffusivity values ranging between 5 and 15  $\text{cm}^2 \text{s}^{-1}$ .

For the broken wave data runs, the  $K_r$  profiles could be determined to 35 cmab due to high sediment concentrations and gradients in the water column (Fig. 3.9b). The  $K_r$  profiles exhibit several distinct partitions. From 0 to 7 cmab, which corresponds to the bottom of the step in the concentration profiles for broken wave data runs (Fig. 3.8b), the  $K_r$  profile does not display a linearly-increasing profile as was seen for the unbroken runs, but rather an S-shaped profile with an exponentially increasing form at the upper limit. The profiles deviate from the very nearbed exponential form at differing elevations, and diverge from one another, resulting in a peak in the eddy diffusivity profile within the nearbed region.

At elevations above approximately 7 cmab, the profiles appear to again increase with height above bed, but at a slower rate than seen below 7 cmab. This increase ranges from almost vertically uniform above the very nearbed region with a maximum of 20  $\text{cm}^2 \text{s}^{-1}$ , to an exponential increase with height above the nearbed region with a maximum of greater than 80  $\text{cm}^2 \text{s}^{-1}$ .

### **3.4 Discussion**

#### **3.4.1 Stratification Correction to Eddy Diffusivity Profile**

Since density stratification of the water column caused by sediment in suspension can inhibit turbulent mixing in the vertical (Adams and Weatherly, 1981; Cacchione and Drake, 1990), a correction to the  $K_r$  profiles may need to be applied. The  $K_r$  values

calculated from suspended sediment profiles as discussed above include any effects due to stratification, and therefore the difference between neutral and stratified  $K_r$  profiles must be considered to make the  $K_r$  profile more applicable to other situations.

The turbulent neutral eddy diffusivities are adjusted through their dependence on the Monin-Obukhov stability parameter ( $z/L$ ), which stems from work on heat stratification done in the atmospheric boundary layer. The Monin-Obukhov scale for sediment induced stratification can be expressed as,

$$L = \frac{U_*^3}{\kappa g(s-1)W_s C} \quad (3.7)$$

where sediment eddy diffusivities are modified according to,

$$K_{st} = \frac{K_n}{\gamma + \beta z/L}, \quad (3.8)$$

(Glenn and Grant, 1987), where  $K_{st}$  and  $K_n$  are the eddy diffusivity for stratified fluids and neutral fluids, respectively, and  $\gamma$  and  $\beta$  are constants. Values for the empirically determined stratification constants have been discussed by Gelfenbaum and Smith (1986) and McLean (1992). The values of McLean are used in this study ( $\gamma = 1$  and  $\beta = 7.3$ ).

The density stratification effect of sand-sized particles in the surf zone on the  $K_r$  profile is shown in two examples, an unbroken wave and broken wave data run. Both the neutral (diamond shaped symbols) and sediment stratified (cross shaped symbols)  $K_r$  profiles are shown in Figure 3.10a and b. The largest differences between the two for all data runs are approximately 10 percent. At this stage of investigating the  $K_r$  profile under breaking waves, the stratification correction found is not considered to be of first-order importance, and is not included in further analysis.

### 3.4.2 Scaling

Scaling of the two regions of the  $K_r$  profile (nearbed and upper water column) are different due to the processes responsible for sediment diffusion in each region. In the bottom boundary layer, theory incorporates an eddy viscosity profile in the wave boundary

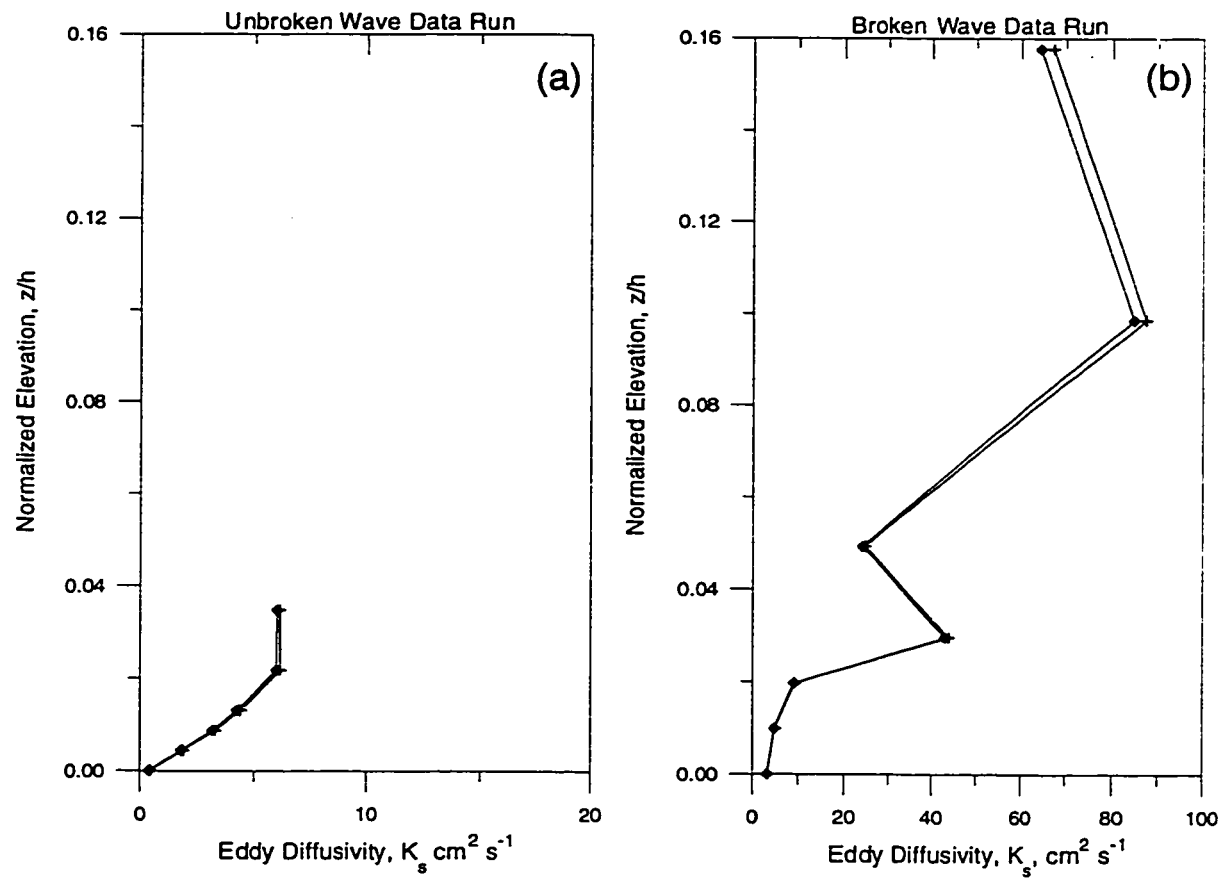


FIGURE 3.10. Profiles of sediment eddy diffusivity show the impact of sediment induced stratification for two examples, a) unbroken wave data run, and b) broken wave data run.

layer that increases linearly with height above bed as  $\kappa U_* z$  (Kajiura, 1964). This relationship was found to be consistent with sediment eddy diffusivity profiles obtained by Sheng & Hay (1995), who used methods similar to those in this study. The linear increase with height above bed is also consistent with results found in the bottom 5 cm of the DUCK94 data for unbroken wave data runs.

For both the unbroken and broken wave data runs, the nearbed  $K_s$  profile can be approximated with a linearly increasing function with height above bed. Scaling by  $\kappa U_* z$  for the eddy viscosity of momentum, as proposed by Smith and McLean (1977) for unidirectional flow, is applied to the  $K_s$  profiles in Figure 3.11a and b for unbroken and broken wave data runs. This scaling causes the  $K_s$  profiles from the unbroken wave data runs (Fig. 3.11a) to collapse onto a single curve. The broken wave data runs still show an S-shape in the nearbed region of the  $K_s$  profile, but the linear approximation can be applied without much loss of information. This S-shape is also seen in the surf zone infragravity wave data of Beach and Sternberg (1988), but is not seen in the data of Sheng & Hay (1995), which was collected under unbroken waves.

Also shown in Figure 3.11 is the predicted  $\kappa U_* z$  relationship for diffusion of momentum (solid line) using  $U_*$  based on the Jonsson friction factor analysis. The scaled  $K_s$  data points always fall above the predicted line, implying that the eddy diffusivity for sediment ( $K_s$ ) is smaller than the eddy viscosity for momentum ( $K_m$ ) in the surf zone ( $\beta < 1.0$ ), or that  $U_*$  has been overpredicted by the Jonsson friction factor analysis. For unbroken wave data runs, the exponential profile of Nowell and Long (1983), Equation 1.8, is plotted in Figure 3.11a using a length scale of  $0.5 h$  (dashed line).

For unbroken wave data runs in the region above the linear region, the form of the exponential approximation (Eq. 1.9) appears to fit the data when using  $0.1$  to  $0.2 h$  as the top of the boundary layer consistent with a bottom boundary layer height of  $10$ - $20$  cm for the unbroken wave data runs. Alternately, a vertically uniform  $K_s$  profile above the bottom 5 cm fits this data, and the limited number of data points and high signal to noise

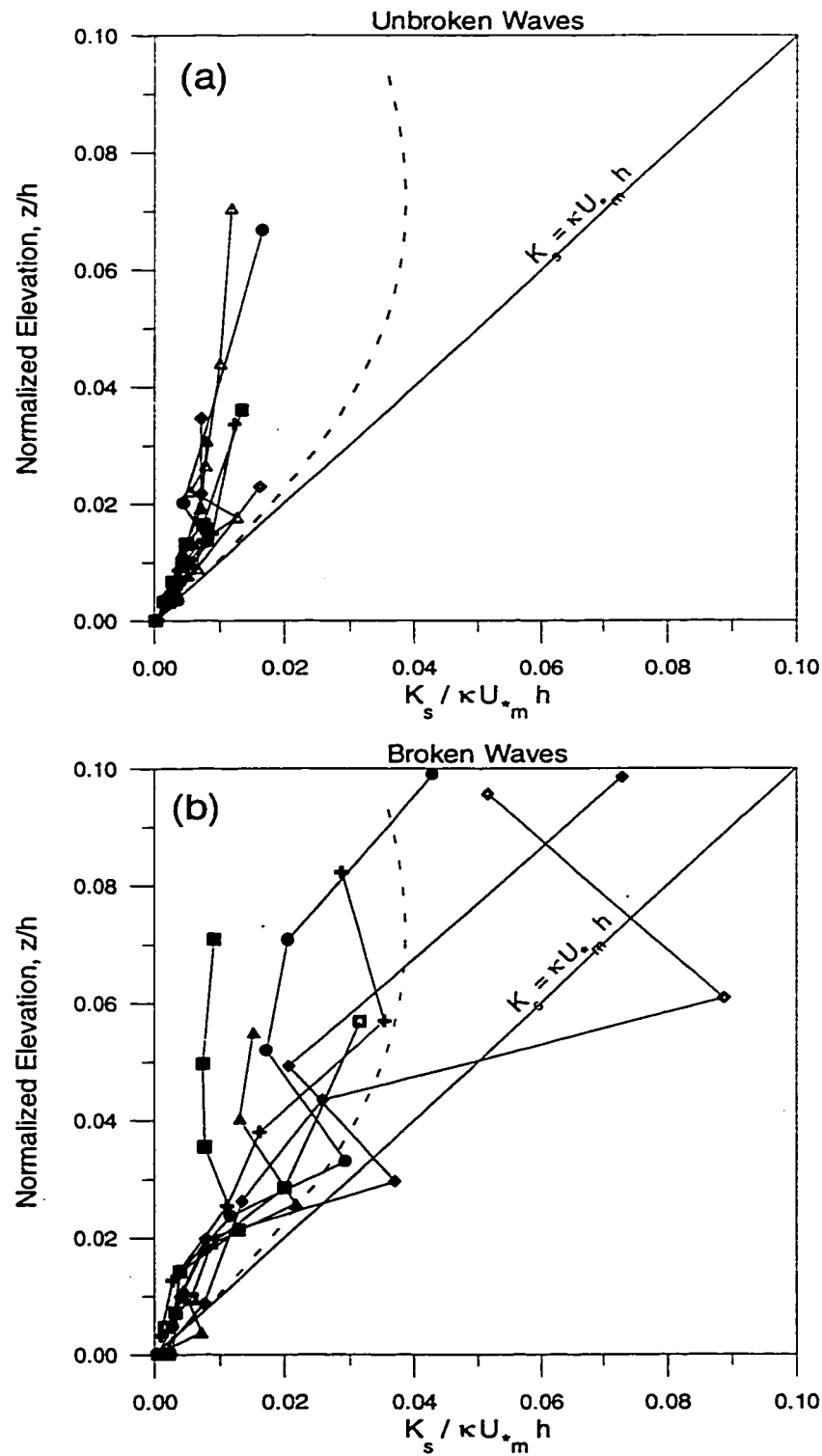


FIGURE 3.11. Profiles of time averaged sediment eddy diffusivity scaled by the eddy viscosity for momentum for, a) the unbroken wave data runs, and b) the broken wave data runs. The solid line indicates a relationship where  $K_s = K_m$  and the dashed line indicates the exponentially decreasing profile found in Nowell and Long (1983).



ratio in computing  $K_s$  values at these upper elevations, make the determination of the best fit profile in the upper water column impossible.

For broken wave data runs, the data points above the top of the nearbed region ( $z > 20$  cm) are scaled by distance from the water surface and wave height, as seen in the wave basin data of Chapter 2. Figure 3.12 suggests a similar increase of the eddy diffusivity profile towards the sea surface as was seen in the wave basin data, discussed in Chapter 2. Despite the large amount of scatter in the data, the trend of an exponentially increasing eddy diffusivity toward the sea surface, rather than becoming vertically uniform or curving back to low values, suggests that turbulence due to wave breaking is reaching into the lower water column, and is controlling the mixing of suspended sediment in the upper water column.

### 3.4.3 Relationship between $K_s$ and $K_m$

This data set enables the estimation of both eddy diffusivity for sediment and eddy viscosity for momentum in the very nearbed region, and the correlation between them. First, the nearbed profile of  $K_m$  was found through the Jonsson friction factor analysis and the relationship,  $K_m = \kappa U_* z$ . Second,  $K_s$  was obtained from the concentration profiles. If we assume  $K_s = \beta K_m$ , then  $\beta$  can be found by a comparison of the slopes of the eddy viscosity and eddy diffusivity profiles in the very nearbed.

The sediment eddy diffusivity profiles were estimated in the very nearbed region, and a linear fit to the data in the nearbed region ( $z < 2\delta$ ) provides the ratio,  $K_s/K_m$  where  $K_m = \kappa U_* z$ , tabulated in Table 3.2. A comparison of  $K_s$  and  $K_m$  at an elevation of 4 cmab is shown in Figure 3.13. The slopes of the sediment eddy diffusivity profiles from the sediment concentration data were found to be substantially smaller than the slopes of the eddy viscosity profile estimated using a Jonsson friction factor. For both broken and unbroken wave data runs the following linear relationship was found,

$$K_s = 0.43 K_m \quad (3.9)$$

where  $\beta = 0.43$ . The value of 0.43 for  $\beta$ , the difference between the eddy diffusivity for

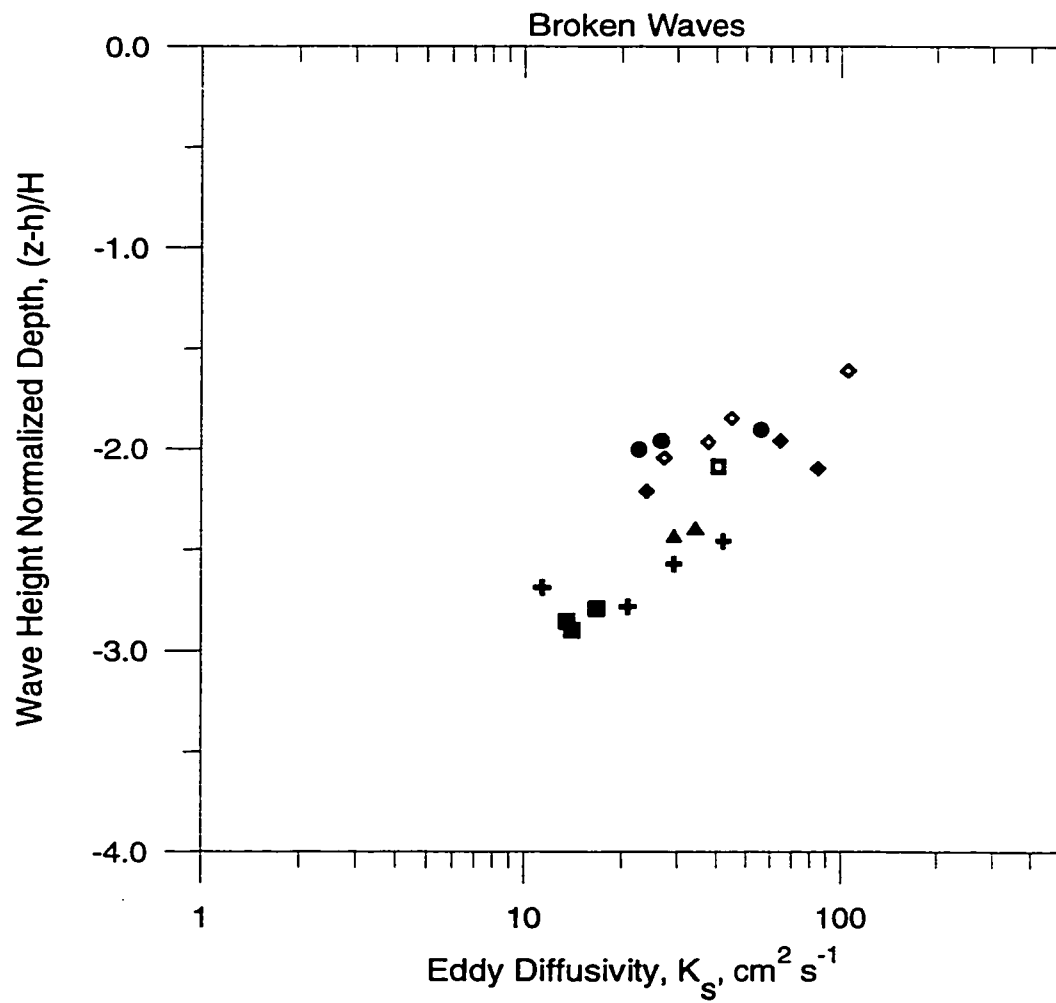


FIGURE 3.12. Upper water column eddy diffusivity values for the broken wave data runs with the depth below the sea surface scaled by the wave height.

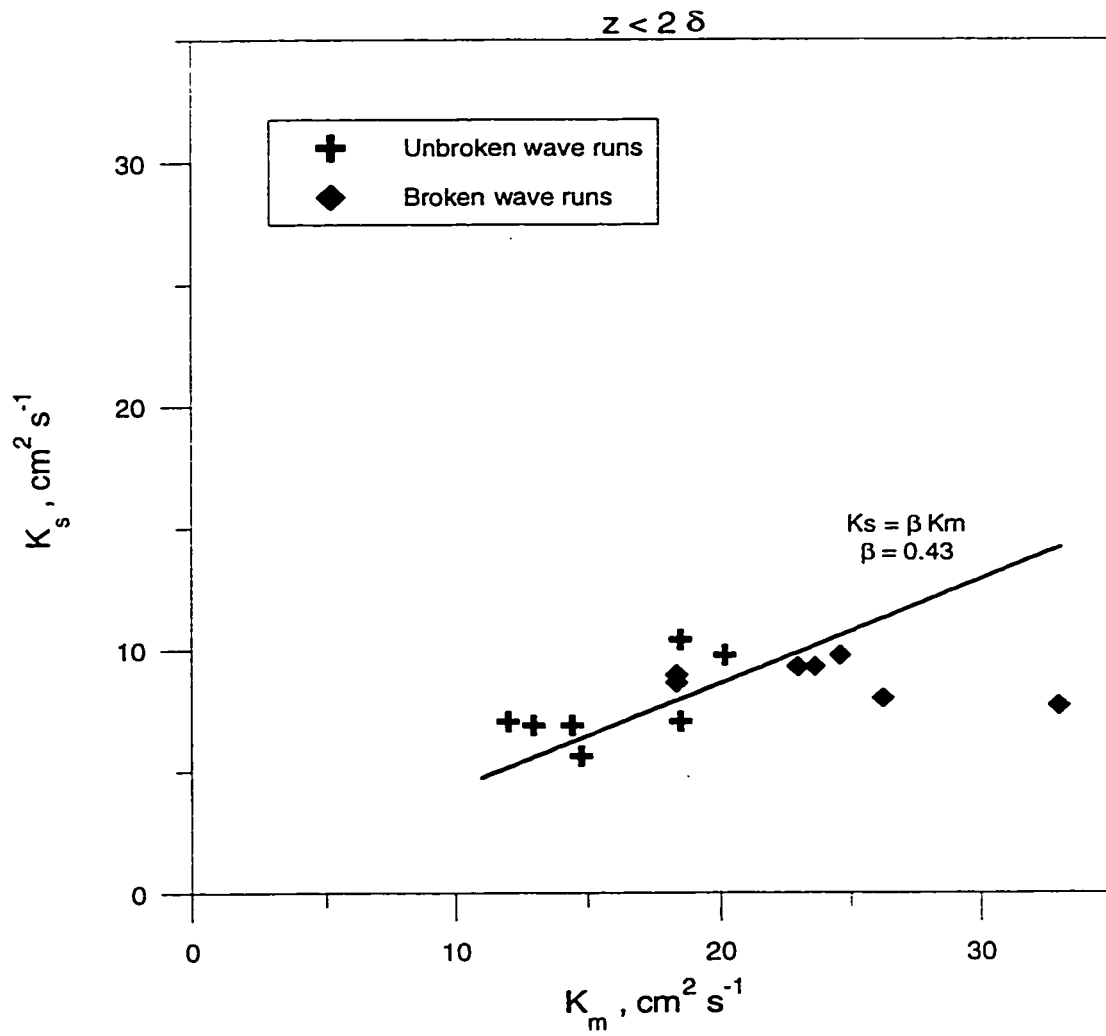


FIGURE 3.13. The relationship between the eddy viscosity for momentum,  $K_m$ , and the sediment eddy diffusivity,  $K_s$ , for all data runs where  $\beta$  is found to be 0.43.

TABLE 3.2 Ratio of eddy diffusivity for sediment to eddy viscosity for momentum.

	Run No.	$K_s/(K_m = \kappa U_* z)$
***Unbroken***	n7815964C	0.48
	n7816206B	0.48
	n7816206C	0.38
	n7816514B	0.56
	n7816514C	0.59
	n7816729B	0.38
	n7816729C	0.53
***Broken***	n7816729A	0.47
	n7817044A	0.49
	n7820881A	0.39
	n7821332A	0.40
	n7822521A	0.30
	n7822655A	0.23
	n7822763A	0.40

sediment and the eddy viscosity for momentum, has been found in other studies to be in the range of 0.2 to 10. In this study, the value of  $\beta$  may also be attributed to several factors. Stratification of the water column due to suspended sediment<sup>9</sup> could affect the nearbed eddy viscosity for momentum, although this was found to be a small factor based on the Monin Obuknov stability parameter above. It is also possible the Jonsson friction factor analysis, which was formulated for unbroken waves, may bias the estimates of  $U_*$  and subsequent estimates of  $K_m$  under broken waves.

The relationship between  $K_s$  and  $K_m$  will be explored in more detail in Chapter 4. Using all of the unbroken and broken wave data runs (Fig. 3.13), the correlation enables the use of a modified Jonsson friction factor method for the nearbed predictions of the friction velocity and the resulting suspended sediment profile in the nearbed,

$$K_s = 0.43\kappa U_* z. \quad (3.10)$$

## **CHAPTER 4. EVALUATION OF THE $K_s$ VS $K_m$ RELATIONSHIP: IMPLICATIONS FOR SURF ZONE DIFFUSION MECHANISMS**

### **4.1 Motivation**

This chapter addresses the details of the relationship between the eddy diffusivity for sediment,  $K_s$ , and the eddy viscosity for momentum,  $K_m$ , which was briefly addressed in Chapter 3. It has been assumed in past work (i.e., Lees, 1981) that the eddy diffusivity of sediment particles is proportional to the eddy viscosity of water ( $K_s = \beta K_m$ ). There has been no general agreement on the value of  $\beta$ , and it has often been taken to be equal to 1.0, suggesting sediment particles act as passive scalars within the fluid field. Van Rijn (1984) found  $\beta$  to be  $> 1$ , implying a centrifugal effect of turbulent eddies where sediment particles are thrown outside the eddies with a subsequent increase in the effective mixing length. Lees (1981) also found  $\beta$  to be generally  $> 1$ , and found it dependent on grain size and sediment concentration. Soulsby et al. (1986) found  $\beta$  to be an almost constant 0.2, using measurements throughout a flood tide. A value of  $\beta < 1$  suggests the inability of sediment grains to fully follow the turbulent velocity fluctuations of the fluid. However, none of the above studies were performed under surf zone conditions, where sediment concentrations are extremely high relative to the tidal channels and shelf environments studied by Lees and Soulsby. In this chapter, suspended sediment measurements and the resulting  $K_s$  and  $K_m$  estimates from Chapter 3 are used to evaluate the relationship between  $K_s$  and  $K_m$  in the nearshore zone, and to discuss the implications of using this relationship, depending on whether waves are unbroken or broken.

### **4.2 Relationship of $K_s$ to $K_m$ in the Nearbed for Unbroken and Broken Waves**

In Chapter 3, a relationship was found for both the unbroken and broken wave data runs between  $K_s$  and  $K_m$  ( $K_s = 0.43 K_m$ ). This relationship was based on the assumption that the same processes are in action under both unbroken and broken waves, whereas, it is clear that wave breaking generated turbulence is an added consideration under broken waves. In this section, the difference between  $K_s$  and  $K_m$  is evaluated under

both unbroken and broken wave conditions, for both the very nearbed ( $z < 5$  cm) and the bottom boundary layer ( $z < 2\delta$ ).

An examination of the assumptions used to estimate  $K_r$  and  $K_m$  provides a means by which to interpret the resulting relationship between them. A first-order assumption applicable to both  $K_r$  and  $K_m$  estimates is that of a steady state process. This requires the vertical mixing of fluids and sediment particles be conservative in time. The non-linearities found in surf zone processes introduce some uncertainty in the estimates of  $K_r$  and  $K_m$ .

#### **4.2.1 Assumptions Leading to Nearbed $K_r$ Estimates**

Determining  $K_r$  from measured sediment concentration profiles (Eq. 3.3) requires the following assumptions:

- net vertical advection due to wave orbital motions is minimal,
- sediment size is unimodal, and therefore a single settling velocity value can be used, and
- $K_r$  is a linear function of height above the bed in the region near the bed.

Under broken waves, the  $K_r$  profile did not show a strictly linear shape nearbed (see Fig. 3.8), but the deviation is small and has an insignificant impact on the predictions of the suspended sediment profile. The unimodal sediment size assumption also provides for confidence in the calibrated sediment concentrations from the optical measurements. The sum of these assumptions was found to have a small accountable effect on the  $K_r$  estimates (on the order of 20 percent) in Chapter 3; and therefore, confidence in the estimates is of that order.

#### **4.2.2 Assumptions Leading to $K_m$ Estimates**

The Jonsson friction factor method of obtaining a friction velocity,  $U_*$ , enables the determination of  $K_m$  from fluid and bed properties (Eq. 3.6), and requires the following assumptions:

- flows are oscillatory and obey linear wave theory, where friction at the bed is the sole mechanism for generating turbulence, and
- bed is planar.

The first assumption ensures that the velocity profile varies from a vertically uniform flow in the upper water column to a logarithmically decreasing bottom boundary layer flow.

Although it is realized that this assumption is violated in the surf zone due to both turbulent wave breaking and the formation of cross shore circulation patterns, it is initially assumed that  $K_m$  can be determined adequately using this method, and the effects of violating the assumptions are discussed later.

#### 4.3 Discussion of $K_s$ and $K_m$ Relationship

The  $K_s$  and  $K_m$  relationships for both the very nearbed ( $z < 5$  cm) and the nearbed region ( $z < 2\delta$ ) are shown in Figures 4.1a and b, respectively. In these figures, a linear relationship between  $K_s$  and  $K_m$  is assumed, and the scatter in the data around this relationship can be used to establish confidence intervals. For this purpose, it is assumed  $K_m$  is the independent variable and uncertainty exists only in  $K_s$ ; therefore, a least squares procedure was used.

For unbroken wave data runs, the estimated eddy diffusivity values appear to follow the model ( $K_s = \beta K_m$ ), both in the very nearbed (Fig. 4.2a,  $z < 5$  cm) and throughout the nearbed region (Fig. 4.2b,  $z < 2\delta$ ), and  $\beta$  was found to be 0.55 and 0.48, respectively. These two slopes are significantly different from a zero slope (a zero slope implying no relationship) at the 95 percent confidence level, but are not significantly different from each other. If it is assumed the intercept need not be forced through zero and is allowed to be free variable, then the relationship,

$$K_s = 0.38 K_m + 1.6 \quad (4.1)$$

is found and the fit to the data is shown in Figure 4.2c. The relationship found, where the intercept is forced through zero (Fig. 4.2b), falls within the confidence intervals of the relationship found where the intercept was not forced through zero (Fig. 4.2c). This

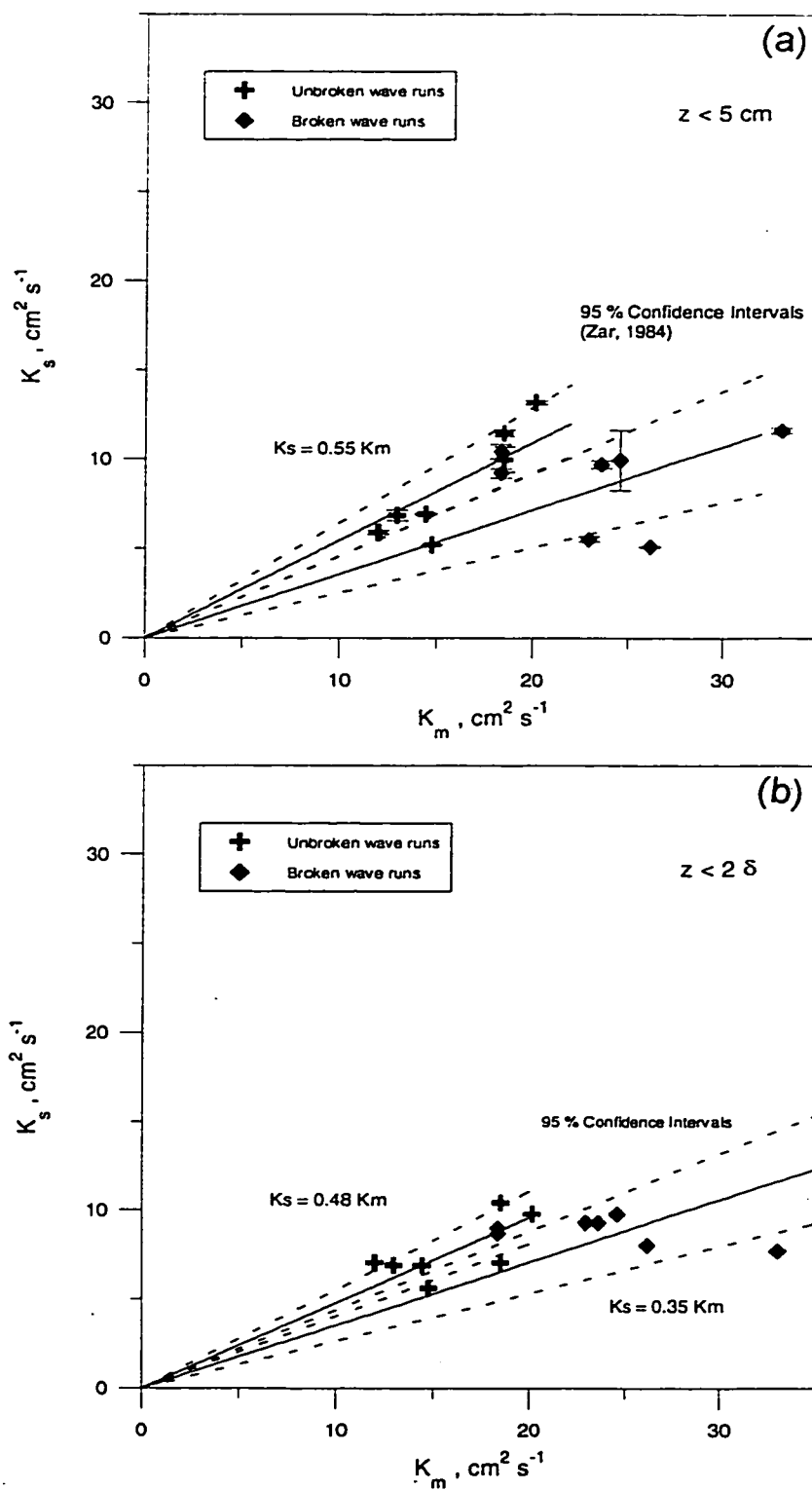


FIGURE 4.1. Relationship of  $K_s$  to  $K_m$  at 4 cmab where  $K_s$  is assumed linear a) within 5 cm of the seabed, and b) within  $2\delta$  of the seabed.



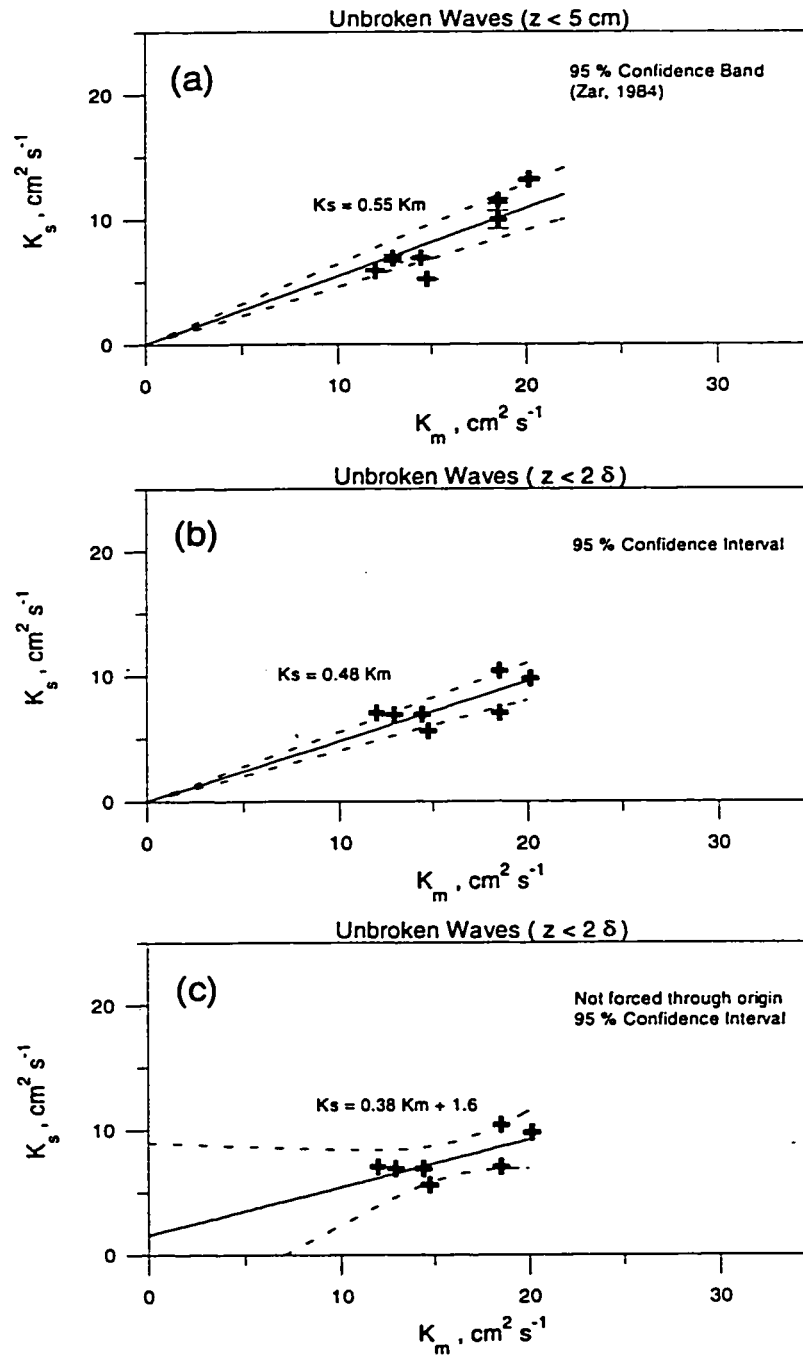


FIGURE 4.2. Relationship of  $K_s$  to  $K_m$  at 4 cmab under unbroken wave conditions and where a) a linear fit through the origin is found and  $K_s$  to is assumed linear with 5 cm of the seabed, b) a linear fit through the origin is found and  $K_s$  to is assumed linear with  $2\delta$  of the seabed, and c) an unconstrained linear fit is found and  $K_s$  to is assumed linear within  $2\delta$  of the seabed.

suggests the model,  $K_r = \beta K_m$ , is appropriate for unbroken wave conditions. Based on this small data set and previous studies of  $\beta$ , the simpler relationship through zero can be assumed to hold, and the  $K_r$  profile can be described as the following function of  $U_*$  and  $z$ ,

$$K_r = 0.48\kappa U_* z. \quad (4.2)$$

For the broken wave data runs, estimates of  $K_r$  vary significantly depending upon the height above bed to which the linear profile is assumed to apply (see differences between Fig. 4.3a and b). This is due to the curvature of the  $K_r$  profile in the nearbed region under broken waves (see Fig. 3.8b), which is not seen under unbroken waves (Fig. 3.8a). Assuming a linear relationship through zero,  $\beta$  is found to be 0.36 below  $z = 5$  cm (Fig. 4.3a). Below  $2\delta$ ,  $\beta$  is found to be virtually the same at 0.36 (Fig. 4.3b), although the confidence interval around  $\beta$  is much larger than the confidence interval around  $\beta$  for  $z < 2\delta$ . For both regions the slope is significantly different from zero, but the broad 95 percent confidence intervals make it difficult to determine the value of  $\beta$ .

When the intercept is allowed to vary from zero for  $K_r$  estimates below  $2\delta$ , a relationship is found that is very weakly dependent upon  $K_m$  (Fig. 4.3c),

$$K_r = 10.7 - 0.08 K_m. \quad (4.3)$$

The slope of this relationship is not significantly different from zero. If the confidence intervals of the parameterizations forced and not forced through zero are compared, as seen in Figures 4.3b and c, the slopes of the two linear fits will not overlap at the 95 percent confidence level. This suggests that under broken waves the relationship between  $K_r$  and  $K_m$  estimates should not be held to the more restrictive relationship formed when the intercept is forced through zero. If it is assumed that  $K_r$  is not dependent upon  $K_m$ , then the  $K_r$  profile can be described by the following function of  $z$ ,

$$K_r = 5.5\kappa z. \quad (4.4)$$

The implication of the relationship between  $K_r$  and  $K_m$  under broken waves is discussed in the following sections.

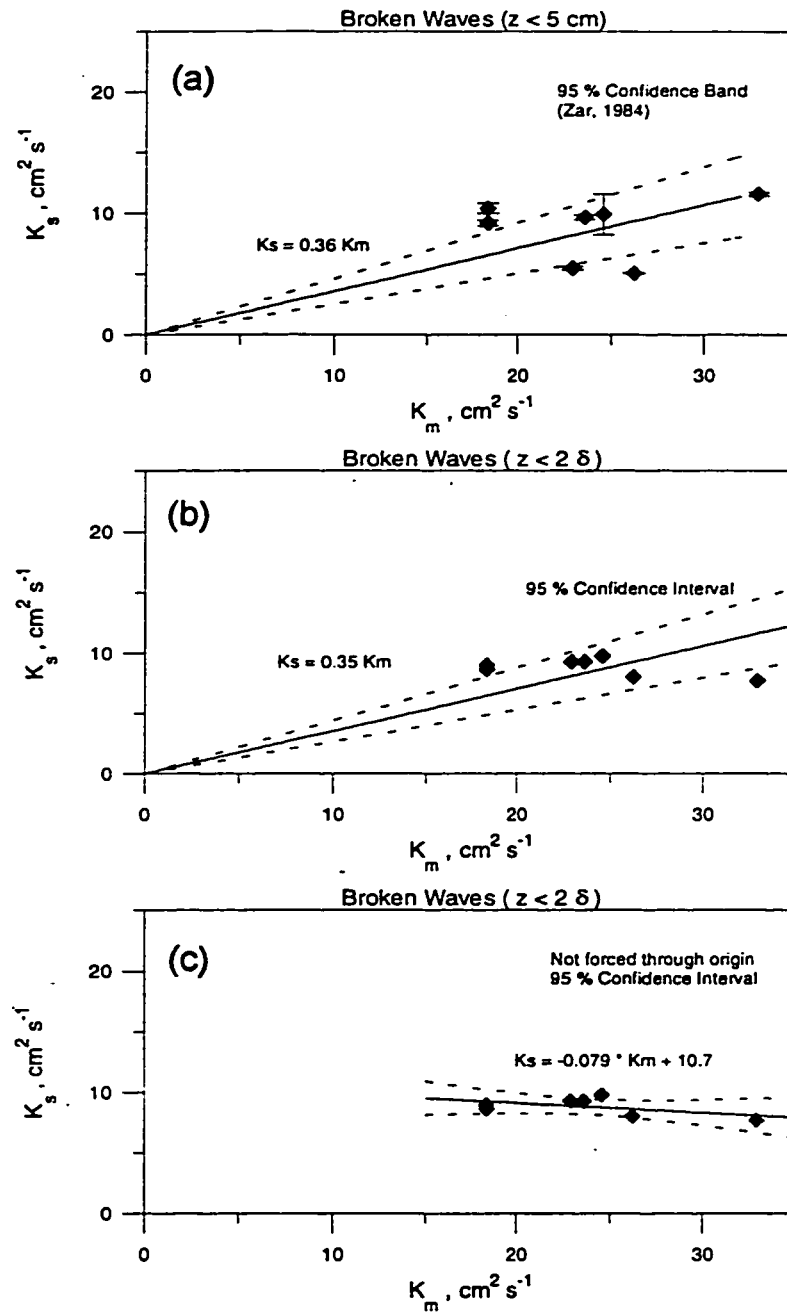


FIGURE 4.3. Relationship of  $K_s$  to  $K_m$  at 4 cmab under broken wave conditions and where a) a linear fit through the origin is found and  $K_s$  to is assumed linear with 5 cm of the seabed, b) a linear fit through the origin is found and  $K_s$  to is assumed linear with  $2\delta$  of the seabed, and c) an unconstrained linear fit is found and  $K_s$  to is assumed linear within  $2\delta$  of the seabed.

#### 4.3.1 Data Variability

Because of the highly turbulent regime, surf zone data typically contains a large amount of variability; it is therefore possible the relationship between  $K_r$  and  $K_m$  for broken waves is simply obscured by the small data set and the degree of scatter. For the  $K_r$  estimates below 5 cm (Fig. 4.1a), most broken wave data points fall outside the confidence intervals for the unbroken wave data points. This suggests that if the assumption of a linear relationship holds, the ratio between  $K_r$  and  $K_m$  would be different for unbroken and broken waves very near the bed. The broken wave  $K_r$  estimates below  $2\delta$  (Fig. 4.1b) do not fall substantially outside the confidence limits of the unbroken wave estimates. If the assumption holds that data scatter is obscuring the linear relationship between  $K_r$  and  $K_m$ , it would be difficult to determine whether  $\beta$  is different for broken and unbroken data runs for  $z < 2\delta$ .

Also, for the  $K_r$  estimates below  $z = 2\delta$ , sediment concentration data were obtained over a range of  $K_m$  values, but the range of  $K_r$  values for the data runs analyzed is very small, and may be inadequate to determine a relationship between  $K_r$  and  $K_m$  (see Fig. 4.3c).

#### 4.3.2 Limitations in Jonsson Friction Factor under Broken Waves

Although it was assumed there was little uncertainty in the estimates of  $K_m$ , it is possible the Jonsson friction factor method of determining a friction velocity,

$$U_* = f_w U_{1/3}^2 / 2 \quad (4.5)$$

is not as applicable under broken waves as it is (and has been extensively used) under unbroken waves. It was seen in Chapter 2 that additional turbulence from wave breaking at the sea surface can penetrate throughout the water column and into the nearbed region. Wave breaking turbulence is not considered when estimating  $U_*$  using the Jonsson friction factor method, and can limit the applicability of this method for determining the eddy viscosity profile in the surf zone.

In addition, the breakdown of wave motions into large eddy motions (Yu et al., 1993) affects the measurements of  $U_{rms}$  and the resulting estimates of  $U_{1/3}$  under broken waves. Adding a turbulent component on top of wave orbital motion causes measurements of  $U_{rms}$  to be larger than measurements where  $U_{rms}$  is due solely to wave orbital motions. The Jonsson friction factor method would then over-estimate the friction velocity which produces bottom boundary shear generated turbulence. Although the turbulent velocities could be capable of adding to the shear at the bed, the time scales may not be sufficient to add substantially to a fully developed bottom boundary layer.

#### 4.3.3 Limit on $K_s$

If the  $K_s$  estimates contained in this small data set and the estimates of  $K_m$  are assumed reasonable despite the issues raised in the previous sections, the relationship in Figure 4.3c implies that, under broken waves, there is a limiting value of  $K_s$  (approximately  $9 \text{ cm}^2 \text{ s}^{-1}$  at 4 cm ab) in the nearbed region. As a wave shoals into shallow water, the bottom orbital velocity increases, which is reflected as an increase in the nearbed estimates of  $K_m$  and increased dissipation of energy at the seabed. A wave breaks when the steepness of the unbroken wave becomes high enough, dissipating energy both at the seabed and throughout the water column. After the wave is broken, the wave orbital velocity at the seabed becomes smaller as the bore propagates across the surf zone, but added turbulent fluctuations cause the measured orbital velocity (based on  $U_{rms}$ ) to appear higher, ultimately causing an overestimation of the nearbed  $K_m$ . Since the wave height to water depth ratio remains relatively constant in a saturated surf zone, it seems feasible that a limit on energy at the seabed would hold throughout the surf zone, independent of the estimated friction velocity.

Alternatively, the extremely high sediment concentrations measured near the bed could cause sediment induced stratification that would damp turbulence generated near the bed under broken waves. There is potential for a self-balancing system in which the high-energy breaking waves suspend high levels of sediment, thereby stratifying the water

column and damping energy at the seabed (Wright et al., in press). An analysis of sediment-induced stratification was performed in Chapter 3 for the time-averaged condition. In the time-dependent case, the role of stratification in sediment mixing may play a larger role due to the episodic high sediment concentration spikes (see Fig. 3.6) that are not accounted for in the description of the time-averaged conditions.

#### 4.4 Proposed $K_r$ and $K_m$ Relationship

Based on the uncertainties discussed in the above sections, a model for the relationship between  $K_r$  and  $K_m$  under broken and unbroken waves is proposed in which two different relationships are invoked, one for unbroken waves (low estimated friction velocities) and another for broken waves (high estimated friction velocities). The relationship is based on the  $K_r$  estimates at elevations less than  $2\delta$  and is shown with confidence intervals in Figure 4.4.

The relationship uses the Jonsson friction factor method to determine  $U_{*}$ , and below a critical value ( $U_{*c} = 11.4 \text{ cm s}^{-1}$ ), the unbroken  $K_r$  to  $K_m$  relationship found in Figure 4.2b is utilized ( $K_r = 0.48 \kappa U_{*} z$ ). Above the critical  $U_{*c}$  value, it is assumed that the waves are broken and there is no relationship between  $K_r$  and  $K_m$ . The  $K_r$  limit for broken waves below  $2\delta$ , as shown in Figure 4.3c, is used when the calculated  $U_{*}$  is above the critical value ( $K_r = 5.5 \kappa z$ ). This parameterization implies there is a distinct separation between broken and unbroken wave runs based on  $U_{*}$ , which is a first approximation only. There is probably an overlap between the unbroken and broken  $K_m$  estimates (as shown with stippling in Fig. 4.4) to which either of the unbroken or broken wave relationships could apply.

It should be noted that the relationship proposed here does not account for some of the details of the sediment concentration profiles below  $2\delta$ , particularly under broken waves. It is suggested in Figure 4.3a, that below 5 cm,  $K_r$  has a larger range of values than is seen below  $2\delta$ . This may be due to either, the relationship is harder to determine

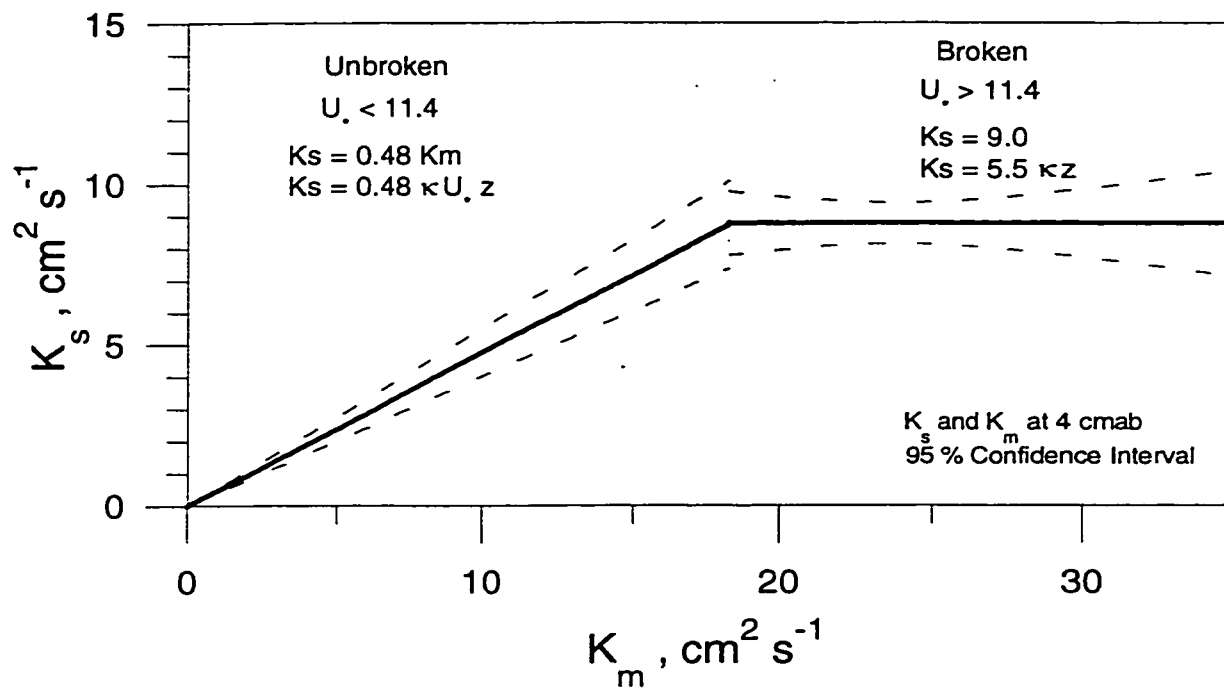


FIGURE 4.4. Proposed relationship of  $K_s$  to  $K_m$  at 4 cmab. The stippling marks the zone of transition between the unbroken wave formulation and the broken wave formulation.

due to the smaller number of concentration data points, or that there are different processes in effect very near the bed which are not seen above 5 cm.

#### 4.5 Summary

This data set provides an opportunity to examine the  $K_r$  to  $K_m$  relationship in the nearbed under unbroken and broken waves. Previous studies outside the surf zone have found  $\beta$  to be within the range of 0.1 to 10, and under unbroken waves, this study found  $\beta$  to be 0.55 for  $z < 5$  cmab and 0.48 for  $z < 2\delta$ . Under broken waves, there may not be a relationship between  $K_r$  to  $K_m$  which suggests that methodology used to describe turbulent diffusion outside the surf zone (i.e., Jonsson friction factor method) is not necessarily applicable inside the surf zone.

Under broken waves, the  $K_r$  and  $K_m$  observations in this data set imply that turbulence generated by bottom boundary shear may not be the primary mechanism responsible for determining the vertical distribution of suspended sediment. As depicted in Figure 4.5a, the commonly accepted view of diffusion of sediments in the surf zone consists of a distinct bottom boundary layer with mixing controlled by shear at the bed, and added mixing near the sea surface due to wave breaking (analogous to Deigaard et al., 1986). In this case, the suspended sediment concentration profile would show a distinct bottom boundary layer (depicted with dashed line Fig. 4.5a) in which suspended sediment is contained. Although there is added mixing due to wave breaking near the sea surface, very little sediment would be mixed above the bottom boundary layer, and a low and relatively vertically uniform sediment concentration profile results in the upper water column. The present data implies that the mixing in the bottom boundary layer may not be controlled by the shear at the bed, but rather by wave-breaking turbulence (Fig 4.5b). The limit on the mixing due to the length scale near the bed would still cause a bottom boundary layer in which the eddy diffusivity is limited by distance from the sea bed. The sediment concentration profile in this case would again show a decrease with height above the bed in the nearbed but the added wave breaking turbulence throughout the water



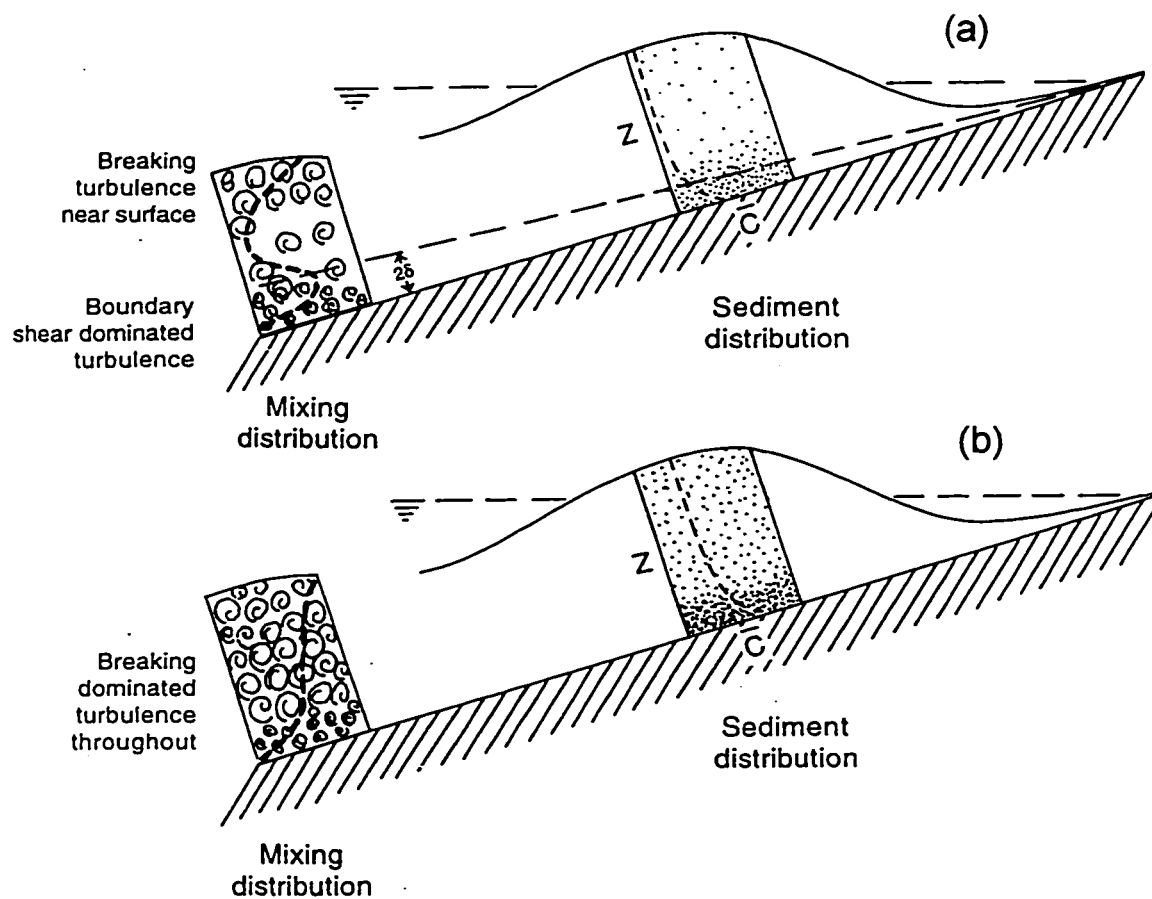


FIGURE 4.5. Conceptual sketch describing the mechanisms of sediment diffusion in the surf zone. In a) a distinct bottom boundary layer is formed with mixing controlled by shear at the bed, and in b) mixing is controlled by the wave breaking turbulence.

column enables mixing of higher sediment concentrations into the upper water column.

The interpretation of the lack of a  $K_s$  to  $K_m$  relationship is not entirely clear, but the alternatives suggest mechanisms by which suspended sediment profiles in the surf zone can be explained. In order to investigate more fully these mechanisms, future work could include expanding the range of surf zone conditions under which suspended sediment data is obtained to determine the range of  $K_s$  and to increase the number of estimates leading to a higher confidence level.

## **CHAPTER 5. COMBINED EDDY DIFFUSIVITY PROFILE AND RESULTING SUSPENDED SEDIMENT PREDICTION**

### **5.1 Motivation**

The Wild Rivers wave basin experiment provided excellent information on turbulence intensity throughout the water column in an artificial surf zone. The application of this information to the full water column under field conditions is limited because the wave basin bottom was a smooth painted surface, and therefore the bottom roughness was very small and the bottom boundary layer very thin (on the order of mm). Also, the wave field was monochromatic and sediment was not available to test estimates of eddy diffusivity obtained from the turbulence intensity estimates.

The DUCK94 field experiment provides a complement to the wave basin experiment since diffusion of sediment in the wave bottom boundary layer was examined under real surf zone conditions. In this chapter, eddy diffusion information obtained in the wave basin and the DUCK94 experiment is combined to gain a full water column formulation of eddy diffusion. This formulation is then used to predict the vertical profile of suspended sediment concentration and flux. The specific objectives are,

- to provide a parameterization for eddy diffusivity of sediment in the surf zone under broken and unbroken waves based on both the wave basin experiment and the DUCK94 field experiment,
- to use the parameterized form of the eddy diffusivity profile to predict suspended sediment concentrations throughout the water column,
- to use velocity measurements and modeling to predict longshore suspended sediment flux, and
- to examine the influence of the parameterized eddy diffusivity profile on predictions of sediment concentration and flux.

## 5.2 Combined Eddy Diffusivities

Eddy diffusion coefficients determined from both the wave basin experiment and the DUCK94 experiment are discussed in Chapters 2 and 3, respectively, and resulting profiles from both experiments are shown normalized by water depth in Figure 5.1. The values from both data sets are of similar magnitude and the fit between the two data sets is reasonably good. They overlap in the vertical at elevations of approximately 4 to 15 cm under unbroken waves and less than 1.0 cm to 30 cm under broken waves. An expanded view of the overlap region of the eddy diffusivity profiles is shown in Figure 5.2a and b for unbroken and broken wave conditions, respectively.

Under unbroken wave conditions, eddy diffusivity profiles in the wave basin experiment and the eddy diffusivity profiles from the DUCK94 experiment (Fig. 5.2a) match well in this region of overlap. It is apparent from the DUCK94 data that a bottom boundary layer develops in the lowest ~10 cm, in which the eddy diffusivity profile increases with height above the bed. Although some individual DUCK94 profiles appear to continue to increase with height above the bed in Figure 5.2a, many are constant or decrease with height above bed above the nearbed region, consistent with the wave basin data. The wave basin data show an eddy diffusivity profile that is constant above the bottom boundary layer, consistent with the concept of very little additional turbulence generated above the bottom boundary layer.

Under broken wave conditions (Fig. 5.2b), the wave basin data and the DUCK94 data also match well within the lower 20 cm. In this region, the DUCK94 eddy diffusivity estimates show a bottom boundary layer with eddy diffusion limited by the distance from the bed. Both the wave basin data and DUCK94 data indicate a decrease in eddy diffusivity just above the very nearbed region, continuing into an exponentially increasing profile with height above bed. The DUCK94 estimates tend to be higher than the wave basin estimates at elevations of ~20 to 30 cmab, but the uppermost points from the DUCK94 data are not very well constrained. At these levels the concentration gradient is

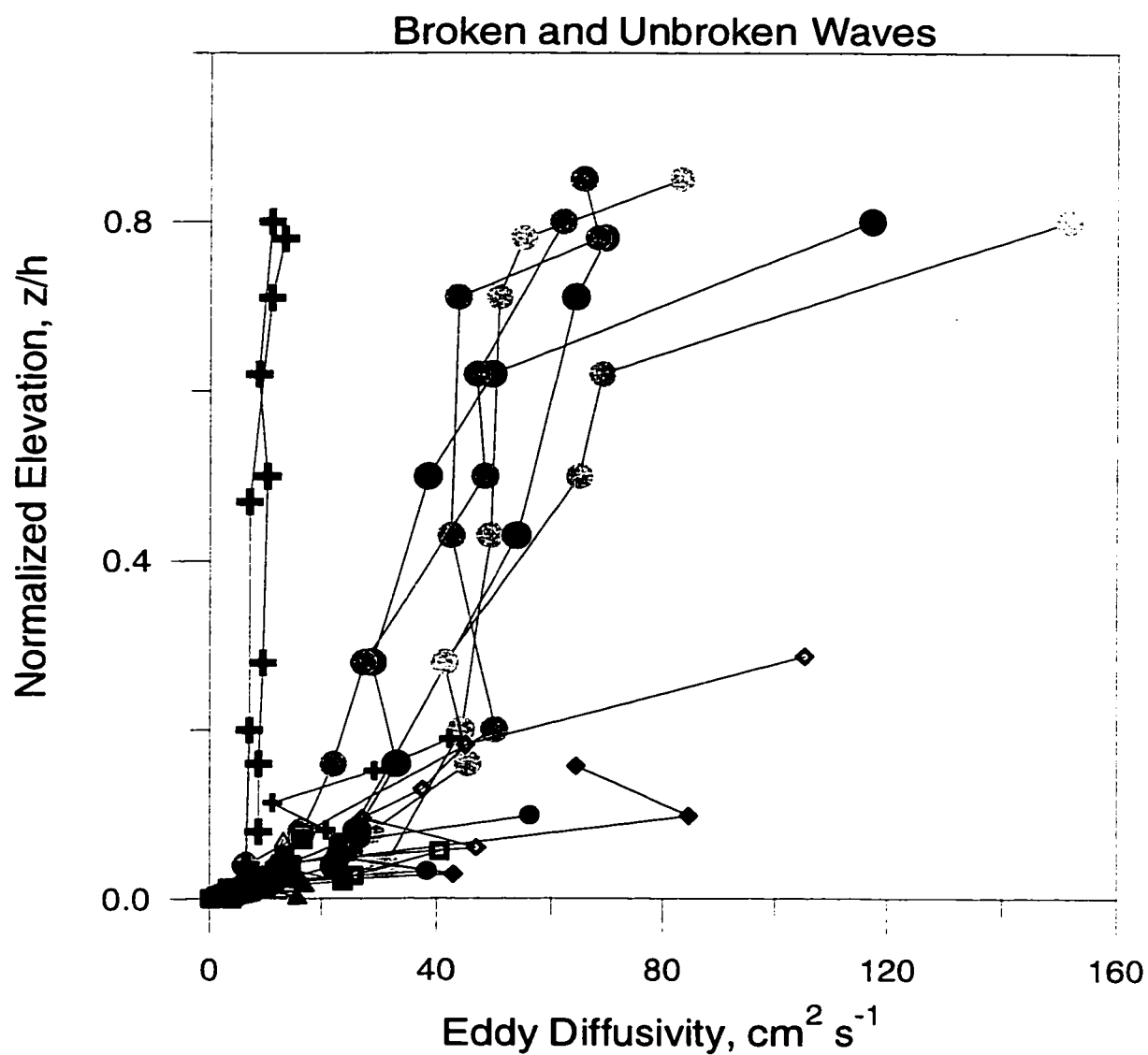


FIGURE 5.1. Eddy diffusivity values from both the wave basin experiment (large shaded symbols) and the DUCK94 experiment (small solid symbols) under both unbroken and broken waves where the elevation is normalized by the water depth.

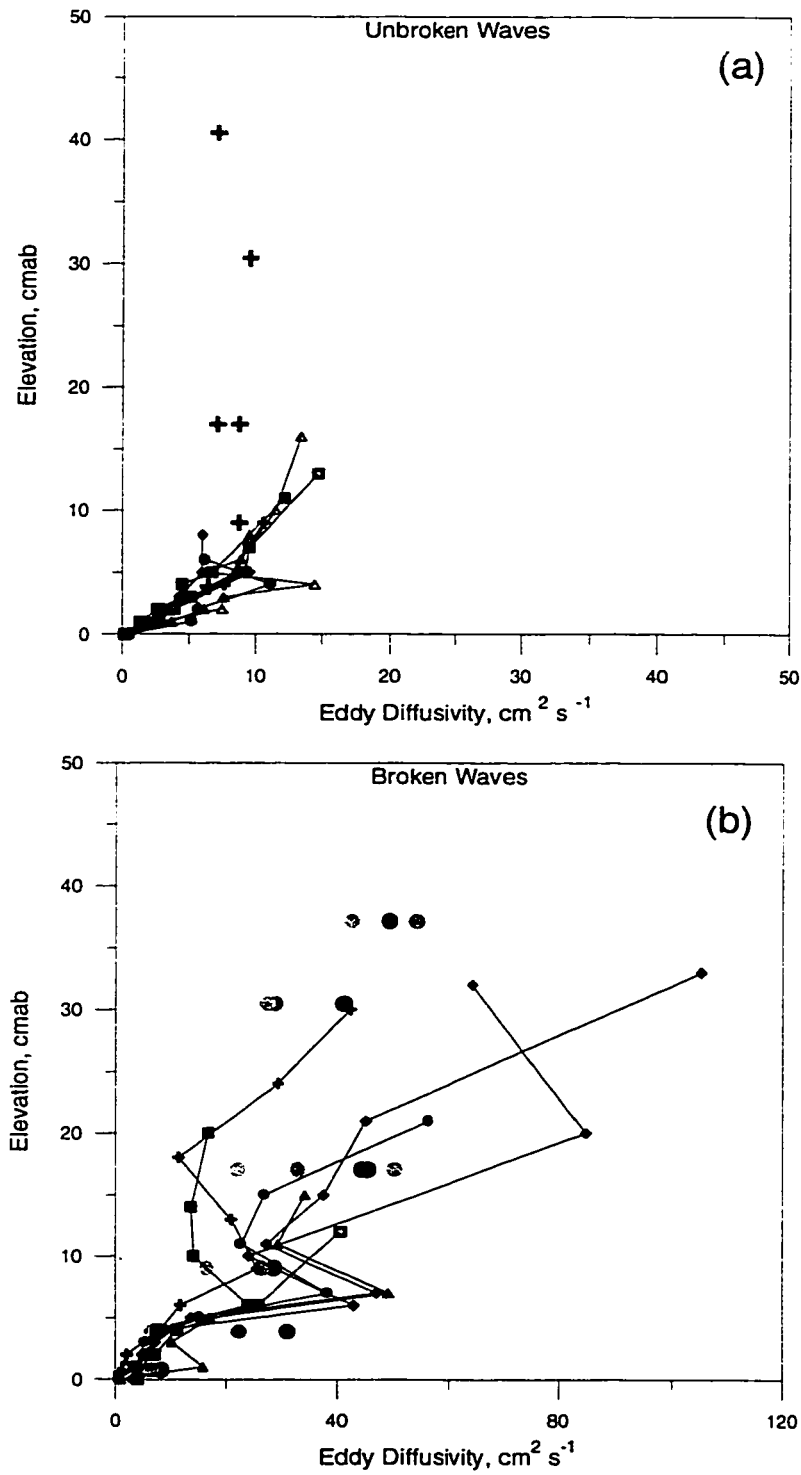


FIGURE 5.2. Region of overlap between the wave basin experiment (large shaded symbols) and DUCK94 (small solid symbols) under both a) unbroken, and b) broken waves.

relatively small compared to instrument precision, which can cause large scatter in eddy diffusivity estimates.

The DUCK94 data in the upper water column region were scaled using the same parameterization as in the wave basin experiment (i.e., depth below water surface scaled by wave height) and are shown along with the wave basin data that were obtained clearly above the bottom boundary layer in Figure 5.3. The upper water column data points from DUCK94 (solid symbols) fall in the lower part of the curve for the wave basin data points (shaded circles) and the overlap and consistency between the two experiments is apparent. The DUCK94 data points closest to the water surface tend to have higher  $K_z$  values than the wave basin data, implying that real surf zone mixing may support even higher eddy diffusivity levels. The shape of the combined set of data points may also imply a non-linearity in the parameterization that was not seen in the wave basin data alone (S-shape of data in Fig. 5.3).

### 5.2.1 Comparison to Other Studies

Acoustic backscatter measurements were used in Sheng and Hay (1995) to determine  $K_z$  on the shoreward side of the nearshore bar. In the nearbed region, their resulting  $K_z$  profiles exhibited a linear scaling with mean maximum friction velocity ( $\kappa U_{*z}$ ), and no universal form above the nearbed region was found. Although Sheng and Hay's nearbed results are consistent with this study (the  $K_z$  profiles found in the nearbed followed the relationship,  $K_z = \kappa U_{*z}$ ), a factor of  $\beta = 0.48$  was found in the relationship,  $K_z = \beta \kappa U_{*z}$ , for unbroken wave data runs of this study. This may be due to substantially higher suspended sediment concentrations found nearbed within the surf zone. The friction velocity could be affected by this in two ways: 1) density stratification effects causing attenuation of vertical momentum transfer (which was found to be only a minor effect in Chapter 3.3), and 2) the  $K_z$  to  $K_m$  relationship could differ between the two environments.

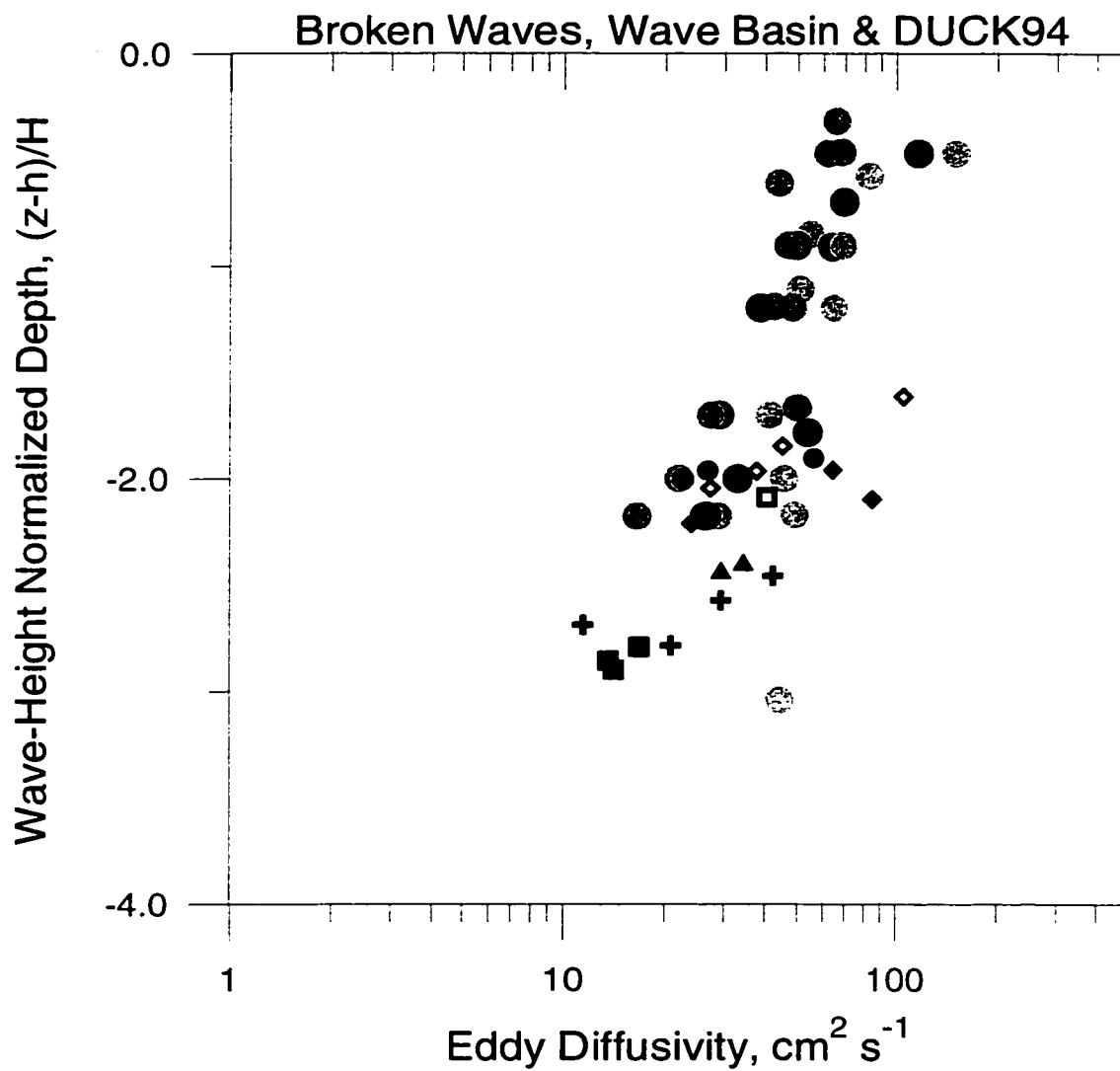


FIGURE 5.3. Eddy diffusivity values above the nearbed region from both the wave basin experiment (large shaded symbols) and DUCK94 (small solid symbols) under both unbroken and broken waves where the depth below the water surface is normalized by the wave height.



Above the nearbed region, eddy diffusivities in Sheng and Hay reach a maximum of approximately  $40 \text{ cm}^2 \text{ s}^{-1}$  and then slowly decrease with height above bed. However, in the present study a nearbed maximum of approximately  $50 \text{ cm}^2 \text{ s}^{-1}$  is seen just above the wave boundary layer, and eddy diffusivity values increase with height above the bed to a maximum exceeding  $100 \text{ cm}^2 \text{ s}^{-1}$ . The smaller peak  $K_z$  value in Sheng and Hay is consistent with the fact that their data was obtained outside the surf zone.

### 5.2.2 Formulation of Combined Eddy Diffusivity Parameterization

The goal of combining the wave basin and DUCK94 eddy diffusion results is to form a parameterized full water column eddy diffusivity profile that can be used for detailed suspended sediment modeling. In the surf zone, it is apparent that turbulence is generated by both bottom boundary friction and surface wave breaking. Therefore in the bottom boundary layer, the parameterization must be a function of distance from the bed, shear velocity, and bottom roughness. This differs in the upper water column where the scaling must be a function of depth from the free surface, wave height, and extent of breaking.

For this reason, the wave basin derived eddy diffusivities and the DUCK94 derived eddy diffusivities are scaled separately and the profiles must be matched where they join at some distance above the bed (Fig. 5.4). In the nearbed region, the eddy diffusivity profile is scaled as,

$$\begin{aligned} K_z &= 0.48\kappa U_* z & U_* < 11.4 \\ K_z &= 5.5\kappa z & U_* > 11.4 \end{aligned} \quad (5.1)$$

The physical arguments behind Eq. 5.1 are found in Chapter 4.3. These formulations are applied at elevations between the bed and twice the calculated wave boundary layer thickness ( $z < 2\delta$ ), which was defined as the height of the nearbed region.

In the upper water column, data from the wave basin experiment constrains the  $K_z$  profile. For unbroken waves, a vertically uniform profile was obtained,

$$K_z = K_1 \quad (5.2)$$

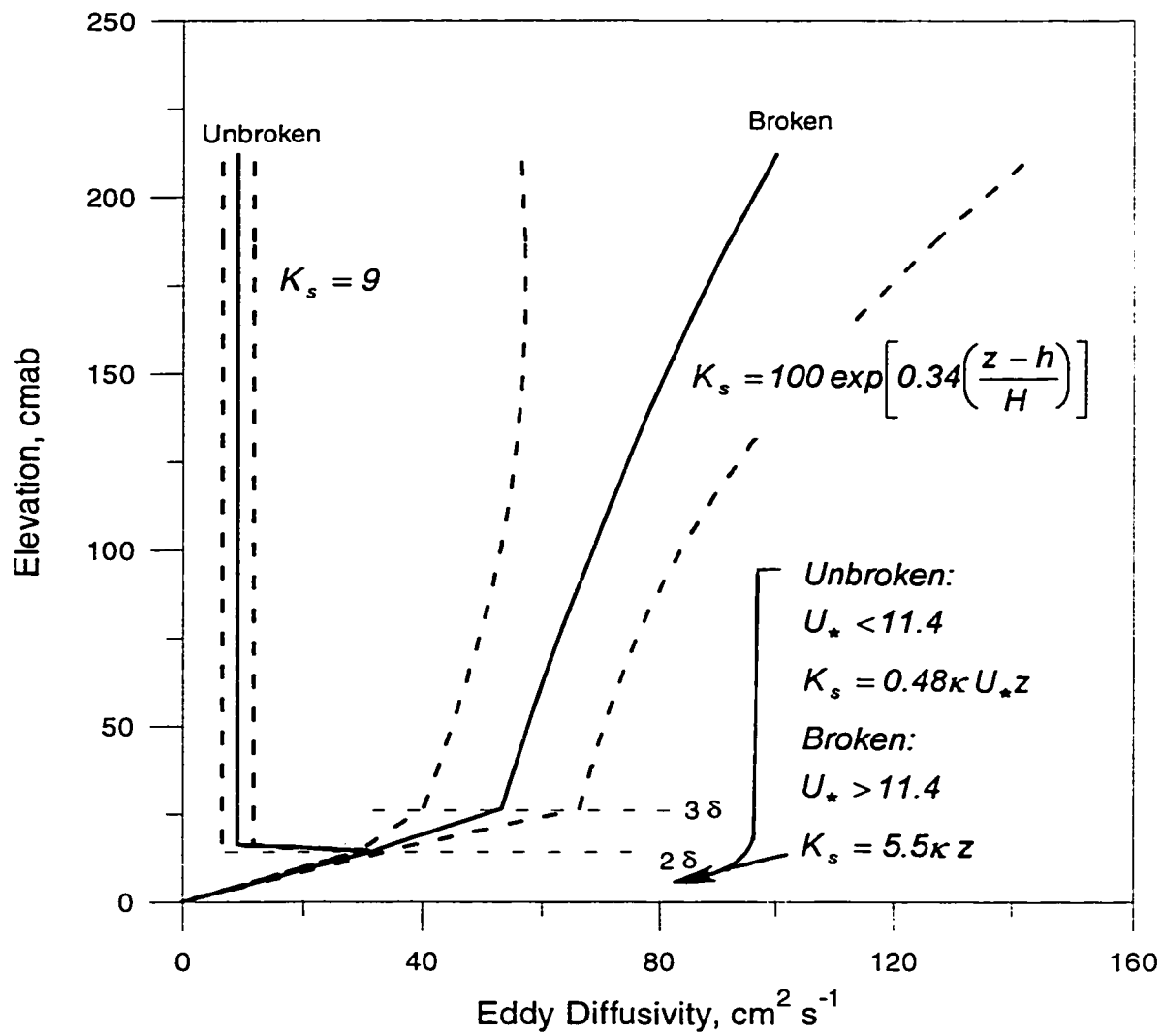


FIGURE 5.4. Conceptual diagram of the eddy diffusivity profile formulated from the wave basin and DUCK94 data.

where  $K_I = 9$  as discussed in Chapter 2. For broken waves, the data points from the highest energy wave runs were fit as shown in Figure 5.5 with the following result:

$$K_s = K_o \exp\left(b^* \frac{(z - h)}{H}\right) \quad (5.3)$$

where  $K_o = 100$  and  $b = 0.34$ . This formulation is applied at elevations above three times the calculated wave boundary layer thickness ( $z > 3\delta$ ). The upper water column formulation is brought from the sea surface down into the water column at a rate dependent upon the wave height. The nearbed formulation is brought from the bed up at a rate dependent upon the friction velocity as shown graphically in Figure 5.4. To avoid a discontinuity at any one elevation, the two profiles are linearly connected between  $2\delta$  and  $3\delta$  (top of the nearbed region).

The form of the resulting eddy diffusivity profile, as seen in Figure 5.4, reflects effects of both bottom boundary shear generated turbulence and surface wave breaking turbulence in the broken wave formulation, and only the bottom boundary shear generated turbulence in the unbroken wave formulation. Although a sharp contact between the upper water column profile and the nearbed profile is shown for unbroken waves, the processes responsible for the shape of eddy diffusivity profile must merge in a more smooth manner than is depicted in Figure 5.4.

The 95 percent confidence intervals around the  $K_s$  profile are shown for both the unbroken wave and broken wave conditions in Figure 5.4, and are based on the degree of scatter in the surf zone data that compose the formulation of an eddy diffusivity profile. The confidence interval on the predictions in the nearbed region ( $z < 2\delta$ ) are based solely on the standard error of estimate in predicting  $\beta$ . There is also error in prediction of  $U_*$  using the Jonsson friction factor method as discussed above. At present that error is not quantifiable, thus the width of the 95 percent confidence intervals in the nearbed may be underestimated. The upper water column formulation is constrained by the wave basin turbulence intensity data. Only eddy viscosity estimates under the highest energy waves in

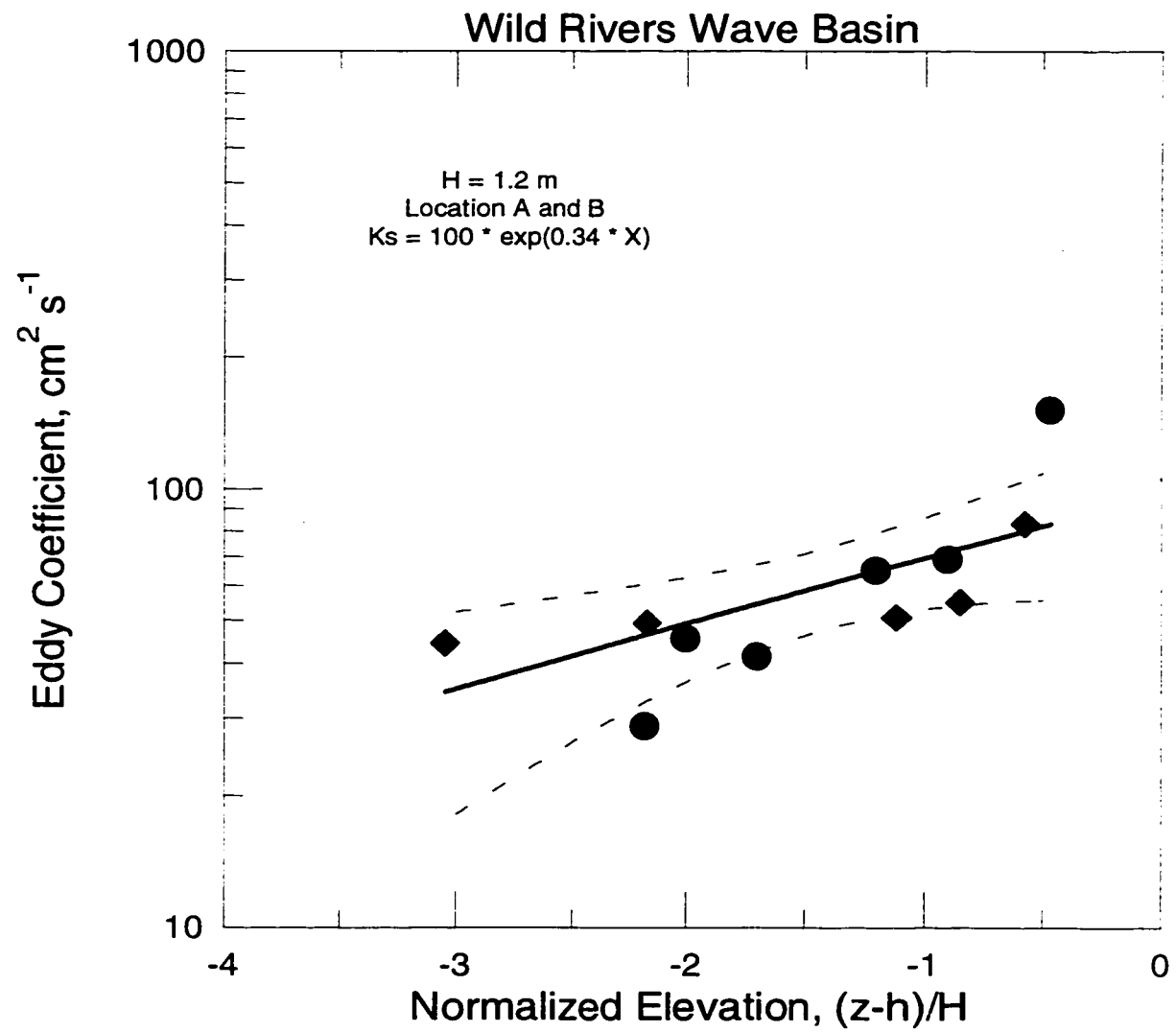


FIGURE 5.5 Fit to the highest energy waves in the wave basin study (1.2 m nominal wave height) at locations A and B.

the wave basin experiment were fit to form the parameterization and the deviation of the data from the assumed relationship used to define confidence intervals (Fig. 5.5).

### 5.3 Prediction of Suspended Sediment Concentration Profiles

A model was developed to calculate suspended sediment concentration profiles and examine implications of the  $K_r$  parameterizations. The model is a simple time averaged prediction of suspended sediment profiles based on input of wave and current characteristics, a reference concentration of suspended sediment, and a  $K_r$  profile. A logarithmically spaced vertical grid is utilized in the one dimensional predictive model, with the lowest element in the grid at the height of the reference concentration and the top element at the elevation of the free water surface.

#### 5.3.1 Physical Processes Input

The model requires input about physical processes that contribute to suspension and flux of sediments. The input requirements for determining the distribution of sediments in the vertical includes significant wave height and period at the measurement location, water depth, and friction velocity obtained from the Jonsson friction factor analysis (see Chapter 3.2). For computation of the longshore flux of sediment, a measured longshore velocity is also necessary from which the velocity distribution over depth can be estimated. The longshore velocity profile is assumed to follow a logarithmically increasing velocity profile,

$$u(z) = \frac{U_{*c}}{\kappa} \ln\left(\frac{z}{z_o}\right) \quad (5.4)$$

where  $U_{*c}$  is the current friction velocity and  $z_o$  is the elevation at which the velocity profile goes to zero. Studies have found  $z_o$  to be relatively constant for fully rough flow over a range of bed conditions and a value of 0.1 cm is used (Sternberg, 1968).

### 5.3.2 Suspended Sediment Input

The model requires input of a reference concentration and elevation. Suspended sediment profiles are calculated from the balance between downward settling and upward diffusion by turbulent mixing (Eq. 1.3). When a reference concentration,  $C_a$  is known at a reference elevation,  $z_r$ , Eq. 1.3 can be integrated vertically to determine the profile  $C(z)$ ,

$$C(z) = C_a \exp\left(\int_{z_r}^z \frac{W_s}{K_s} dz\right) \quad (5.5)$$

Analytical solutions can be obtained when  $K_s(z)$  has a simple functional form, but for more complicated profiles of  $K_s(z)$ , as formulated in Figure 5.4, suspended sediment profiles above the reference concentration are determined by numerical integration of Eq. 5.5.

The reference concentration is determined from field data as the suspended sediment concentration at an elevation which appears to be immediately above the bed load layer. This is noted in the concentration profiles as a large jump in concentration within the first couple of centimeters of the bed. Reference concentrations ranged between 1.9 and 10.2 g l<sup>-1</sup> at elevations of 1 to 3 cmab. A settling velocity for a single grain size sediment is used in the model. In the sections below, sensitivities of the model to both the eddy diffusivity profile and the sediment settling velocity are tested.

### 5.3.3 Eddy Diffusivity Profiles

Any eddy diffusivity profile formulation can be input into the model, and as a test of the sensitivity of the suspended sediment profile to the form of the  $K_s$  profile, suspended sediment concentration profiles were predicted using a variety of previously published  $K_s$  formulations. The  $K_s$  profiles and corresponding predicted sediment concentration profiles are shown in Figure 5.6 for an example broken wave data run. Measured suspended sediment concentration profiles are also shown with star symbols. The  $K_s$  profiles used in this comparison (Fig. 5.6a) are discussed in more detail in Chapter 1.2. Line A represents a linearly increasing profile with elevation above the bed, line B represent the exponential profile of Nowell and Long (1983), line C represents the two part profile of Grant and Madsen (1986), and lines D1 and D2 represent the unbroken and broken wave profiles

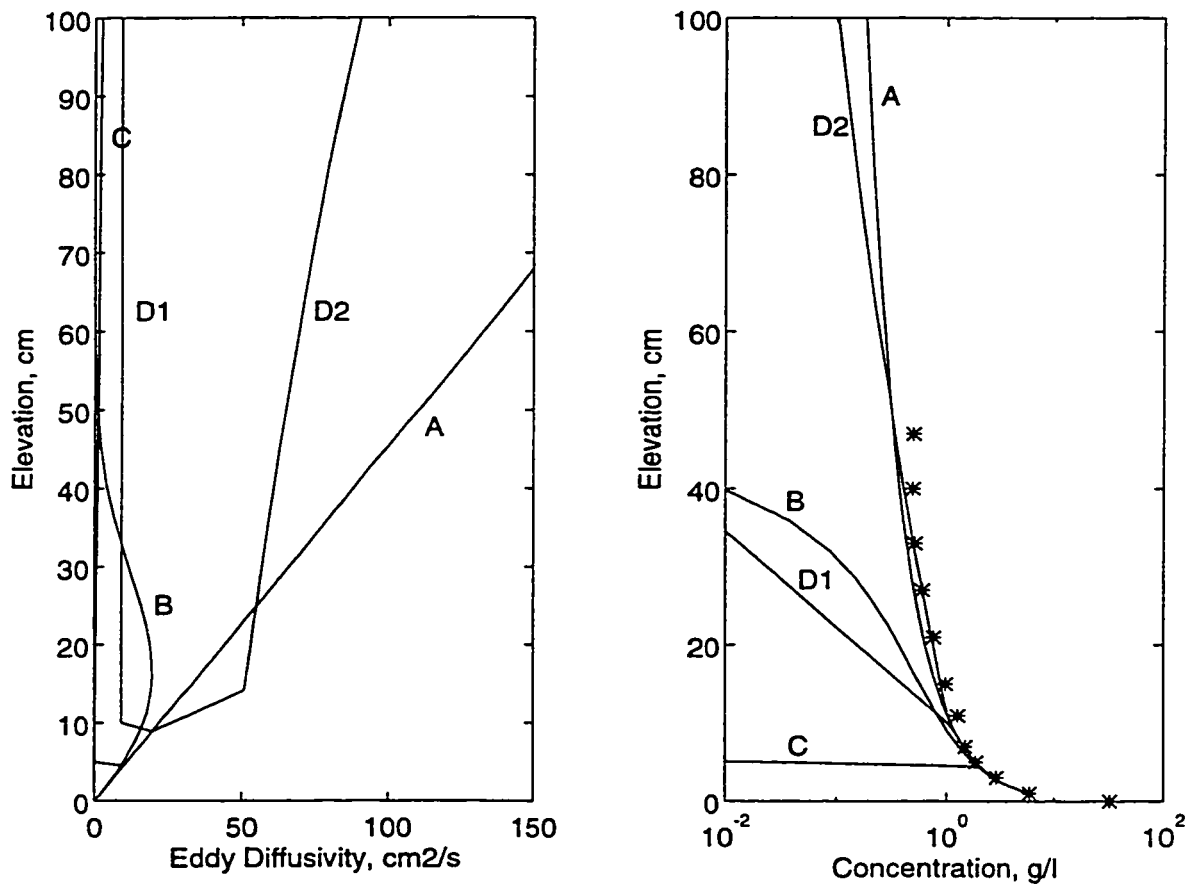


FIGURE 5.6. Profiles of a) eddy diffusivity as used in model studies (see Chapter 1 for explanation of profiles A-C) and as obtained in this study (D1 and D2), and b) measured (symbols) and predicted suspended sediment concentration profile using the corresponding eddy diffusivity profile.

from this study, respectively. All of the profiles scale similarly in the nearbed region for the broken wave data run example (Fig. 5.6). In the nearbed, the concepts behind all of the  $K_t$  profiles agree that the length scale of turbulent eddies is limited by the proximity to the bed and thus controls vertical diffusion of sediment particles. Of the two profiles used in models applied outside the surf zone (lines B and C), the exponential profile (line B in Fig. 5.6a) appears to provide the closest fit to the surf zone data points (Fig. 5.6b), but the fit falls off rapidly with height above bed. The linear profile which uses a current friction velocity above the wave boundary layer (line C in Fig. 5.5a), does not enable enough sediment to get above the wave boundary layer due to the small friction velocity generated almost solely by longshore mean currents. In the surf zone, longshore current is not the only mechanism that creates diffusion in the upper water column.

A linearly increasing  $K_t$  profile which applies the wave friction velocity, determined by the Jonsson friction factor method, throughout the water column (line A in Fig. 5.6) appears to fit the measured data well. This profile reflects the fact that there is increased mixing towards the sea surface, but the concepts behind it implies that turbulence throughout the water column is being generated at the seabed, and that the wave boundary layer is as thick as the water depth both of which are physically incorrect.

The broken wave  $K_t$  profile formulated in this study (line D2 in Fig. 5.6a) reflects mixing due to both bottom boundary layer friction and wave breaking and provides suspended sediment predictions that fit the data points well for this broken wave data run. The unbroken wave  $K_t$  profile (line D1 in Fig. 5.6a) which only reflects bottom boundary layer mixing works well in the bottom boundary layer, but does not allow sediment to be mixed into the upper water column for this broken wave data run. Therefore it underpredicts the suspended sediment concentration above the bottom boundary layer for this broken wave data run.

The effect of the  $K_t$  profile on predicted suspended sediment concentration profiles provides supporting evidence to the concepts sketched in Figure 4.5. High measured suspended sediment concentrations in the upper water column are observed under broken



TABLE 5.1. Sediment size and settling velocity

Sediment Size	Gibbs Settling Velocity	Integrated Concentration (g cm <sup>-2</sup> )
Measured data		0.045
$D_{15} = 0.30$ mm	3.6 cm s <sup>-1</sup>	0.062
$D_{50} = 0.22$ mm	2.3 cm s <sup>-1</sup>	0.024
$D_{85} = 0.16$ mm	1.4 cm s <sup>-1</sup>	0.012
$D_{bestfit} = 0.18$ mm	1.7 cm s <sup>-1</sup>	0.043
$D(z) = 0.22$ to $0.17$ mm	2.3 cm s <sup>-1</sup> to 1.5 cm s <sup>-1</sup>	0.027

waves, and the only  $K_z$  profile that adequately models the suspended sediment concentration in the upper water column and is consistent with the results of this study is one in which diffusion from breaking waves is high throughout the water column, only being limited near the bed by the length scales involved (as depicted in Fig 4.5b).

#### 5.3.4 Settling Velocity

The settling velocity of suspended particles is an important factor in balancing the upward diffusion of particles and is based on size and density of the suspended sediment particles. The size of the sediment particles in suspension is a complex function of the bed sediment size distribution, selective resuspension of sediment particles, the ability of the diffusive forces to maintain particular size classes in suspension, and the density of sand grains (typically taken to be 2.65 g cm<sup>-3</sup>). Fortunately, in the surf zone, sand grains are typically well sorted by the action of waves and currents. As was seen in Chapter 3.2, this is true for the DUCK94 field experiment except for the shoreface sediment samples in which a shell hash was combined with sand particles to form a bimodal distribution.

To test the dependence of the predictive model on settling velocity of the grain size in suspension, a range of sediment sizes corresponding to the  $D_{15}$ ,  $D_{50}$  and  $D_{85}$  of the bed sediment and resulting Gibbs et al. (1971) settling velocity estimates (see Eq. 1.5), as shown in Table 5.1, were used as input to the model and compared to the measured data for a DUCK94 broken wave data run. The suspended sediment profile measurements and predictions are shown in Figure 5.7, and it can be seen that predictions using a settling

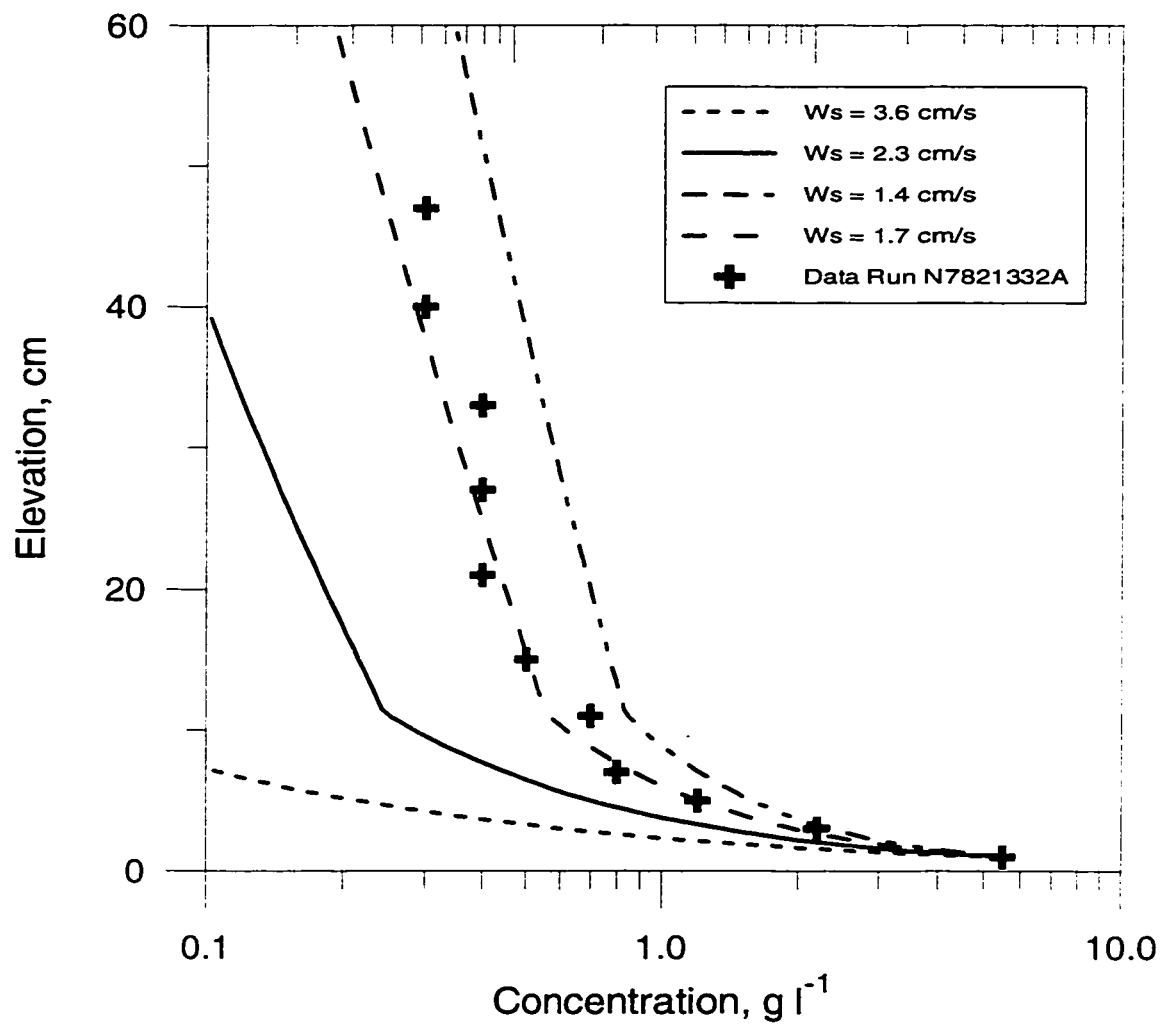


FIGURE 5.7. Comparison of predicted suspended sediment concentration profiles (solid and dashed lines) to measurements (crosses) showing the effect of settling velocity on the predictions.

velocity in excess of  $2.3 \text{ cm s}^{-1}$  are substantially lower than the measured concentrations. The predicted concentrations using a settling velocity of  $1.4 \text{ cm s}^{-1}$  are high and the predictions that fit the measurements best occur with a settling velocity of  $1.7 \text{ cm s}^{-1}$  which corresponds to the  $D_{75}$  grain size in suspension of  $0.18 \text{ mm}$ .

The effects of varying suspended sediment grain size as a function of elevation above bed can be preliminarily investigated using grain size measurements from acoustic instruments as used in Sheng and Hay (1995). The FOBS instrumentation used in the present study do not have that capability to determine grain size. Suspended sediment mean grain size profiles in Sheng and Hay (1995) indicate that the change in mean grain size with height is small for their nearshore experiment (outside the surf zone). Using a typical decrease in mean grain size from the Sheng and Hay study of  $0.05 \text{ mm}$  over  $50 \text{ cm}$  of elevation, a linearly decreasing mean grain size from  $0.22 \text{ mm}$  (mean bed grain size) at the reference concentration to  $0.17 \text{ mm}$  at  $50 \text{ cm}$  above the reference level was used as input to the predictive model and is shown in Figure 5.8 (dashed line). Also shown in Figure 5.8 are concentration profile predictions for a uniform grain size of  $0.22 \text{ mm}$  ( $Ws = 2.3 \text{ cm s}^{-1}$ ) and the best fit result,  $0.18 \text{ mm}$  ( $Ws = 1.7 \text{ cm s}^{-1}$ ). Both of the predictions with elevation dependent grain size and uniform grain size of  $0.22 \text{ mm}$  underpredict the observed data. Although there is probably a sediment grain size gradient in the vertical, it appears that the change in settling velocity due to the grain size variation is not a major factor in the predictions as shown by the very small change in slope of the concentration profile. It appears that selecting a grain size representative of the bulk of particles in suspension has a much greater impact on predictions of suspended sediment profiles. Therefore, since grain size information for the suspended particles is not available and for simplification, the sediment size in suspension is assumed to be constant in the vertical and approximately  $0.04 \text{ mm}$  smaller than the mean bed size ( $D = 0.18 \text{ mm}$ ,  $Ws = 1.7 \text{ cm s}^{-1}$ ).

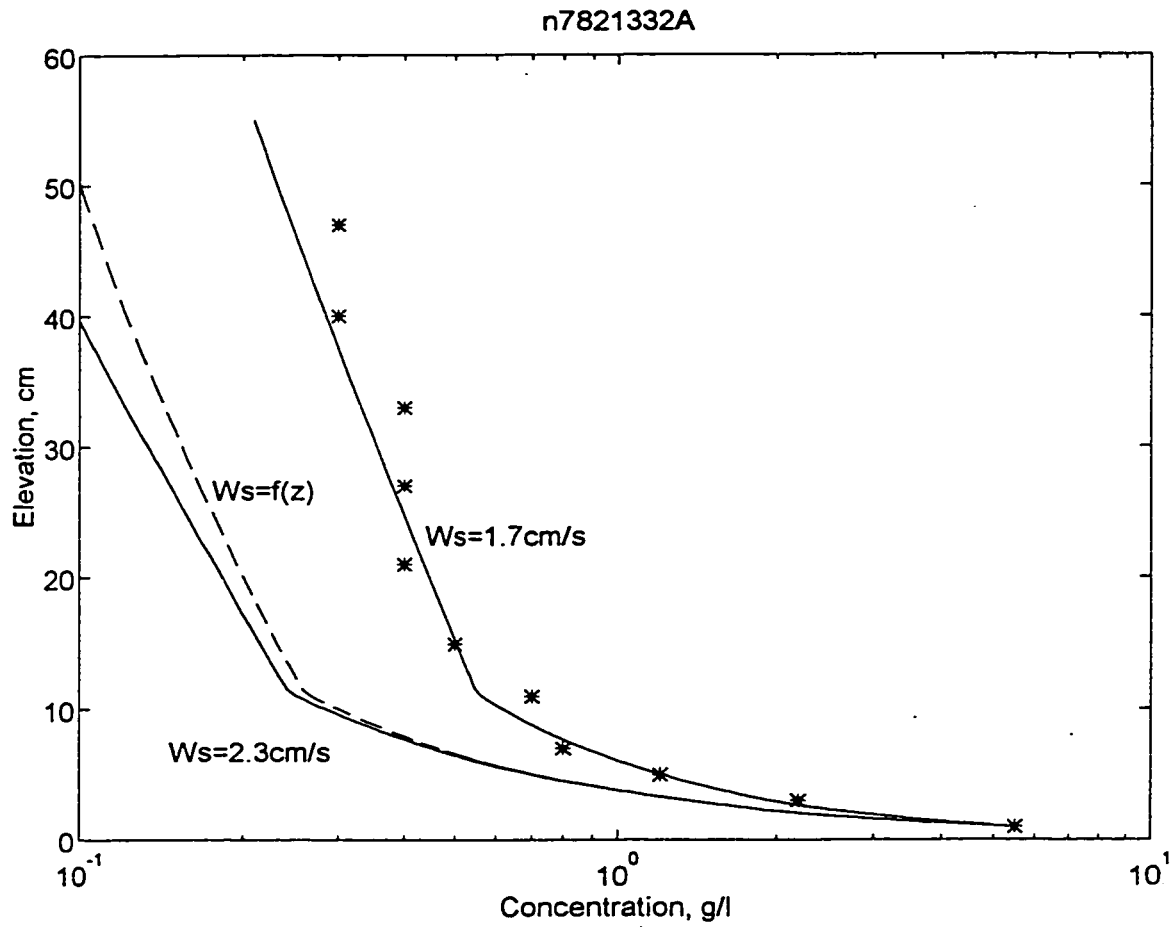


FIGURE 5.8. Comparison of predicted suspended sediment concentration profiles (solid and dashed lines) to measurements (symbols) showing the effect of using an elevation dependent settling velocity on the predictions.

TABLE 5.2. Integrated concentration and flux

	Unbroken Wave Data Run		Broken Wave Data Run	
	Integrated Concentration ( $\times 10^{-3} \text{ g cm}^{-2}$ )	Integrated Flux ( $\times 10^{-3} \text{ g cm}^{-1} \text{ s}^{-1}$ )	Integrated Concentration ( $\times 10^{-3} \text{ g cm}^{-2}$ )	Integrated Flux ( $\times 10^{-3} \text{ g cm}^{-1} \text{ s}^{-1}$ )
Measured Data	5.02	0.014	37.0	0.16
Predictions				
Broken Wave $K_r$	4.85	0.013	41.7	0.19
Unbroken Wave $K_r$	4.34	0.012	30.8	0.12

#### 5.4 Model Results

The predictive model was run for the conditions of all 14 data runs summarized in Chapter 3, with the confidence intervals as discussed above, and resulting profiles are contained in Appendix A for both unbroken and broken wave data runs. Predicted and measured suspended sediment profiles are shown for two example surf zone conditions in Figures 5.9 and 5.10.

##### 5.4.1 Suspended Sediment Profile

Figure 5.9 shows the predictive model results and a comparison to an unbroken wave data run. The concentration predictions (Fig. 5.9b) were obtained using both the unbroken and broken wave  $K_r$  profiles (Fig. 5.9a). For this example, the two predictions fall so close to one another, they are indistinguishable. The results show both the unbroken and broken  $K_r$  profile predict the suspended sediment concentrations very well, and both data and predictions show that very little sediment is suspended above the nearbed region. The form of the  $K_r$  profile above the nearbed region does not appear to have a large impact on the concentration profile in this example because of the very small amounts of suspended sediment above the bottom boundary layer. Therefore both of the predictions fall very close to one another. The vertically integrated sediment mass in the lower 50 cm of the water column is given in Table 5.2, with the unbroken wave  $K_r$ ,

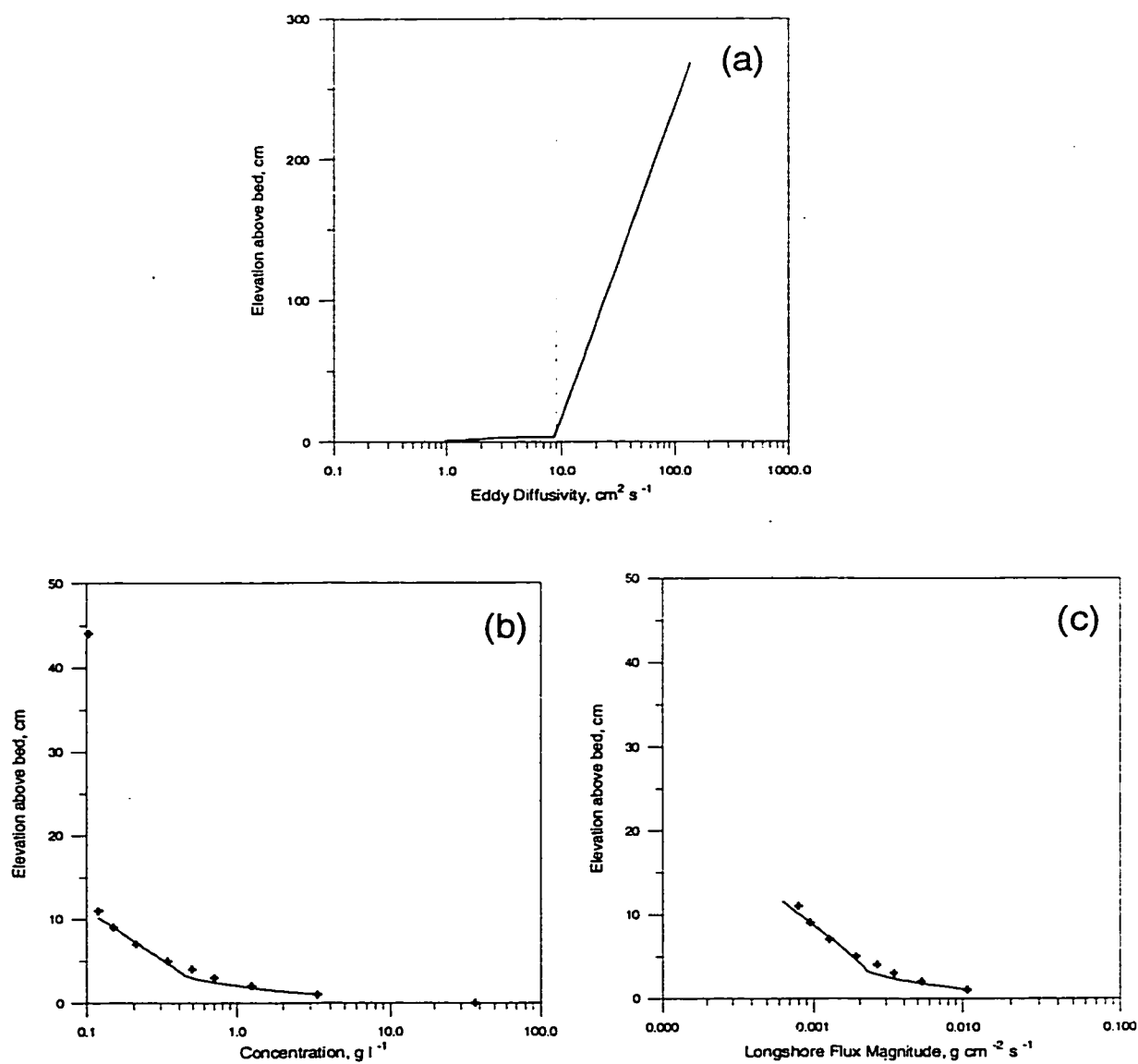


FIGURE 5.9. Example unbroken wave data run profiles of a) eddy diffusivity with (dashed line) and without (solid line) wave breaking incorporated, b) measured (crosses) and predicted (dashed and solid lines) suspended sediment concentration, and c) measured (crosses) and predicted (dashed and solid lines) longshore sediment flux.

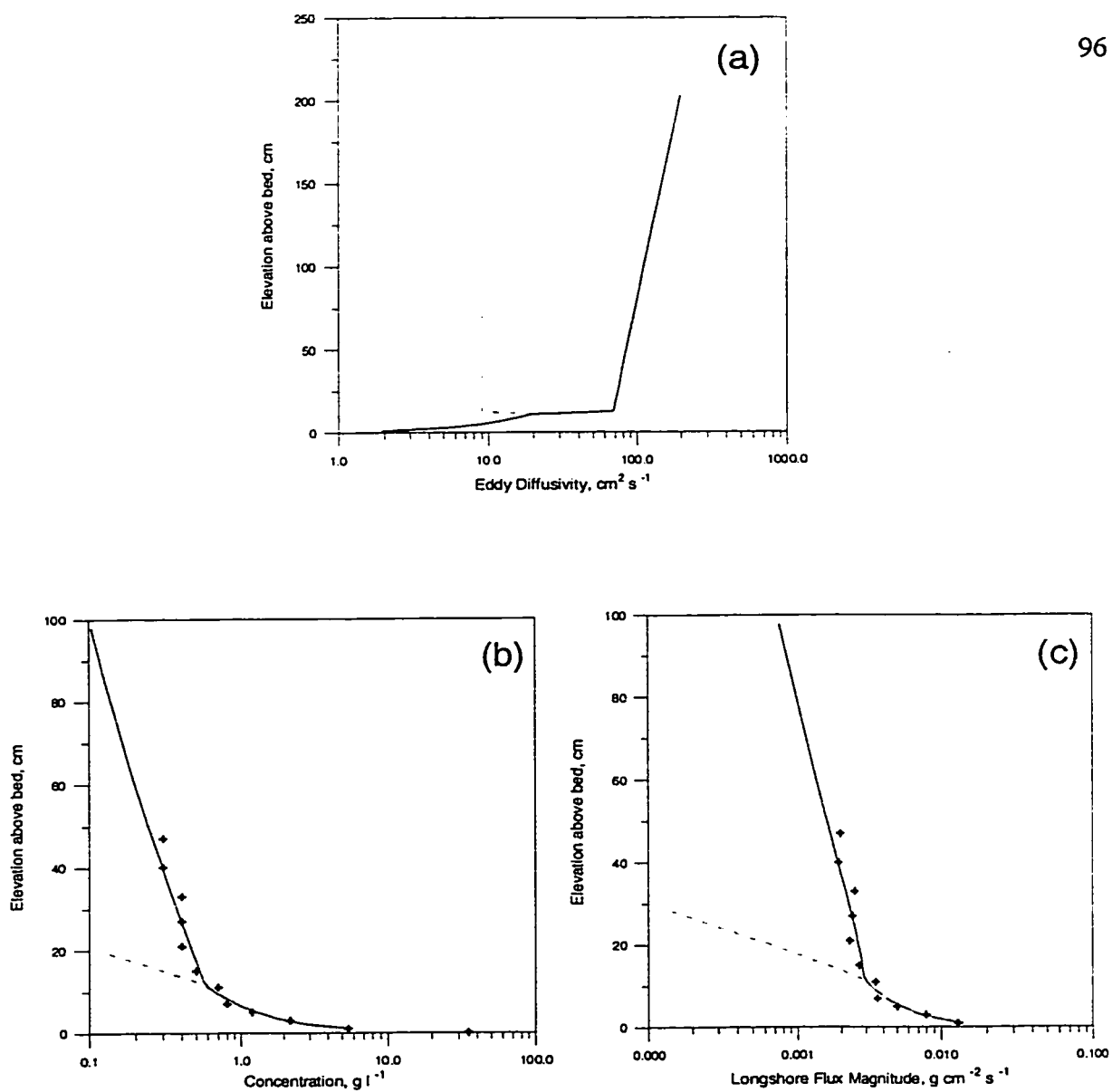


FIGURE 5.10. Example broken wave data run profiles of a) eddy diffusivity with (dashed line) and without (solid line) wave breaking incorporated, b) measured (crosses) and predicted (dashed and solid lines) suspended sediment concentration, and c) measured (crosses) and predicted (dashed and solid lines) longshore sediment flux.

prediction yielding about 86 percent and the broken wave  $K_r$  prediction yielding about 97 percent of the measured mass of sediment for this example unbroken wave data run.

Figure 5.10 shows the predictive model results and a comparison to a broken wave data run. As in the unbroken wave data run, suspended sediment concentrations were predicted using both the unbroken wave (dashed line in Fig. 5.10a) and broken wave (solid line in Fig 5.10a)  $K_r$  profile. Because of the high friction velocity that controls the  $K_r$  profile near the bed, there is a discontinuity in the  $K_r$  profile at the top of the nearbed region. The two predicted concentration profiles (Fig. 5.10b) show large differences in the upper water column. Above the nearbed region, the profiles diverge sharply and the broken wave  $K_r$  prediction fits the measured data points well, whereas the unbroken wave  $K_r$  prediction contains much lower suspended sediment concentrations in the upper water column. The vertically integrated sediment mass in the lower 50 cm of the water column is contained in Table 5.2. The broken wave  $K_r$  prediction yields 112 percent of the measured sediment mass while the unbroken wave  $K_r$  prediction yields only 83 percent.

#### 5.4.2 Sediment Flux Profile

The predicted sediment concentration profiles were combined with the longshore velocity profile to form a profile of longshore sediment flux. Predicted and measured longshore sediment fluxes are shown in Figure 5.9c and 5.10c for the unbroken and broken wave example runs. For the unbroken wave data run (Fig. 5.9c), the flux is contained in the nearbed region and both predictions show a good correspondence to the measured longshore flux data points. The predictions diverge from the measured data at a height of approximately 12 cmab, but this corresponds with the height at which the concentration measurements fall below  $0.1 \text{ g l}^{-1}$ , which is the lower limit of the sensor resolution. The vertically integrated longshore sediment flux in the lower 50 cm of the water column is given in Table 5.2 with both predictions yielding slightly less integrated sediment flux than the measurements (86 to 97 percent).

For the broken wave data run (Fig. 5.10c), a large portion of the vertically integrated flux is contained in the upper water column, and therefore the form of the water



TABLE 5.3. Integrated sediment concentration in the lower 50 cm.

INTEGRATED SEDIMENT CONCENTRATION (C > 0.1 g l <sup>-1</sup> )					
Run No.	Predictions			C <sub>Ks-un</sub> / C <sub>data</sub>	C <sub>Ks-br</sub> / C <sub>data</sub>
	C <sub>data</sub>	C <sub>Ks-un</sub>	C <sub>Ks-br</sub>		
***Unbroken Wave					
Data Runs***					
n7815964C	8.15	7.17	7.21	0.88	0.88
n7816206B	11.90	9.93	11.77	0.83	0.99
n7816206C	6.35	7.89	9.22	1.24	1.45
n7816514B	5.21	3.56	3.95	0.68	0.76
n7816514C	4.61	3.59	3.58	0.78	0.78
n7816729B	5.02	4.34	4.85	0.86	0.97
n7816729C	5.02	3.08	3.35	0.61	0.67
				0.84	0.93
***Broken Wave					
Data Runs***					
n7816729A	52.9	36.9	61.5	0.70	1.16
n7817044A	54.0	30.4	49.4	0.56	0.91
n7820881A	34.1	19.5	27.4	0.57	0.80
n7821332A	37.0	30.8	41.7	0.83	1.13
n7822521A	109.7	105.8	128.6	0.96	1.17
n7822655A	35.6	31.9	39.5	0.90	1.11
n7822763A	81.0	57.8	77.2	0.71	0.95
				0.75	1.03

column eddy diffusivity has a large impact on predictions of the longshore sediment flux. The vertically integrated longshore sediment flux in the lower 50 cm of the water column is given in Table 5.2 with the broken wave prediction yielding 119 percent of the measured flux and the unbroken wave prediction yielding only 75 percent of the measured flux.

### 5.5 Discussion

The suspended sediment concentration was integrated over the bottom 50 cm for all 14 data runs for both predictions and measurements and ratios of predictions to measurements are tabulated in Table 5.3. For unbroken wave data runs, the prediction to measurement ratio using the unbroken wave  $K_r$  profile ranges from 0.61 to 1.24 with a mean of 0.84. The same ratio using the broken wave  $K_r$  profile ranges from 0.67 to 1.45 with a mean of 0.93. This implies the difference between the predictions using an

TABLE 5. 4. Integrated longshore sediment flux in the lower 50 cm.

INTEGRATED SEDIMENT FLUX					
Run No.	Predictions			$F_{Ks-un}/$	$F_{Ks-br}/$
	$F_{data}$	$F_{Ks-un}$	$F_{Ks-br}$	$F_{data}$	$F_{data}$
***Unbroken Wave					
Data Runs***					
n7815964C	0.052	0.044	0.045	0.85	0.87
n7816206B	0.076	0.061	0.078	0.80	1.03
n7816206C	0.050	0.068	0.086	1.36	1.72
n7816514B	0.018	0.011	0.013	0.61	0.72
n7816514C	0.021	0.015	0.015	0.71	0.71
n7816729B	0.014	0.012	0.013	0.86	0.93
n7816729C	0.032	0.016	0.018	0.50	0.56
***Broken Wave				0.81	0.93
Data Runs***					
n7816729A	0.038	0.023	0.047	0.61	1.24
n7817044A	0.042	0.019	0.038	0.45	0.90
n7820881A	0.028	0.013	0.021	0.46	0.75
n7821332A	0.16	0.12	0.19	0.75	1.19
n7822521A	1.16	1.14	1.52	0.98	1.31
n7822655A	1.23	1.00	1.31	0.80	1.07
n7822763A	1.45	0.92	1.39	0.63	0.96
				0.67	1.06

unbroken wave  $K_r$  profile and using a broken wave  $K_r$  profile is only around 10 percent.

For broken wave data runs, the prediction to measurement ratio using the  $K_r$  profile for unbroken waves ranges from 0.56 to 0.96 with a mean of 0.75, implying that integrated sediment mass predictions using the unbroken wave  $K_r$  profile are low by approximately 25 percent in the bottom 50 cm. The same ratio using the broken wave  $K_r$  profile ranges from 0.80 to 1.17 with a mean of 1.03. The difference between predictions using an unbroken wave  $K_r$  profile verses using a broken wave  $K_r$  profile is substantially larger (28 percent) than in the case of the unbroken wave data runs (9 percent). The difference between the predictions using the unbroken wave  $K_r$  profile and the broken wave  $K_r$  profile, as well as the difference between the predictions and measurements, would become larger as the depth under which the concentration is integrated increases due to the difference in slopes of the predicted concentration profile in the upper water column.

The longshore sediment flux was integrated over the bottom 50 cm for all 14 data runs for both predictions and measurements and ratios of predictions to measurements are tabulated in Table 5.4. The ratios show even larger differences between predictions of integrated longshore sediment flux and measurements than with the integrated suspended sediment concentrations. The predictions of integrated longshore flux for broken wave data runs is only 67 percent of the measured data when using an unbroken wave  $K_s$  profile. Again, as the depth over which the integration is performed increases, the under-prediction would increase. The broken wave  $K_s$  profile predicts the measured data within 6 percent.

#### **5.5.1 Implications of Model Results**

The model results show that the vertical structure of the  $K_s$  profile is a very important factor in predicting the suspended sediment concentration profile in the surf zone, perhaps more important than in locations outside the surf zone where bottom boundary layer friction is the primary mechanism in controlling suspension and distribution of suspended sediment. The prediction of longshore sediment flux is more strongly influenced by the  $K_s$  profile because even small quantities of sediment that are suspended into the upper water column are subjected to faster currents than in the nearbed under steady currents.

#### ***Breaking vs. Non-breaking***

Under unbroken wave conditions, the suspended sediment profile can be modeled using any of the  $K_s$  profiles discussed above, since they all consistently use a linearly increasing diffusion with height above bed in the nearbed region. The  $K_s$  form in the upper water column is not as important under unbroken waves because the amount of sediment suspended into the upper water column is so small that the flux of sediment in the upper water column is not a large contributor to the overall flux.

Under broken wave conditions, nearbed controls on the mixing of suspended sediment appear to be the same for unbroken wave conditions due to the limitation on the

length scales of turbulent eddies by the proximity of the bed. However, in the upper water column ( $z > 3\delta$ ), predictions of suspended sediment must also reflect the turbulence generated by broken waves at the sea surface. The form of the  $K_z$  profile in the upper water column significantly impacts the predicted suspended sediment profile and large enough suspended sediment concentrations are present in the upper water column to impact the integrated sediment load and resulting sediment flux.

***Proportion of Sediment Flux Occurring due to Increased  $K_z$***

In the surf zone strong shears exist in both the cross shore and longshore vertical current profiles (e.g., Yu et al., 1993). In the longshore direction, currents have been found to follow a logarithmic profile, and therefore velocities farther from the bed are larger than velocities near the bed. In the cross shore direction, current profiles are complicated by undertow (e.g., Nadaoka, 1982; Longuet-Higgins, 1983), and mean currents near the sea surface can be in the opposite direction as currents near the bed. The vertical distribution of suspended sediments above the bed affects the flux of sediment by exposing sediment particles to transport by different currents at different elevations. Predicted suspended sediment profiles were found to be strongly dependent on the water column  $K_z$  profile under broken waves, but not so under unbroken waves. In the broken wave data run example shown in Figure 5.10, the amount of sediment flux that would have been predicted using an unbroken wave  $K_z$  is substantially less than that predicted using a broken wave  $K_z$ . This corresponds to a potential under-estimation of longshore flux in excess of 33 percent if a  $K_z$  profile that does not take into account wave breaking is used in the surf zone under broken wave conditions. In the unbroken wave example shown in Figure 5.9, the upper water column form of  $K_z$  does not contribute significantly to the magnitude of the predicted sediment flux.

Although there are no measurements of cross shore sediment flux, implications of wave breaking on the longshore sediment flux apply also to the cross shore flux. In the cross shore direction, predictions of sediment flux could even be in error directionally if a

*K*<sub>r</sub> profile is used that does not reflect wave breaking due to complicated mean current profiles in the surf zone (i.e. fluid velocities in the upper water column are directed opposite of the nearbed velocities).

## **CHAPTER 6 . SUMMARY AND CONCLUSIONS**

Two experiments provided data for the investigation of the influence of wave breaking on suspended sediment concentration profiles and longshore sediment flux in the nearshore zone. The first experiment, a prototype wave basin experiment, provided systematic velocity fluctuation data in the upper water column, and the second experiment, the DUCK94 field experiment, provided detailed suspended sediment concentration data in the nearbed region as well as detailed profiles in the bottom 50 cm of the water column. The results from the two experiments are used to formulate sediment eddy diffusivity profiles for unbroken and broken wave conditions. The relationship between the sediment eddy diffusivity and the eddy viscosity for momentum is investigated and a simple model for prediction of suspended sediment profiles is formulated.

In Chapter 2, the wave basin methods are presented and the turbulence intensities obtained from the velocity fluctuations are combined with a length scale to form an eddy viscosity profile under unbroken and broken waves. The turbulence intensity results show wave breaking in the surf zone not only causes increased levels of turbulence near the water surface, but also causes increased levels of turbulence throughout the water column. The eddy viscosity profiles suggest that wave breaking can affect mixing and diffusion throughout the entire water column. Because the diffusion of sediment can be related to the eddy diffusion of momentum ( $K_s = \beta K_m$ ), this implies that suspended sediment profiles would look different between unbroken and broken wave conditions. The wave basin had painted surfaces, and therefore the wave boundary layer was very small (on the order of 1 millimeter), which is not representative of field conditions. In addition, the wave basin did not have sediment on the bed in order to examine the eddy diffusions concepts.

In Chapter 3, the DUCK94 suspended sediment concentration profile data provides a means to examine the nearbed eddy diffusivity of sediment under unbroken and broken waves in the surf zone. In the nearbed region, the eddy diffusivity profile was found to increase linearly with height above the bed. Under broken wave data runs, the

nearbed eddy diffusivity profile exhibits an S-shape, but a linear fit to the curve is not unreasonable. It was found that the nearbed eddy diffusivity profile can be estimated using

$$K_r = \beta \kappa U_* z \quad (6.1)$$

where  $U_*$  is based on the Jonsson friction factor analysis.

Limited information is available above the nearbed region from the DUCK94 data set due to small concentration gradients, but it appears that eddy diffusivity profiles for unbroken waves approach either a uniform value or decrease exponentially as in Nowell and Long (1983). For broken wave data runs, the eddy diffusivity profile scaled by the wave height and distance from the sea surface in the upper water is consistent with the wave basin results of Chapter 2, and provides the indication that wave breaking adds to the mixing throughout the water column.

The DUCK94 data set also provides an opportunity to examine the  $K_r$  to  $K_m$  relationship in the nearbed under unbroken and broken waves, as discussed in Chapter 4. Previous studies outside the surf zone have found  $\beta$  to be within the range of 0.1 to 10 and under unbroken waves, this study found  $\beta$  to be 0.55 for  $z < 5$  cm and 0.48 for  $z < 2\delta$ . Under broken waves, there may not be a relationship between  $K_r$  to  $K_m$ , which suggests that methodology used to describe turbulent diffusion outside the surf zone (i.e. Jonsson friction factor method) is not necessarily applicable inside the surf zone.

Under broken waves, the  $K_r$  to  $K_m$  observations in this data set imply bottom boundary shear may not be the primary mechanism responsible for determining the vertical distribution of suspended sediment. Rather, the turbulence generated in wave breaking may control the turbulent transfer of sediment particles in the vertical. In order to more fully investigate these mechanisms, future work could include expanding the range of surf zone conditions under which suspended sediment data are obtained to determine the range of  $K_r$  and to increase the number of estimates leading to a higher confidence level.

The water column wave basin information and the nearbed DUCK94 information are combined in Chapter 5 to formulate two full water column  $K_r$  profiles, one for unbroken waves and one for broken waves. A simple one-dimensional model is created to

examine the impacts of the  $K_z$  profile, and results show the vertical structure of the  $K_z$  profile is a very important factor in predicting the suspended sediment concentration profile in the surf zone, more important than in locations outside the surf zone where bottom boundary layer friction is the primary mechanism in controlling the suspension and distribution of suspended sediment.

Under unbroken wave conditions, the suspended sediment profile can be modeled using a  $K_z$  profile that uses a linearly increasing diffusion with height above the bed in the nearbed region. The  $K_z$  form in the upper water column is not as important under unbroken waves because only a small amount of sediment is suspended into the upper water column, and this sediment does not contribute significantly to the integrated mass of sediment in the water column.

Under broken wave conditions, the nearbed controls on the mixing of suspended sediment appear to be the same as for the unbroken case due to the limited length scales of turbulent eddies due to proximity to the bed. But in the upper water column ( $z > 3\delta$ ), predictions of suspended sediment must also reflect the turbulence generated by broken waves at the sea surface. The form of the  $K_z$  profile in the upper water column significantly impacts the predicted suspended sediment profile and high suspended sediment concentrations are present in the upper water column which impact the integrated mass of sediment.

In the surf zone strong shears exist in both the cross shore and longshore vertical current profiles (i.e., Yu et al., 1993). In the longshore direction, currents have been found to follow a logarithmic profile and therefore velocities farther from the bed are larger than velocities near the bed. In the cross shore direction, current profiles are complicated by undertow (i.e., Nadaoka, 1982; Longuet-Higgins, 1983), and mean currents near the sea surface can be in the opposite direction from currents near the bed. The vertical distribution of suspended sediments above the bed affects the flux of sediment by exposing the sediment particles to transport by different currents at different elevations. Predicted suspended sediment profiles are found to be strongly dependent upon the water



column  $K_z$  profile under broken waves, but not so under unbroken waves. In all of the broken wave data runs, the amount of longshore sediment flux predicted using an unbroken wave  $K_z$  is substantially less than the amount of flux that is predicted using a broken wave  $K_z$ . This corresponds to a potential under-estimation of longshore flux of at least one third if a  $K_z$  profile that does not take into account wave breaking is used in the surf zone under broken wave conditions. In the unbroken wave data runs, the upper water column form of  $K_z$  does not contribute significantly to the magnitude of the predicted longshore sediment flux.

Although there are no measurements of cross shore sediment flux, the implications of wave breaking on the longshore sediment flux apply also to the cross shore flux. In the cross shore direction, predictions of sediment flux could even be in error directionally if a  $K_z$  profile is used that does not reflect wave breaking due to the complicated mean current profiles in the surf zone (i.e. fluid velocities in the upper water column are directed opposite of the nearbed velocities).

**APPENDIX A. MODEL RUNS**

# Unbroken Wave Data Runs

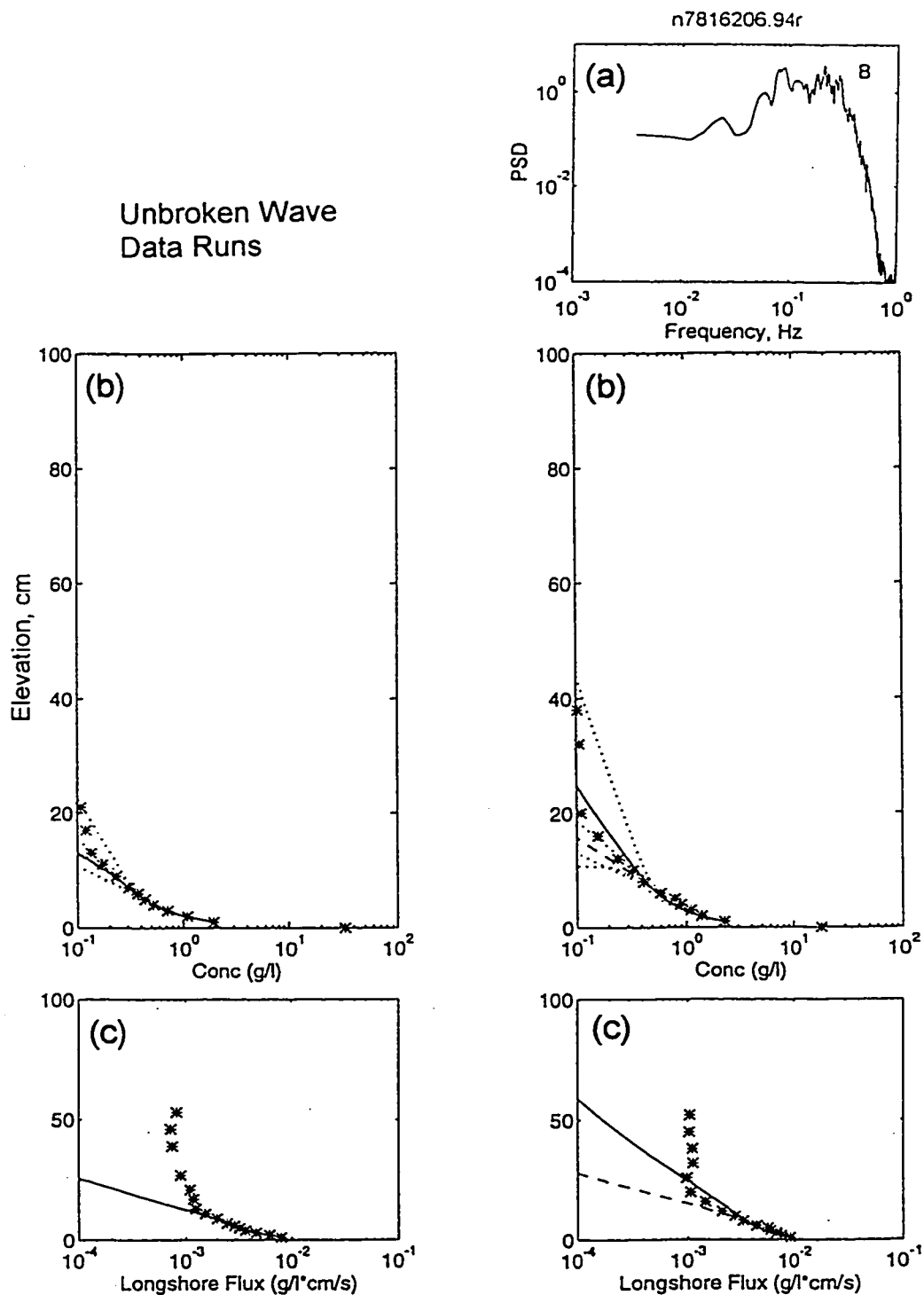


FIGURE A.1. Measurements and predictions of unbroken wave data runs, showing a) pressure power spectral density, b) sediment concentration measurements (stars), predictions (solid and dashed lines), and confidence intervals on predictions (dotted lines), and c) longshore sediment flux measurements (stars) and predictions (solid and dashed lines).

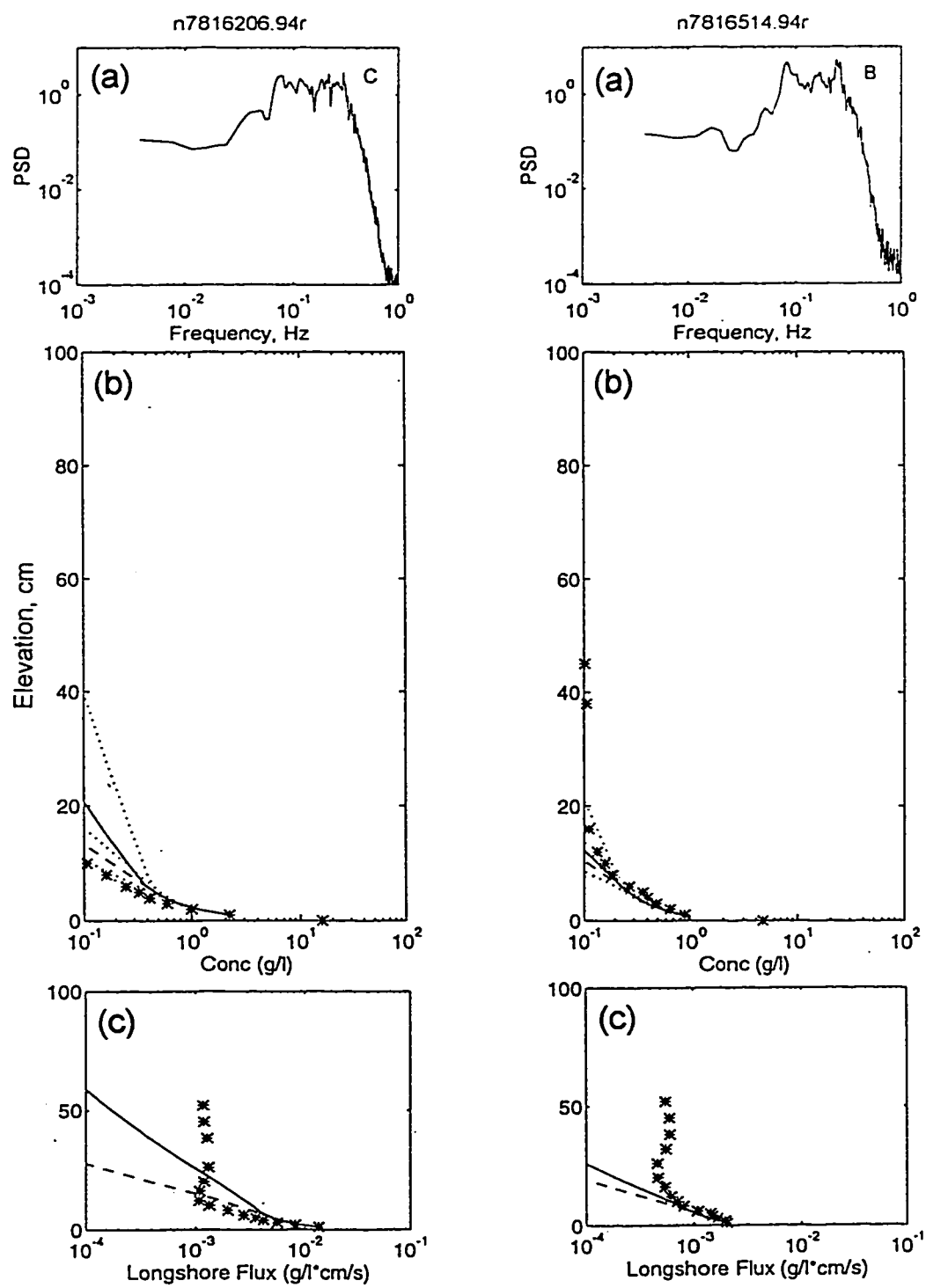


FIGURE A.1. Continued.

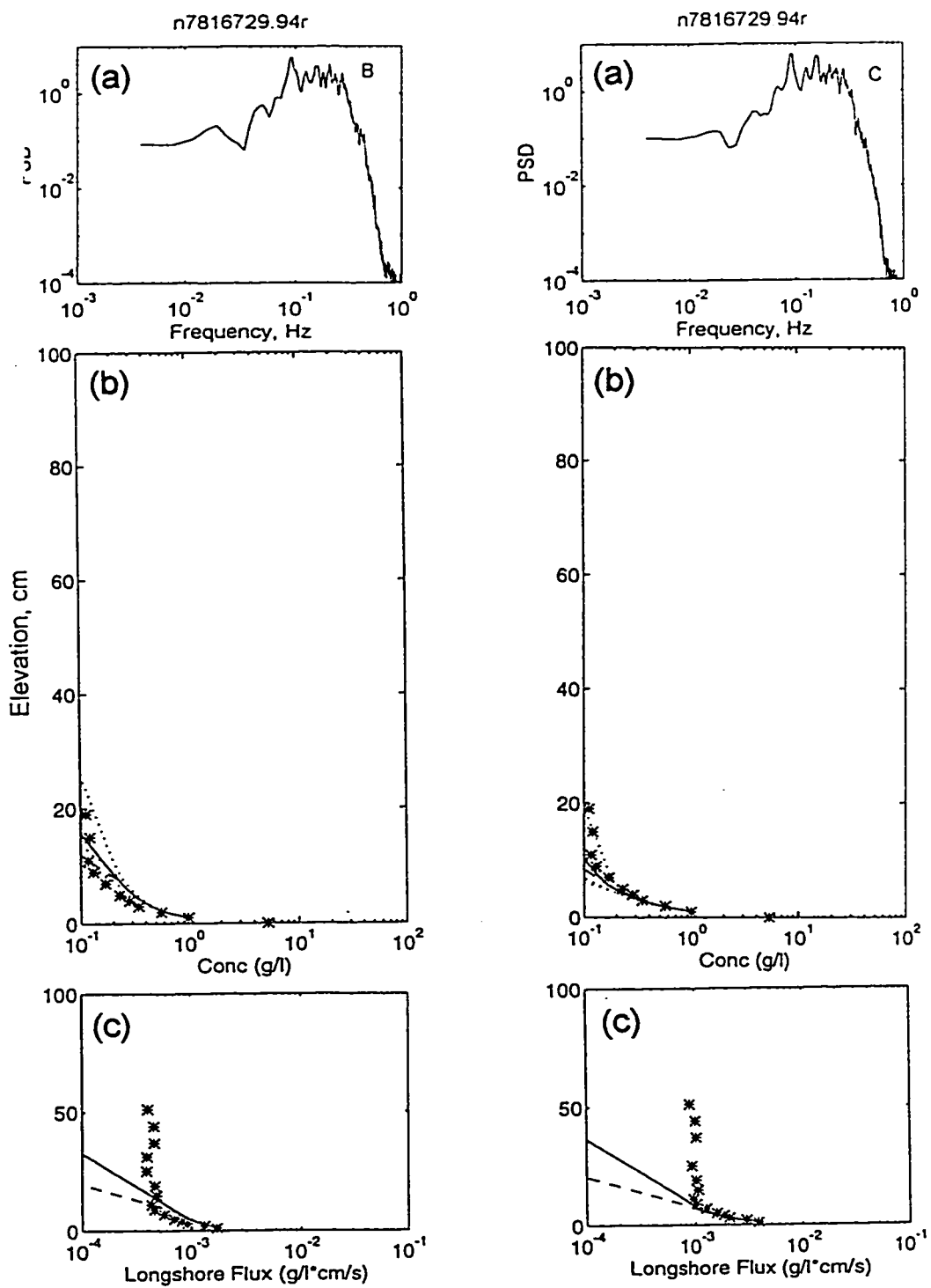


FIGURE A.1. Continued.

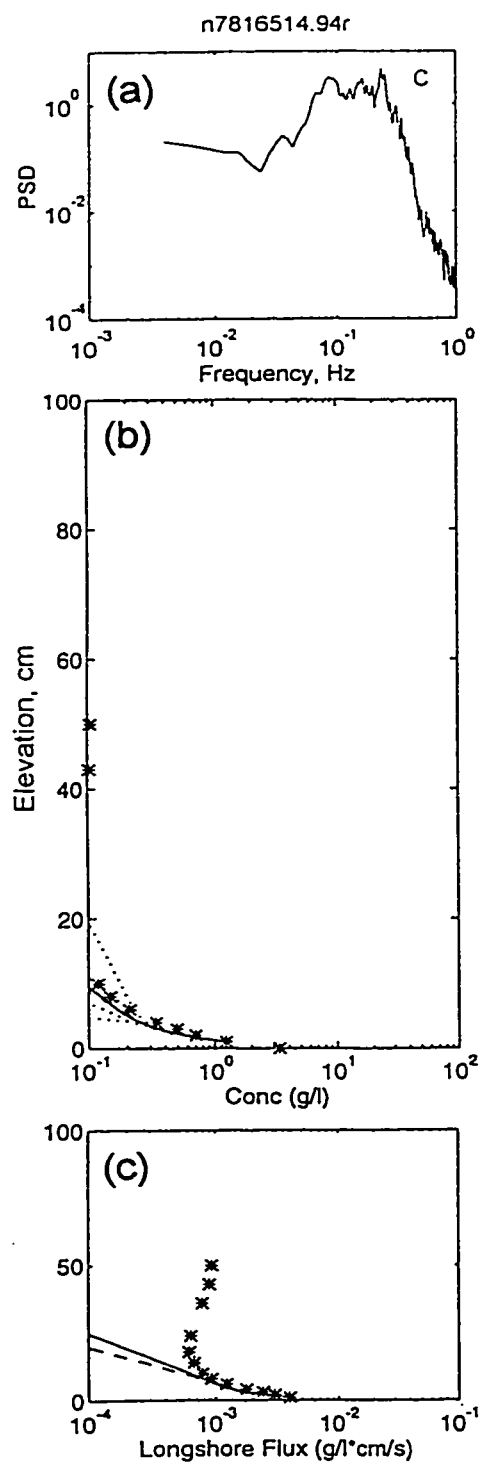


FIGURE A.1. Continued.

# Broken Wave Data Runs

112

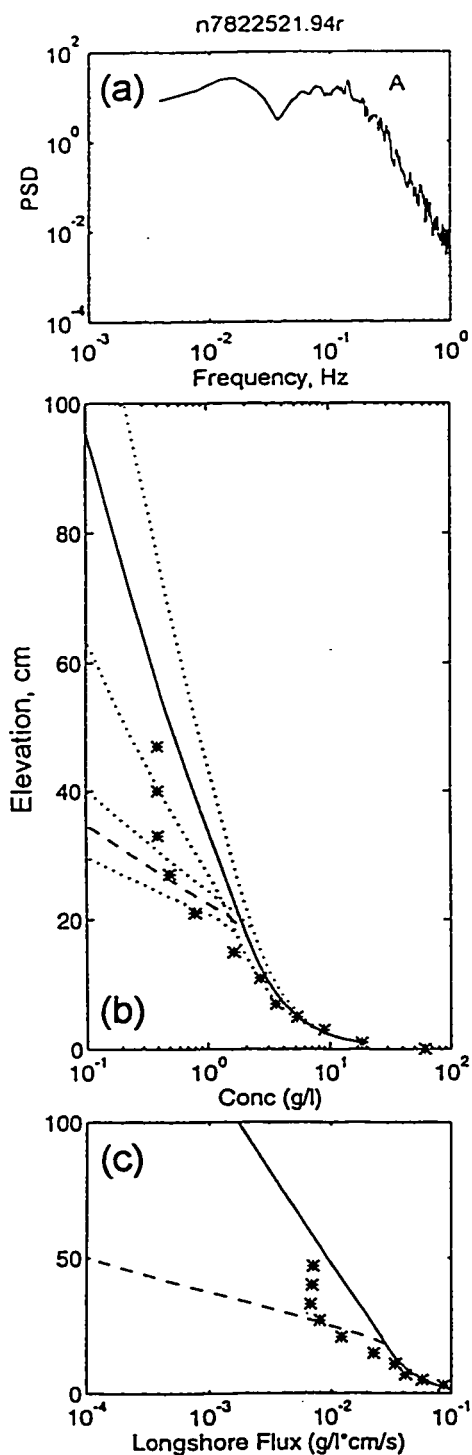


FIGURE A.2. Measurements and predictions of broken wave data runs, showing a) pressure power spectral density, b) sediment concentration measurements (stars), predictions (solid and dashed lines), and confidence intervals on predictions (dotted lines), and c) longshore sediment flux measurements (stars) and predictions (solid and dashed lines).

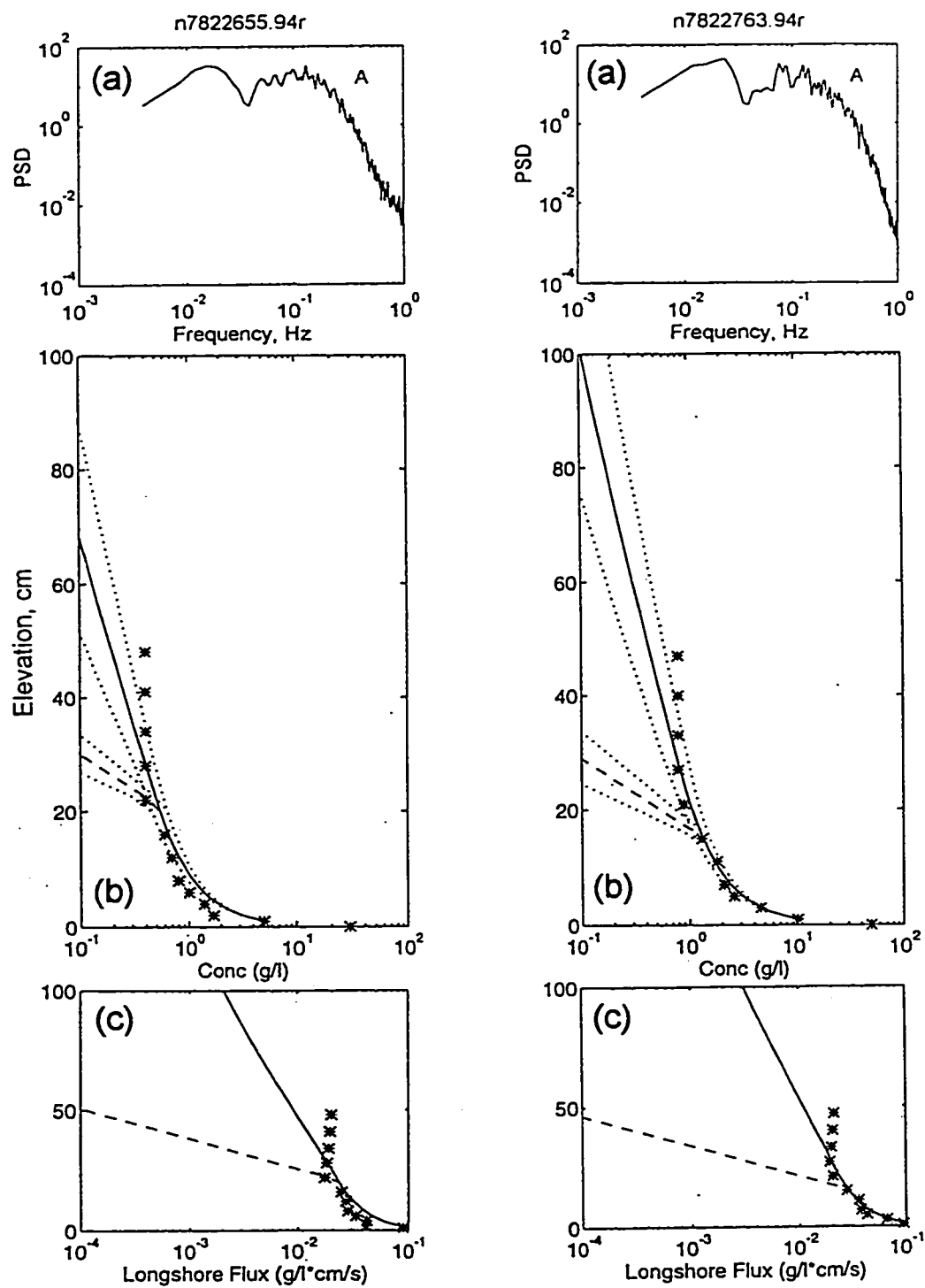


FIGURE A.2. Continued.



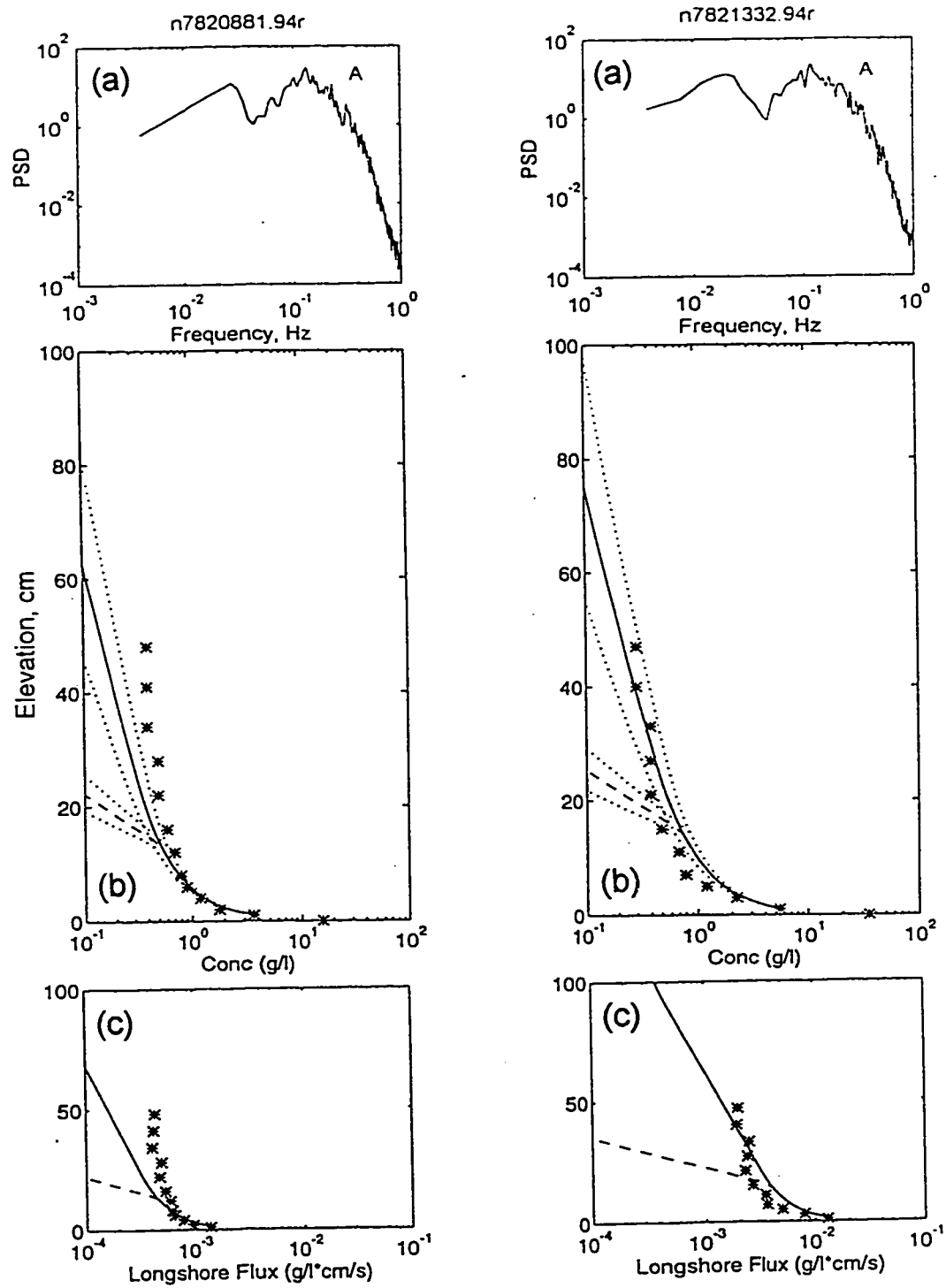


FIGURE A.2. Continued.

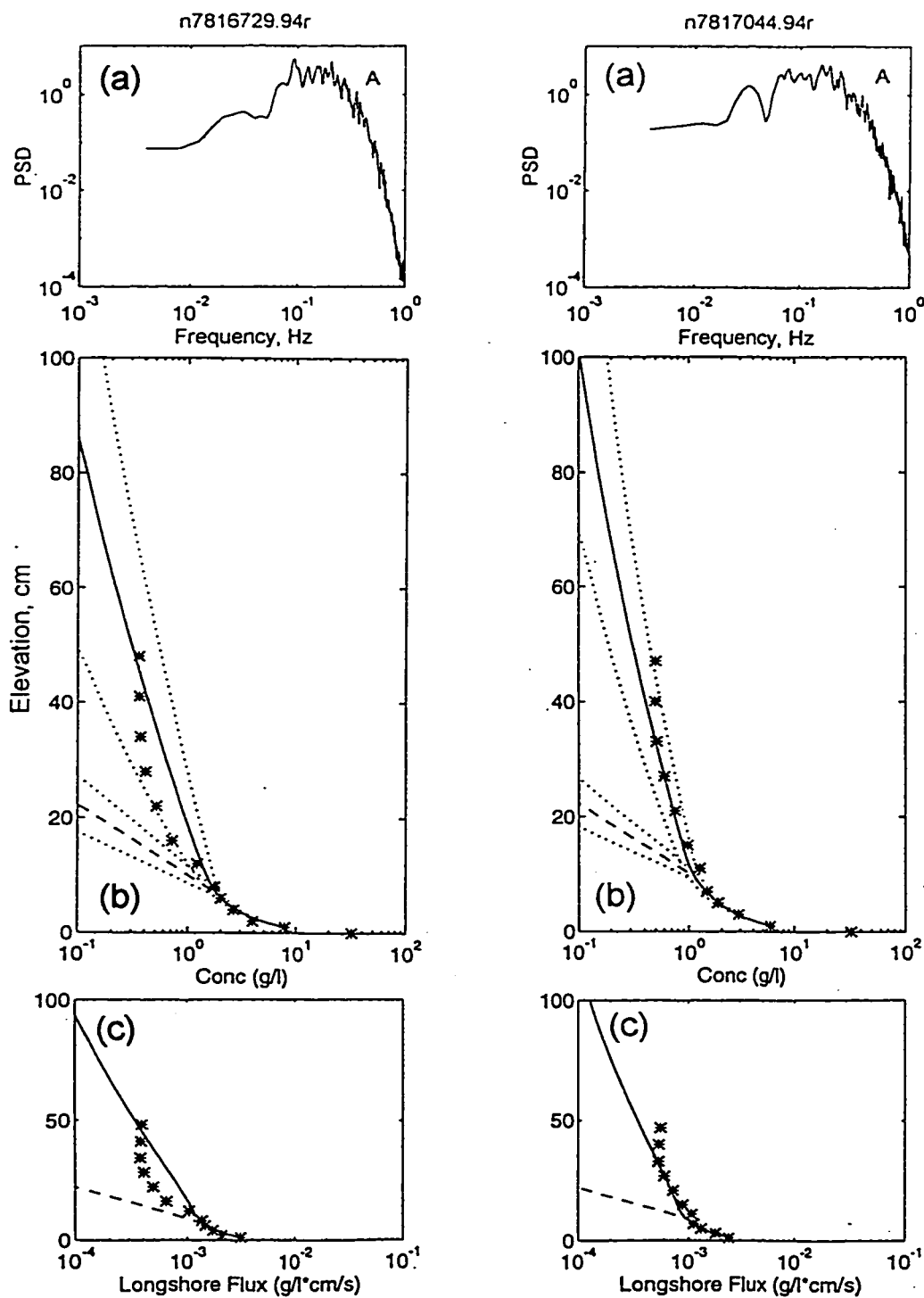


FIGURE A.2. Continued.

## LIST OF REFERENCES

- Adams, C. E. and G. L. Weatherly (1981), Some effects of suspended sediment stratification on an oceanic bottom boundary layer. *Journal of Geophysical Research*, Vol. 19, pp. 4161-4172.
- Agrawal, Y. C. and D. G. Aubrey (1992), Velocity observations above a rippled bed using laser Doppler velocimetry. *Journal of Geophysical Research*, Vol. 97, pp. 20249-20259.
- Agrawal, Y. C., E. A. Terray, M. A. Donelan, P. A. Hwang, A. J. Williams III, W. M. Drennan, K. K. Kahma and S. A. Kitaigorodskii (1992), Enhanced dissipation of kinetic energy beneath surface waves. *Nature*, Vol. 359, pp. 219-220.
- Asher, W., L. Karle, B. Higgins, P. Farley, C. Sherwood, W. Gardiner, R. Wanninkhof, H. Chen, T. Lantry, M. Steckley, E. Monahan, Q. Wang, and P. Smith (1995), Measurement of gas transfer, whitecap coverage, and brightness temperature in a surf pool: an overview of WABEX-93. In: *Proceeding of the Third International Symposium on Air-Water Gas Transfer*, B. Jaehne and E. C. Monahan, editors, Aeon Verlag, Heidelberg, Germany, July 24-27, pp. 205-216.
- Battjes, J. A. (1974), Surf similarity. *Proceedings 14th Coastal Engineering Conference*, ASCE, pp 466-480.
- Beach, R. A. and R. W. Sternberg, (1992) Suspended sediment transport in the surf zone: response to incident wave and longshore current interaction. *Marine Geology*, Vol. 108, pp. 275-294.
- Beach, R. A. and R. W. Sternberg (1988), Suspended sediment transport in the surf zone: response to cross-shore infragravity motion. *Marine Geology*, Vol. 80, pp. 61-69.
- Beach, R. A., R. W. Sternberg and R. Johnson (1992), A fiber optic sensor for monitoring suspended sediment. *Marine Geology*, Vol. 103, No. 1-3, pp. 513-520.
- Boussinesq, J. (1877), Theorie de l'ecoulement tourbillant [Theory of Turbulent Flow]. *Memoires presentes par diverse savants a l'academie des sciences de l'institut de France*, Vol. 23, pp. 46.
- Cacchione, D. A. and D. E. Drake (1990), Shelf sediment transport: An overview with applications to the northern California continental shelf. In: *The Sea*, Vol. 9 Part B, B. Lemehaute and D. M. Hanes, editors, Wiley Interscience, New York.

- Deigaard, R., J. Fredsoe and I. B. Hedegaard (1986), Suspended sediment in the surf zone, *Journal of Waterway, Port, Coastal and Ocean Engineering*, Vol. 112, pp. 115-128.
- Downing, J. P. (1983), Field studies of suspended sand transport, Twin Harbors beach, Washington. Dissertation to University of Washington, 121pp.
- Downing, J. P. and R. A. Beach (1989), Laboratory apparatus for calibrating optical suspended solids sensors. *Marine Geology*, Vol. 86, pp. 243-249.
- Dyer, K. R. (1986), *Coastal and Estuarine Sediment Dynamics*, John Wiley and Sons, Ltd., Great Britain, 342pp.
- Dyer, K. R. and R. L. Soulsby (1988), Sand transport on the continental shelf. *Annual Review of Fluid Mechanics*, Vol. 20, pp. 295-324.
- Field Research Facility (1994), Preliminary Data Summary October 1994, Coastal Engineering Research Center, U.S. Army Corps of Engineers, Vicksburg, MS.
- Foster, D. L. (1996), Dynamics of the nearshore wave bottom boundary layer. Dissertation to Oregon State University, 114pp.
- Gallagher, E. L., W. Boyd, S. Elgar, R. T. Guza, and B. Woodward (1996), Performance of a sonar altimeter in the nearshore. *Marine Geology*, Vol. 133, no. 3-4, pp. 241-248.
- Gelfenbaum, G. and J. D. Smith (1986), Experimental evaluation of a generalized suspended-sediment transport theory. In: *Shelf Sands and Sandstones, Memoir II*, R.J. Knight and J. R. McLean, editors, Canadian Society of Petroleum Geologists, pp. 133-144.
- George, R., R. E. Flick and R. T. Guza (1994), Observations of turbulence in the surf zone, *Journal of Geophysical Research*, Vol. 99, pp. 801-810.
- Gibbs, R. J., M. D. Matthews and D. A. Link (1971), The relationship between sphere size and settling velocity, *Journal of Sedimentary Petrology*, Vol. 41, pp. 7-18.
- Glenn, S. M. and W. D. Grant (1987), A suspended sediment stratification correction for combined wave and current flows. *Journal of Geophysical Research*, Vol. 92, pp. 8242-8264.
- Grant, W. D. and O. S. Madsen (1986), The Continental shelf bottom boundary layer. *Annual Review of Fluid Mechanics*, Vol. 18, pp. 265-305.

- Gross, T. F., A. J. Williams and E. A. Terray (1994), Bottom boundary layer spectral dissipation estimates in the presence of wave motions. *Continental Shelf Research*, Vol. 14, pp. 1239-1256.
- Herbers, T. H. C. and R. T. Guza (1993), Comment on "Velocity observations above a rippled bed using laser doppler velocimetry" by Y. C. Agrawal and D. G. Aubrey. *Journal of Geophysical Research*, Vol. 98, pp. 20331-20333.
- Johns, B. (1983), Turbulence modelling beneath waves over beaches. In: *Physical Oceanography of Coastal and Shelf Seas*, B. Johns, editor, Elsevier, Amsterdam, pp. 111-133.
- Jonsson, I.G. (1966), Wave boundary layers and friction factors. *Proceedings of the 10th International Conference on Coastal Engineering, 1966*, ASCE. pp. 127-148.
- Kachel, N. and J. D. Smith (1989), Sediment transport and deposition on the Washington continental shelf. In: *Coastal Oceanography of Washington and Oregon*, Vol. 47, M. R. Landry and B. M. Hickey, editors, Elsevier Oceanography Series, Elsevier, Amsterdam, pp. 287-348.
- Kajiura, K. (1964), On the bottom friction in an oscillatory current. *Bulletin of Earthquake Research Institute, Univ. Tokyo*, Vol. 42, pp. 147-174.
- Kana, T. W. (1979), Suspended sediment in breaking waves, Coastal Research Division Technical Report, No. 18-CRD, Univ. of S. Carolina, 153pp.
- Kawanisi, K. and S. Yokosi (1997), Characteristics of suspended sediment and turbulence in a tidal boundary layer. *Continental Shelf Research*, Vol. 17, no. 8, pp. 859-875.
- Kineke, G. C. and R. W. Sternberg (1992), Measurements of high concentration suspended sediments using the optical backscatterance sensor. *Marine Geology*, Vol. 108; No. 3-4, pp 253-258.
- Kitaigorodskii, S. A., M. A. Donelan, J. L. Lumley and E. A. Terray (1983), Wave-turbulence interactions in the upper ocean. Part II: Statistical characteristics of wave and turbulent components of the random velocity field in the marine surface layer. *Journal of Physical Oceanography*, Vol. 13, pp. 1988-1999.
- Komar, P. D. and M. K. Gaughan (1972), Airy wave theory and breaker height prediction. *Proceedings 13th International Conference on Coastal Engineering*, pp. 405-418.

- Kroon, A. and L. C. Van Rijn (1993), Suspended sediment fluxes in the nearshore zone at Egmond, The Netherlands. Dept. of Physical Geography, Univ. of Utrecht, The Netherlands.
- Kraus, N. C., A. Lohrmann, R. Cabrera (1994), New acoustic meter for measuring 3D laboratory flows. *Journal of Hydraulic Engineering*, ASCE.
- Lavelle, J. W. and H. O. Mofjeld (1983), Effects of time-varying viscosity on oscillatory turbulent channel flow. *Journal of Geophysical Research*, Vol. 88, pp. 7607-7616.
- Lee, T. H. and D. M. Hanes (1995), Direct inversion method to measure the concentration profile of suspended particles using backscattered sound. *Journal of Geophysical Research*, Vol. 100, pp. 2649-57.
- Lees, B. J. (1981), Relationship between eddy viscosity of seawater and eddy diffusivity of suspended particles. *Geo-Marine Letters*, Vol. 1, no.3-4.
- Longuet-Higgins, M. S. (1993), Wave set-up, percolation and undertow in the surf zone. *Proceedings Royal Society, London*, Vol. 390, no. 1799, pp. 283-291.
- Mei, C. C. (1992), *The Applied Dynamics of Ocean Surface Waves*, World Scientific Publishing, New Jersey, 740pp.
- McLean, S. R. (1992), On the calculation of suspended load for noncohesive sediments. *Journal of Geophysical Research*, Vol. 97, pp. 5759-5770.
- Nadaoka, K. (1982), Laboratory measurements of velocity field structure in the surf zone by LDV. *Coastal Engineering, Japan*, Vol. 25, pp. 125-145.
- Nadaoka, K., M. Hino and Y. Koyano (1989), Structure of the turbulent flow field under breaking waves in the surf zone. *Journal of Fluid Mechanics*, Vol. 204, pp. 359-387.
- Nielson, P., M. O. Green and F. C. Coffey (1982), Suspended sediment under waves, Department of Geography, The Univ. of Sidney, Coastal Studies Unit, *Technical Report No. 8216*.
- Nielson, P. (1992), *Coastal Bottom Boundary Layers and Sediment Transport*, World Scientific Publishing, New Jersey, 324pp.
- Nowell, A. R. M. and C. E. Long (1983), An evaluation of von Karman's constant. In: *Pollutant Transfer and Sediment Dispersal in the Washington-Oregon Coastal*

- Zone: Report of Progress, 1 August 1982-31 July 1983.* B. M. Hickey, editor, Dept. of Energy, Univ. Washington, Rep. RLO 2225 TA25-64.
- Ogston, A. S., C. R. Sherwood, and W. E. Asher (1995), Estimation of turbulence dissipation rates and gas transfer velocities in a surf pool: Analysis of results from WABEX-93. In: *Proceeding of the Third International Symposium on Air-Water Gas Transfer*, B. Jaehne and E. C. Monahan, editors, Aeon Verlag, Heidelberg, Germany, July 24-27, pp. 255-267.
- Pedersen, C., R. Deigaard and J. Sutherland (1993), Turbulence measurements under broken waves, *Progress Report of the Institute of Hydrodynamics and Hydraulic Engineering; Technical University of Denmark*, Vol. 74, pp. 81-97.
- Press, W. H., S. A. Teukolsky, W. T. Vetterling and B. P. Flannery (1992), *Numerical Recipes in FORTRAN: the Art of Scientific Computing*. Cambridge University Press, New York, 963pp.
- Sheng, J. and A. E. Hay (1995), Sediment eddy diffusivities in the nearshore zone, from multifrequency acoustic backscatter. *Continental Shelf Research*, Vol. 15, pp. 129-147.
- Sherwood, C. R. (1995), Measurements and Modeling of Suspended-Sediment Transport on the Northern California Continental Shelf. Dissertation to the University of Washington, 175pp.
- Smith, J. D. and S. R. McLean (1977), Spatially averaged flow over a wavy surface. *Journal of Geophysical Research*, Vol. 82, pp. 1735-1746.
- Soulsby, R. L., A. P. Salkield, R. A. Haine, and B. Wainwright (1986), Observations of the turbulent fluxes of suspended sand near the sea-bed. In: *Transport of Suspended Solids in Open Channels*, W. Bechteler, editor, Balkema, Rotterdam.
- Sternberg, R. W. (1968), Transport and accumulation of river-derived sediment on the Washington continental shelf, USA. *Journal of the Geological Society, London*, Vol. 143, pp. 945-956.
- Svendsen, I. A. (1987), Analysis of surf zone turbulence. *Journal of Geophysical Research*, Vol. 92, pp. 5115-5124.
- Swart, D. H. (1974), Offshore sediment transport and equilibrium beach profiles. *Delft Hydraulic Lab Publication*, No. 131.

- Thornton, E. and R. Guza (1982), Energy Saturation and phase speeds measured on a natural beach. *Journal of Geophysical Research*, Vol. 87, pp. 9499-9508.
- Trowbridge, J. H. and O. S. Madsen (1984), Turbulent wave boundary layers 1. Model formulation and first-order solutions. *Journal of Geophysical Research*, Vol. 89, pp. 7999-8007.
- Van Rijn, L. C. (1984), Sediment Transport, Part III: Alluvial Roughness. *Journal of Hydraulic Engineering*, ASCE, Vol. 110, No.12.
- Wiberg, P. L. and J. D. Smith (1983), A comparison of field data and theoretical models for wave-current interaction at the bed on the continental shelf. *Continental Shelf Research*, Vol. 2, pp 147-162.
- Williams, A. E. (1995), Duck '94 caps Engineers' efforts. *Sea-Technology*, Vol. 36, no. 1, pp. 36-37.
- Wright L. D. (1995), *Morphodynamics of Inner Continental Shelves*. CRC Press, Boca Raton, Florida, 241pp.
- Wright L. D., S.-C. Kim and C. T. Friedrich (in press), Across-shelf variations in bed roughness, bed stress and sediment suspension on the Northern California shelf: Field measurements in STRATAFORM. *Marine Geology*.
- Wyngaard, J. C. and O. R. Cote (1971), The budgets of turbulent kinetic energy and temperature variance in the atmospheric surface layer. *Journal of Atmospheric Science*, Vol. 28, pp. 190-201.
- Yu, Y., R. W. Sternberg, and R. A. Beach (1993), Kinematics of breaking waves and associated suspended sediment in the nearshore zone. *Continental Shelf Research*, Vol. 13, No. 11, pp 1219-1242.



## **VITAE**

**Andrea Susanna Ogston**

**Address:** School of Oceanography  
Box 357940  
University of Washington  
Seattle, WA 98195  
**Phone:** (206) 543-0768  
**e-mail:** ogston@ocean.washington.edu

## **EDUCATION**

Ph.D., 1997 Oceanography, University of Washington, Seattle, Washington  
M.S., 1993 Oceanography, University of Washington, Seattle, Washington  
B.S., 1987 Civil Engineering, Oregon State University, Corvallis, Oregon  
B.S., 1987 Physics, Eastern Oregon State College, LaGrande, Oregon

## **RESEARCH INTERESTS**

Marine sediment transport processes, in both the nearshore and continental shelf environments.

## **PROFESSIONAL EXPERIENCE**

1990 - present University Of Washington, School of Oceanography, Research Assistant (MS degree and Ph.D. Candidate). Developed and performed experimental surf zone research project. Worked with spectral data analysis tools and sediment transport theory and modeling as well as field instrumentation and laboratory techniques. Also involved with long-term monitoring continental shelf project.

1989 - 1990 Hartman Associates, Associate Engineer. Managed and performed work on projects pertaining to beach erosion, dredge material disposal, and sediment sampling plans.

1987 - 1989 Ogden Beeman & Associates, Consulting Engineer. Performed estuarine sedimentation analyses, river flow and backwater studies, and stormwater modeling.

## **PROFESSIONAL AFFILIATIONS**

American Geophysical Union  
American Society of Civil Engineers, Associate member  
Tau Beta Pi, Engineering Honor Society

## PUBLICATIONS

- Ogston, A.S. and R.W. Sternberg (submitted), Sediment transport events on the northern California shelf. *Marine Geology*, Special Issue on The Formation of Sedimentary Strata on Continental Margins.
- Sternberg, R.W., I. Berhane, and A.S. Ogston (submitted), Measurement of size and settling velocity of suspended aggregates on the northern California continental shelf. *Marine Geology*, Special Issue on The Formation of Sedimentary Strata on Continental Margins.
- Ogston, A.S., (1997), *Influence Of Breaking Waves On Sediment Concentration Profiles And Longshore Sediment Flux In The Nearshore Zone*. Ph.D. Dissertation, University of Washington, Seattle, WA.
- Sternberg, R.W., A.S. Ogston, and R.V. Johnson (1996), A Video System for in-situ Measurement of Size and Settling Velocity of Suspended Particulates. *Journal of Sea Research*, Vol. 36, The Netherlands, pp. 127-130.
- Ogston, A.S., C.R. Sherwood, and W.E. Asher (1995), Estimation of Turbulence-Dissipation Rates and Gas-Transfer Velocities in a Surf Pool: Analysis of the Results from WABEX-93, In: *Air-Water Gas Transfer*, eds B. Jahne and E. Monahan, AEON Verlag, pp. 255-267.
- Ogston, A.S. and R.W. Sternberg (1995), On the importance of nearbed sediment flux measurements for estimating sediment transport in the surf zone. *Continental Shelf Research*, Vol. 15, No.13, pp. 1515-1524.
- Hartman, G.L., A.S. Ogston, and M. Hanson (1991), Analysis of Transport Processes on Ocean Disposal Mound. *Coastal Sediments '91 Proceedings*, ASCE, Seattle, WA, pp. 2027-2036.